

**DOKUZ EYLÜL UNIVERSITY**  
**GRADUATE SCHOOL OF NATURAL AND APPLIED**  
**SCIENCES**

**SLOPE STABILITY ASSESSMENT OF THE**  
**OPEN PIT ALBITE MINE IN THE ÇİNE-**  
**KARPUZLU (AYDIN) AREA**

by

**Tümay KADAKCI**

**March, 2011**

**İZMİR**

**SLOPE STABILITY ASSESSMENT OF THE  
OPEN PIT ALBITE MINE IN THE ÇİNE-  
KARPUZLU (AYDIN) AREA**

**A Thesis Submitted to the  
Graduate School of Natural and Applied Sciences of Dokuz Eylül University  
In Partial Fulfillment of the Requirements for the Degree of Master of Science  
in Geological Engineering, Applied Geology Program**

**by**


**Tümay KADAKCI**

**March, 2011**


**İZMİR**

**M.Sc THESIS EXAMINATION RESULT FORM**


We have read the thesis entitled “**SLOPE STABILITY ASSESSMENT OF THE OPEN PIT ALBITE MINE IN THE ÇİNE- KARPUZLU (AYDIN) AREA**” completed by **TÜMAY KADAKÇI** under supervision of **PROF. DR. M. YALÇIN KOCA** and we certify that in our opinion it is fully adequate, in scope and in quality, as a thesis for the degree of Master of Science.

  
Prof. Dr. M. Yalçın Koca

Supervisor

  
Prof. Dr. Ferhan Şimşir

(Jury Member)

  
Dr. Dr. A. Bahadır Yavuz

(Jury Member)



Prof. Dr. Mustafa SABUNCU  
Director  
Graduate School of Natural and Applied Sciences

## ACKNOWLEDGEMENTS

I wish to express my sincere appreciation to Prof. Dr. M. Yalçın Koca for his guidance and encouragement and to Prof. Dr. Ergun Karacan for his suggestions and comments. Furthermore, I want to thank to Dr. Ahmet Turan Arslan and Dr. Cem Kıncal for their selfless and insight help throughout the research. I also thank to Çine Akmaden Company staff for their help during the site investigation. Finally, I owe my husband and mother a debt of gratitude for their support.

Tümey KADAKCI

# **SLOPE STABILITY ASSESSMENT OF THE OPEN PIT ALBITE MINE IN THE ÇİNE- KARPUZLU (AYDIN) AREA**

## **ABSTRACT**

Slope failure is often the result of insufficient geological investigation and inadequate interpretation of ground conditions prior to design. In this work, it was investigated that, to ensure the stability, how high or how steep an overall slope depending on the slope conditions can be. The study area is an open pit albite mine which has been operating by Çine Akmaden Company since 1996 in Aydın, Çine-Karpuzlu. In the mine, only leucocratic orthogneisses are exposed. The elevation of the base of the albite open pit is 395 m at present and 45 m thickness from the present base has been planned to be mined out. The main goal of this study is to determine the optimum overall slope angle for different slope conditions at the time which the mining operations are terminated. In this context, field investigation and numerical studies to analyse the slope instabilities were conducted. Input data to the stability analysis was obtained from detailed field observation of the rock mass and laboratory studies performed on rock material.

In numerical modelling, applicability of the finite element method (FEM) involving shear strength reduction (SSR) technique by considering the Generalized Hoek-Brown Criterion and Equivalent Mohr-Coulomb parameters to jointed rock slopes in the eastern part of the Alipaşa open pit was investigated. In this process, firstly five geotechnical cross-sections perpendicular to the tension cracks observed in the field and passing through the area affected from local block slides were taken; secondly stability analyses of overall slopes along these cross-sections considering the variations of Geological Strength Index (GSI), seismic acceleration ( $\alpha_s$ ), slope angle ( $\alpha_{\text{slope}}$ ) and water table location (WTL) were conducted using the Phase<sup>2</sup> V.7.013 software which utilizes FEM with SSR technique in terms of Generalized Hoek-Brown and equivalent Mohr-Coulomb parameters. The causes and mechanisms of slope instabilities, also the factor of safety values for each cross-section were determined.

The results obtained from each criterion were compared to each other by utilizing a statistical computer program SPSS (Statistical Package for Social Sciences) to determine the optimum overall slope angle for each cross-section in terms of the best fitting criterion for the orthogneisses.

As a result, considering the SRF (Shear Reduction Factor) values obtained from both methods, the optimum overall slope angle was determined as 32° when the GSI, WTL and  $\alpha_s$  values were taken as 42, 70% and 0.1g, respectively. Accordingly, the present overall slope angle 27° should be increased to 32° by trimming the units from upper slope face to the base of the mine after the mining operations. Besides, at the time either the slope becomes fully saturated after heavy rainstorms or an earthquake with a magnitude greater than 6.5 occurs, it will be unavoidable that the slope becomes instable even for 32° slope angle.

**Keywords:** Generalized Hoek-Brown Criterion, Equivalent Mohr-Coulomb parameters, Finite element Method (FEM), Slope stability, Orthogneiss, Albite open pit mine.

# ÇİNE-KARPUZLU (AYDIN) YÖRESİNDEKİ AÇIK OCAK ALBİT MADENİNİN ŞEV STABİLİTE DEĞERLENDİRMESİ

## ÖZ

Şev yenilmesi, şev tasarımından önceki zemin koşullarının yetersiz yorumlanması ve eksik jeolojik incelemelerin bir sonucudur. Bu çalışmada, duraylılığı sağlamak için, şevin ne kadar dik ve yüksek olacağı, şev koşulları doğrultusunda incelenmiştir. Çalışma alanı, Çine Akmaden Şirketi tarafından 1996'dan beri işletilmekte olan, Aydın, Çine-Karpuzlu'da bulunan bir açık ocak albit madenidir. Madende sadece lökokratik ortognayslar yüzlek vermektedir. Albit açık ocak işletmesinin bugünkü taban kotu 395 m iken, tabandan itibaren 45 m daha işletilmesi planlanmıştır. Bu çalışmanın asıl amacı, maden çalışmalarının sona erdiği durumdaki değişik şev koşullarında optimum şev açısının belirlenmesidir. Bu kapsamda, şev duraysızlıklarını analiz etmek için, arazi incelemeleri ve numerik çalışmalar yapılmıştır. Duraylılık analizleri için gerekli olan girdiler, kaya kütlelerinin ayrıntılı arazi gözlemleri ve kaya materyali üzerinde yapılan laboratuvar çalışmalarından sağlanmıştır.

Numerik analizlerde, kesme direnci indirgeme (SSR) tekniğini içeren, Genelleştirilmiş Hoek-Brown Kriteri ve Eşdeğer Mohr-Coulomb parametrelerini dikkate alan, sonlu elemanlar yönteminin (FEM) Alipaşa açık ocak işletmesinin doğusunda bulunan çatlaklı kaya şevine uygulanabilirliği incelenmiştir. Bu süreçte, öncelikle arazideki yerel blok kaymalarından etkilenen alandan geçen, tansiyon çatlaklarına dik uzanan beş adet jeoteknik kesit alınmıştır. Daha sonra bu kesitlere ait şevlerin duraylılık analizleri, değişik Jeolojik Dayanım İndeksi (GSI) değerleri, sismik ivme ( $\alpha_s$ ), şev açısı ( $\alpha_{slope}$ ) ve yeraltı su durumu (WTL) değerleri kullanılarak, iki boyutlu FEM analizi yapan bilgisayar programı Phase<sup>2</sup> V.7.013 ile yürütülmüştür. Analizlerin sonucunda, şevin yenilme mekanizması ve nedenleri; ayrıca güvenlik katsayısı (SRF) değerleri elde edilmiştir.

Her iki yöntemden elde edilen SRF değerleri, bir istatistik programı olan SPSS (Statistical Package for Social Sciences) kullanılarak karşılaştırılmış ve çalışma alanındaki ortognaysları en iyi temsil eden kriter doğrultusunda, nihai şev açısı belirlenmiştir.

Sonuç olarak, her iki yöntemden elde edilen SRF değerleri gözönünde bulundurularak, GSI, WTL and  $\alpha_s$  değerlerinin sırasıyla 42, 70% and 0.1g olduğu durumda, optimum şev açısının  $32^\circ$  olduğu belirlenmiştir. Buna bağlı olarak bugünkü  $27^\circ$ 'lik şev açısı, şev tepesinden tabanına doğru uygun miktarda malzemenin temizlenmesi ile  $32^\circ$ 'ye arttırılabilir. Bunun yanı sıra şevin, şiddetli yağış sonrası tamamen doymun hale gelmesi ve/veya moment büyüklüğü 6.5'dan büyük bir depremin oluşması sonucunda,  $32^\circ$ 'lik şevin de duraysız hale gelmesi kaçınılmazdır.

**Anahtar kelimeler:** Genelleştirilmiş Hoek-Brown Kriteri, Eşdeğer Mohr-Coulomb parametreleri, Sonlu elemanlar yöntemi, Şev duraylılığı, Ortognays, Albit açık ocak işletmesi.



## CONTENTS

	<b>Page</b>
THESIS EXAMINATION RESULT FORM.....	<b>Error! Bookmark not defined.</b>
ACKNOWLEDGEMENTS .....	ii
ABSTRACT .....	iv
ÖZ.....	vi
<b>CHAPTER ONE - INTRODUCTION .....</b>	<b>1</b>
1.1 Location of the Study Area.....	1
1.2 Rainfall .....	2
1.3 The Çine-Akmeden Company .....	2
1.4 Main Scope of The Study .....	3
1.5 Preliminary Site Investigation of Alipaşa Open Pit Albite Mine .....	3
1.6 Safety Factor .....	6
1.7 Slope Stability Analyses .....	6
<b>CHAPTER TWO - METHODS.....</b>	<b>9</b>
2.1 Numerical Modelling with Finite Element Method (FEM).....	9
2.2 The Shear Strength Reduction (SSR) Technique in FEM .....	11
<b>CHAPTER THREE - REGIONAL GEOLOGY.....</b>	<b>13</b>
3.1 Stratigraphy.....	13
3.2 Tectonics .....	14
3.2.1 Büyük Menderes Graben.....	16
<b>CHAPTER FOUR - GEOLOGY OF THE STUDY AREA .....</b>	<b>17</b>
4.1 Çine Submassif .....	17
4.2 Mineral Composition of Ore Bearing Zone .....	17

4.3 Occurrence of Albite Deposits .....	18
<b>CHAPTER FIVE - SEISMICITY.....</b>	<b>20</b>
<b>CHAPTER SIX - ENGINEERING GEOLOGY.....</b>	<b>24</b>
6.1 Quantitative Description of Discontinuities in Rock Masses .....	24
6.1.1 Type of Discontinuity .....	25
6.1.2 Orientation of Discontinuities .....	26
6.1.3 Spacing of Discontinuities .....	27
6.1.4 Persistence of Discontinuities .....	28
6.1.5 Roughness of a Discontinuity Surface .....	28
6.1.6 Discontinuity Wall Strength.....	29
6.1.7 Discontinuity Aperture.....	30
6.1.8 Filling of Discontinuity Apertures .....	30
6.1.9 Seepage Through Discontinuity Planes .....	31
6.1.10 Block Size and Shape.....	31
6.2 Rock Mass Strength .....	32
6.3 In-situ Tests .....	33
6.3.1 Tilt Tests .....	33
6.4 Laboratory Tests .....	33
6.4.1 Unit Weight Determination.....	33
6.4.2 Uniaxial Compressive Strength Test.....	33
6.5 Kinematic Analysis Of The Eastern Slope of Alipaşa Open Pit Mine .....	34
6.6 Water Table Condition .....	37
<b>CHAPTER SEVEN - SLOPE STABILITY ANALYSIS CONSIDERING THE GENERALIZED HOEK-BROWN FAILURE CRITERION .....</b>	<b>41</b>
7.1 Applicability of the Generalized Hoek-Brown Failure Criterion .....	41
7.2. Input Data for Slope Stability Analyses Based on Generalized Hoek-Brown Criterion.....	42

7.3 The Slope Stability Analyses Results Based on Generalized Hoek-Brown Criterion .....	52
<b>CHAPTER EIGHT - SLOPE STABILITY ANALYSIS USING THE EQUIVALENT MOHR COULOMB PARAMETERS .....</b>	<b>57</b>
8.1 Applicability of Equivalent Mohr-Coulomb Criterion .....	57
8.2 Input Data for Slope Stability Analyses Based on Equivalent Mohr-Coulomb Criterion .....	58
8.3 The Slope Stability Analyses Results Based on Equivalent Mohr Coulomb Parameters .....	60
<b>CHAPTER NINE - COMPARISON OF THE RESULTS OBTAINED FROM TWO METHODS .....</b>	<b>66</b>
<b>CHAPTER TEN - CONCLUSIONS.....</b>	<b>70</b>
<b>REFERENCES .....</b>	<b>75</b>
<b>APPENDICES .....</b>	<b>81</b>
APPENDIX A - LABORATORY TEST RESULTS .....	82
APPENDIX B - MEASUREMENTS OF WATER TABLE LEVEL .....	82
APPENDIX C - GENERALIZED HOEK-BROWN ANALYSES RESULTS .....	83
APPENDIX D - MOHR-COULOMB ANALYSES RESULTS .....	86
APPENDIX E - MULTIVARIATE ANALYSES RESULTS .....	89
APPENDIX F - PAIRED SAMPLES T TEST RESULTS .....	91

# CHAPTER ONE

## INTRODUCTION

### 1.1 Location of the Study Area

Çine-Akmeden Company carries on its operations on the 33<sup>rd</sup> km of the Aydın-Karpuzlu highway in Çaltı village in Çine, Aydın. The open pits are located in 14 km south from the company building (Figure 1.1). There are 18 albite open pits with deep excavation slopes in this area (Figure 4.1).

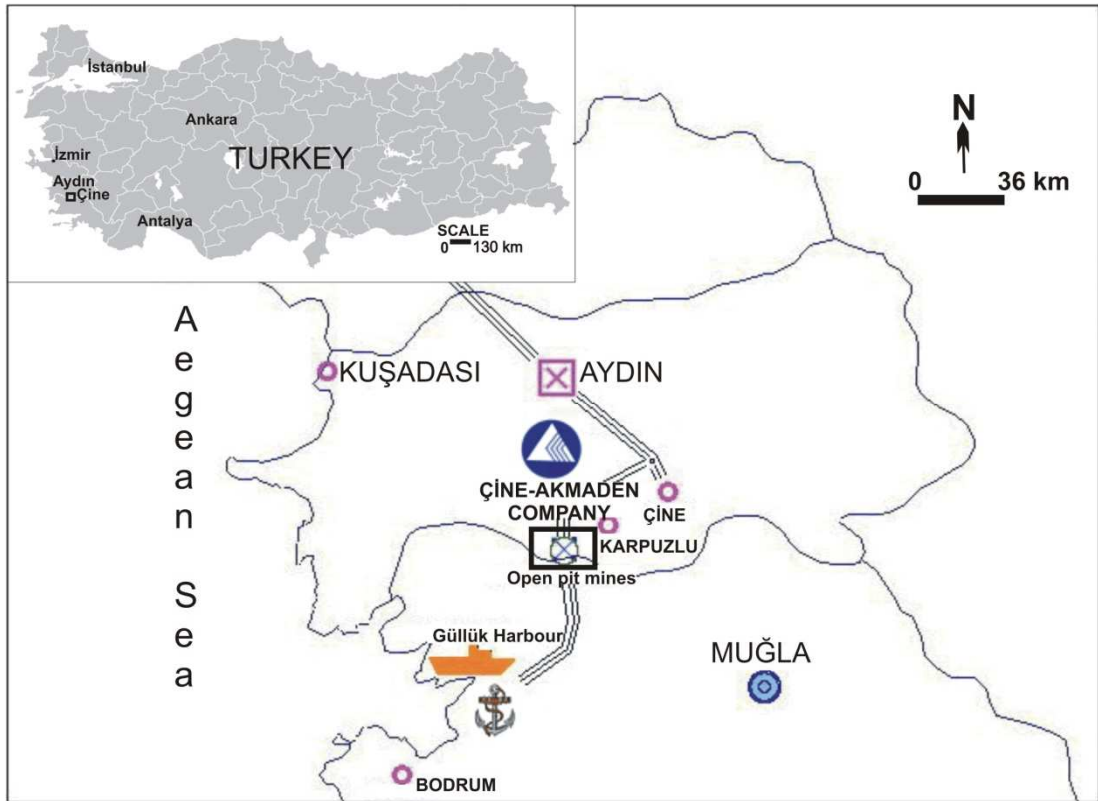


Figure 1.1 Location map of the open pit mines.

## 1.2 Rainfall

Rainfall in the region is mostly confined to the winter and spring months, with the highest average annual rainfall reported on the Çine-Madran mountains. The amount of precipitation values for Çine, Aydın region were derived from the data published on Turkish State Meteorological Service's (DMI) website (Table 1.1).

Table 1.1 Annual average rainfall data for Aydın published on DMI's website

Average Rainfall (mm) (Period: 1970-2009)											
Months											
1	2	3	4	5	6	7	8	9	10	11	12
96	92.2	71.8	54.6	33.1	12.6	4.1	2.5	11.2	43.1	87.4	110.4
Annual Average Rainfall (Period: 1970-2009) : 619 mm											

There is strong evidence of prior slab slides on the benches in the pit. Koca et al. (2009) cites slab slides in the pit and identifies intensive rainfalls (March, 2007) and occurrences of the earthquakes along the Büyük Menderes fault zone in the magnitude range from 3.0 to 5.5 in the past.

## 1.3 The Çine-Akmeden Company

The Çine-Akmeden company consists of crushing-sieving, flotation, granulation and drying units. The floated feldspar in Akmeden is popular for its low amount of  $\text{Fe}_2\text{O}_3$  (0.02 %),  $\text{TiO}_2$  (0.05 %) and high amount of  $\text{Na}_2\text{O}$  (>10.5 %) constituent. Na-feldspar is widely used in glass industry as a source of various compounds. The proven Na-feldspar reserve was determined as a result of drilling and computations as 100.646.548 tons and the annual production is 400.000 tons in Alipaşa open pit. This explicit that the production from the Alipaşa open pit provides a significant amount of raw material to the industry.

## 1.4 Main Scope of The Study

The stability of slope is controlled by many factors as well as by local geological conditions, seismic activities, change in water table level, and, pore pressure. Besides, the causes given by humans are excavation of slope toe, overloading, wrong and deficient slope design, destroying the vegetation, and poor blasting. One of the goals of this study is to determine the main and secondary reasons of slope instabilities in Alipaşa open pit albite (Na-feldspar) mine which is being mined since 1996 in Aydın, Çine-Karpuzlu; furthermore to prewise the potential slope failure and outline the mechanism of progressive failure. This process requires the post failure characteristics of the rock mass. Investigated slopes in the eastern part of the open pit are stable at present, but the main purpose is to estimate the optimum overall slope angle in terms of stability for the final condition of the mine. In other words, right after the mining operations are terminated, the optimum overall slope angle at which the slopes will be stable are to be estimated in this study.

## 1.5 Preliminary Site Investigation of Alipaşa Open Pit Albite Mine

The Alipaşa open pit is dominated by the orthogneisses with schist anclavas which are the most typical lithologies of the core series of Menderes Massif. The orthogneisses in the study area are moderately foliated-fractured rock units at dip angles in the range from 25° to 42°. They have the wide outcrops in both sides of the Alipaşa open pit albite mine. The shear zone with an outcrop width of 50-60 m and alength of 400-450 m in the mine is trending in N25E direction (Figure 1.4). Ore-bearing zone with the mineralogical composition of Na-feldspar was settled

along the shear zone. Length of the albite deposit runs in N25E direction and is approximately 450, m that of width in the direction of N65W is 55 m.

The first engineering geological investigations were performed following the continued instability of the benches and overall slope in eastern part of the mine. There are 18 open pit albite mines in Menderes Massif and 10 of them are still being mined. Only Alipaşa open pit mine which is investigated in this study has shown some slope instabilities in eastern part of this mine in previous years (Figure 1.2). On

the basis of previous failures on benches, it is estimated that the visible tension cracks present on the berms signifies slow movements that already occurred. At present, slope failures only occurs on some benches. It is supposed that the discontinuities in the open pit mine sector which do not daylight on the overall slope face can trigger the slope movements. There is not any clear evidence to show that bench failures trigger overall slope failures. Accordingly, mass movements occurred on the benches may be defined as “local planar slides” (Figure 1.3). Except this kind of failure, a rotational failure starting from the tension cracks on the berms can be expected in overall slope only when the failure conditions are provided. Reversely, in the western part of the mine, as the foliation planes are towards into the slope, slope instabilities have not occurred.



Figure 1.2 Panoramic view of the eastern slope of the Alipaşa open pit mine

Tension cracks were determined behind the slope crest. Their presence is an occasional phenomena on excavated slopes. Barton (1978) found that in jointed rock slopes, tension crack resulted from small shear movements within the rock mass. Although these individual movements were very small, their cumulative effect was that there was a significant displacement of the slope surfaces sufficient to cause separation of vertical joints behind the slope crest and to form tension cracks. The fact that the tension crack is caused by shear movements in the slope is important. When a tension crack becomes visible in the surface of a slope, it is suggested that shear failure has initiated within the rock mass.

The dominant rock type orthogneiss in the albite mine consists of foliation planes and more than one joint sets. Foliation planes were observed as they cut to the slope face and commonly as dipping to NW with a strike in the direction of NE-SW. Engineering properties of discontinuities such as spacing, aperture and persistence,

the previous bench-scale failure traces (cracks) are examined and water seepage points were observed and plotted on the 1/1000 scaled topographic map (Figure 6.5).



Figure 1.3 A shear displacement occurred on the foliation planes in the benches called as local planar slides.

All geological units in the region are deformed by the shear zone. In accordance with this shear zone, shear joints were developed perpendicular to the foliation surfaces. These opened joints are daylighting on the slope face and working like a drainage path.

Since a probable failure is expected to occur on the foliation planes, a detailed field investigation of engineering properties of foliation planes was performed. Accordingly, Geological Strength Index (GSI) value was chosen in a range that the Generalized Hoek-Brown Criterion uses as a base, furthermore the equivalent Mohr-Coulomb parameters were obtained by proposed formulation from the Generalized Hoek-Brown Criterion. Thus, these values only provided prevision about the strength characteristics of the foliation planes.



## 1.6 Safety Factor

Traditional designs have been based upon a factor of safety against sliding. Especially for rock slopes, some discontinuities involve the potential for sliding along well-defined failure surfaces such as foliation surfaces into the gneiss rock masses. The numerical values of the factor of safety chosen for a particular design depends upon the level of confidence which the designer has in the shear strength parameters, ground water pressures, the location of the critical failure surface and the magnitude of the external driving forces acting upon the structure.

If a very low factor of safety is used, there may be a significant probability of failure. On the other hand, in order to minimize this failure probability, sometimes a high value for the factor of safety is used. A comprehensive program of site investigations and uniaxial compressive strength tests have been carried out and the external loads acting on the slope have been defined. In addition, studies of the water table location and pressure distributions into the rock mass have been carried out. Consequently, the ranges of shear strength and driving stress values, which have to be considered in the design, are smaller.

In the design of deep rock slopes there is a tendency to move away from high factors of safety between 1.3 and 1.5 which have been used in the past, provided that care is taken in choosing sensible conservative shear strength parameters, particularly for jointed rock masses.

## 1.7 Slope Stability Analyses

Slope stability analyses were performed firstly kinematically and secondly by numerical modelling based on finite element method (FEM).

In kinematic analyses, two dominant foliation plane orientations on which the failure expected to occur and two release surfaces were used. Whether the potential of plane failure of the overall slope was to occur or not was investigated.

In numerical analyses, two dimensional FEM software Phase<sup>2</sup> was used considering two cases; first one modelled with Mohr-Coulomb Criterion regardless

of joint pattern that uses equivalent Mohr-Coulomb parameters obtained by fitting the Hoek-Brown failure envelope and second one modelled by the material strength of Generalized Hoek-Brown Failure Criterion.

The uniaxial compressive strength tests were performed on rock samples to determine the uniaxial compressive strength of intact rock ( $\sigma_{ci}$ ). Besides, unit weight of the rock was determined by laboratory tests.

To undertake slope stability analysis, five geotechnical cross-sections passing through the affected area from the rock slides and perpendicular to the tension cracks on the berms and to main shear zone present in the study area were taken. The distance between these cross-sections are 50 m. and they are parallel to each other. The cross-sections were named as A-A', B-B', C-C', D-D', E-E' consecutively from NW to SE direction (Figure 1.4). Slope heights belonging to these cross-sections are 135 m, 123 m, 132 m, 121 m, 101 m, respectively. The finite element slope stability analyses were performed for all cross-section lines for the slope angles 30°, 32°, 34°, 36° and 40°. The main goal was to determine the optimum and also economic overall slope angle. The parameters such as GSI, seismic coefficient also vary in each computation, and, the disturbance factor (D), and,  $m_i$  which were chosen from the charts are constant in all models. Degree of water saturation for the slope as an input data was taken 50%, 70% and 100%, respectively.

Finally, the failure mechanism and optimum overall slope angle were determined and the results obtained from two methods were compared to point out the applicability of both methods on the slope stability of jointed rock masses.

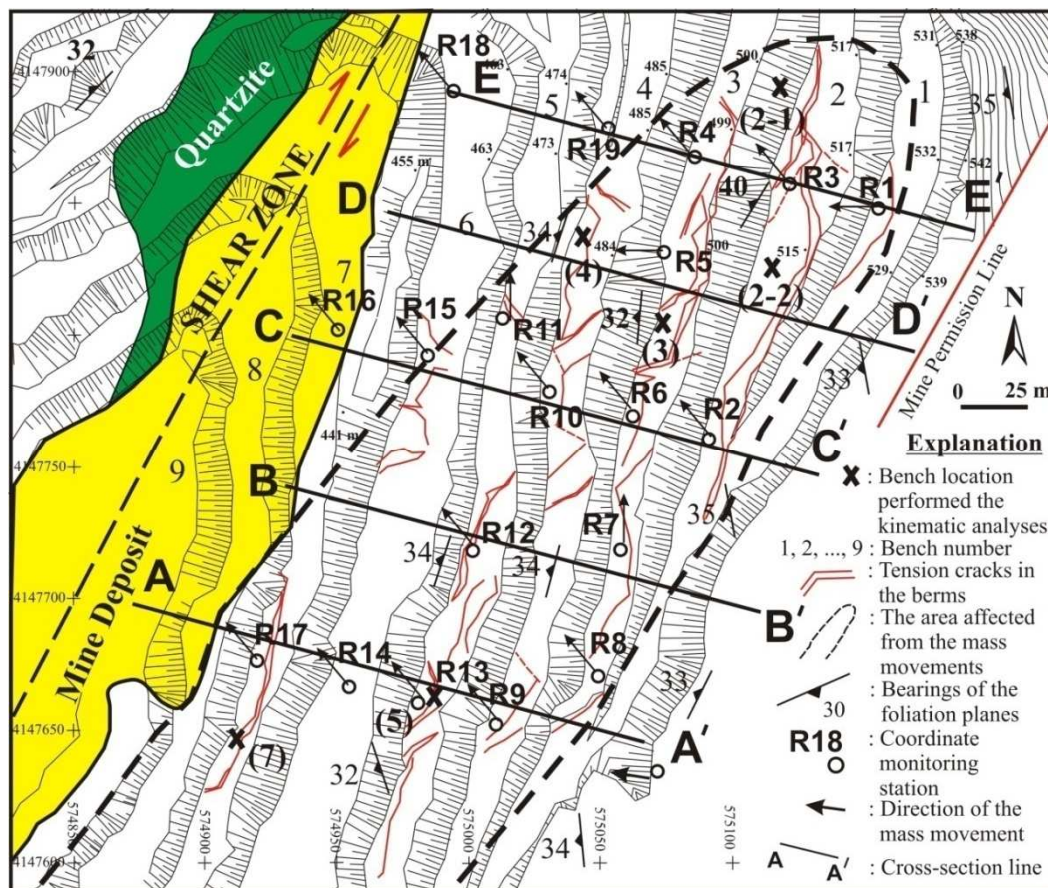


Figure 1.4 Geological and ground fracture trace map of the eastern part of the open pit mine (Koca et al., 2009)

## **CHAPTER TWO**

### **METHODS**

#### **2.1 Numerical Modelling with Finite Element Method (FEM)**

Slope stability analysis has a great importance in safe and economical slope design in excavation, road fill, earth dam, spoil pile and dumping operations. Unlike the other methods, numerical analysis examines deeply the slope movements and the development of the failure zone by considering the distribution of the stresses under or over the failure surface and progressive failure. In this study, to analyse the stability of slopes in the mine, a two dimensional hybrid element model called Phase<sup>2</sup> Finite Element Program (RocScience, 2010) was used. Basically, FEM involves the representation of continuum as an assembly of elements which are connected at discrete points called nodes. The problem domain is divided into discrete elements of various shapes such as triangles and quadrilaterals in two dimension cases. All forces are assumed to be transmitted through the body by the forces that are set up at the nodes. Expressions for these nodal forces, which are essentially equivalent to forces acting between elements, are required to be established. Continuum problem is analyzed in terms of sets of nodal forces and displacements for the problem domain.

The displacement components within the finite elements are expressed in terms of nodal displacements. Derivation of these displacements describes strain in the element. The stiffness of the medium to this induced strain determines stress in the element.

The disadvantage of this method is that considerable time is required in computation of the model especially when simulating the fractures mainly due to the limitation of small element size according to the meshing accompanied with various joint sets. Despite these limitations, the direct inclusion of the geological information into the analysis and geometrical complexities, directional rock properties and various lithological units associated with surface topography, fault zones, igneous intrusions, existing excavations can be readily accommodated in FE approach.

Phase<sup>2</sup> 7.0 is a powerful 2D elasto-plastic finite element slope stability stress analysis program for underground and surface excavations in rock or soil. In this study, all the slopes belong to the Aydın Çine open pit albite mine were modelled by the slope stability analysis software program Phase<sup>2</sup> 7.0 considering the Generalized Hoek-Brown Failure Criterion and Mohr-Coulomb Criterion that uses equivalent Mohr-Coulomb parameters.

6 noded triangles were used to construct the meshes in 2D analysis assuming plane strain conditions (Figure 2.1).

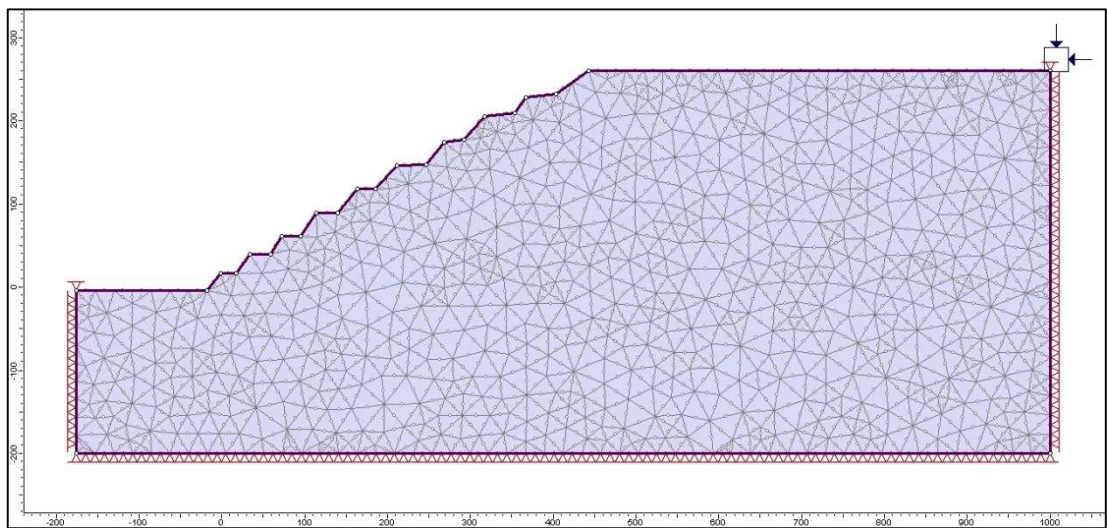


Figure 2.1 FEM mesh (6 noded triangular elements)

Amount of displacement is computed by the forces acting on the nodes of the triangular elements and by the elastic parameters of the material (Young's modulus and Poisson's ratio) as shown in the Figure 2.2 below.



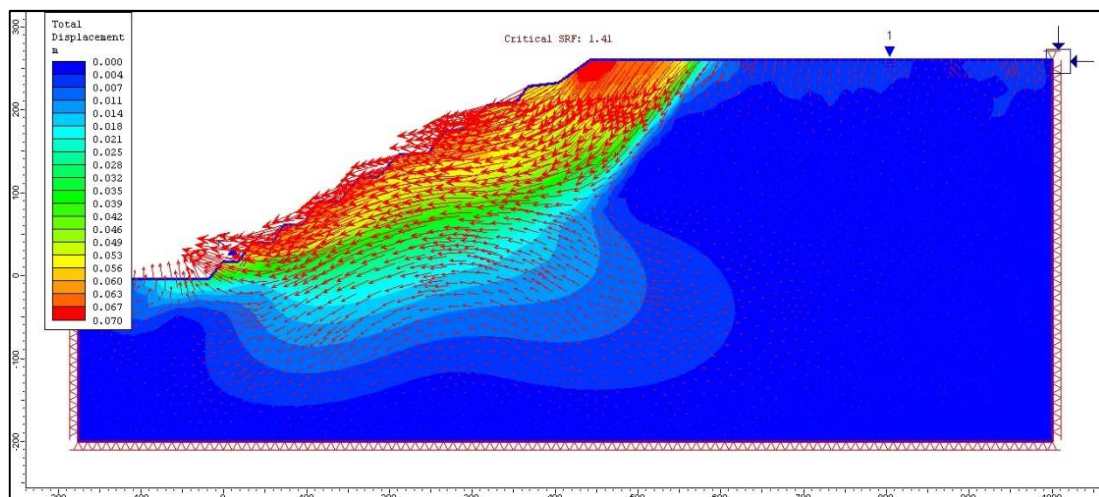


Figure 2.2 Distribution of displacement within the elements

With respect to the achieved displacements, stress and deformation distribution for each element are determined (Figure 2.3). As a result, the surfaces at which the failure starts and continues can be outlined.

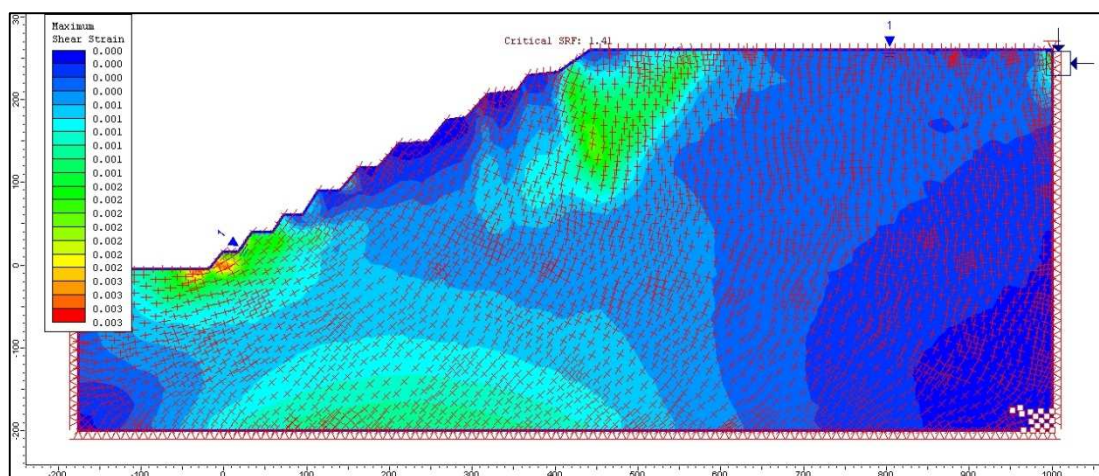


Figure 2.3. The distribution of the tensile and compressive stresses within the rock mass.

## 2.2 The Shear Strength Reduction (SSR) Technique in FEM

The SSR technique for slope stability analysis involves systematic use of finite element analysis to determine a stress reduction factor (SRF) or factor of safety values that brings a slope to the verge of failure. The shear strengths of all the

materials in a FE model of a slope are reduced by the SRF (Hammah et al., 2005). This technique is widely used with the Mohr-Coulomb Criterion and also with Generalized Hoek-Brown Criterion. The basic idea is calculating the factored (reduced by SRF) strength parameters for each criterion.

Numerical techniques have been used for slope stability analysis for some time. The interest in the use of the Shear Strength Reduction technique explained by Dawson et al. (1999) as that it enables the finite element method to calculate factors of safety for slopes. The methodology is summarized by Lorig and Varona (2004). A basic assumption in the SSR finite element technique is that elasto-plastic strength is assumed for slope materials. Simulations are then run for a series of increasing trial factors of safety ( $F_s$ ). Subsequently, actual shear strength properties (cohesion,  $c$  and internal friction angle,  $\Phi$ ) are reduced for each trial accordingly to the following equations;

$$\Phi^{\text{trial}} = \text{arc tangent} \left[ \frac{1}{F_s} \text{ tangent } \Phi \right] \quad (1)$$

$$c^{\text{trial}} = \left[ \frac{1}{F_s} \right] \times c \quad (2)$$

The trial factor of safety is then gradually increased until the slope fails. This is the condition when the factor of safety equals the trial safety factor.

## **CHAPTER THREE**

### **REGIONAL GEOLOGY**

#### **3.1 Stratigraphy**

Menderes Massif is a metamorphic unit which extends along with a strike of NE-SW. It is surrounded with West Taurus (Lycia) Nappes from south and İzmir-Ankara suture zone composed by ophiolitic rock units from north (Dora et al., 1987).

Candan and Dora (1998) states that the Menderes Massif is composed of a Pan-African basement named core and the overlying Lower Paleozoic-Paleocene aged cover series. The core series are primarily composed of clastic sedimentary rocks, asidic volcanic originated leptitic gneiss and migmatites also the metagranite and metagabbro cutting these units. Cover series involve metasediments, at low levels clastics and at high levels carbonates are dominant.

As a result, the general stratigraphic sequence in Menderes Massif as shown in Figure 3.1 starts from Precambrian gneisses and upwards continues with Lower Paleozoic mica-schists, Permo-Carboniferous metaquartzite, black phyllite and dark recrystallized neritic limestones. Paleocene and Lower Eocene is represented by recrystallized pelagic limestones and schist (Okay, 1989).

Okay (1989) defines that the main metamorphism formed the Menderes Massif is the Eocene aged Barrowian type regional metamorphism. This metamorphism is caused by the settlement of Western Taurus (Lycia) Nappes over the Menderes Massif and the effect of related compressional regime.



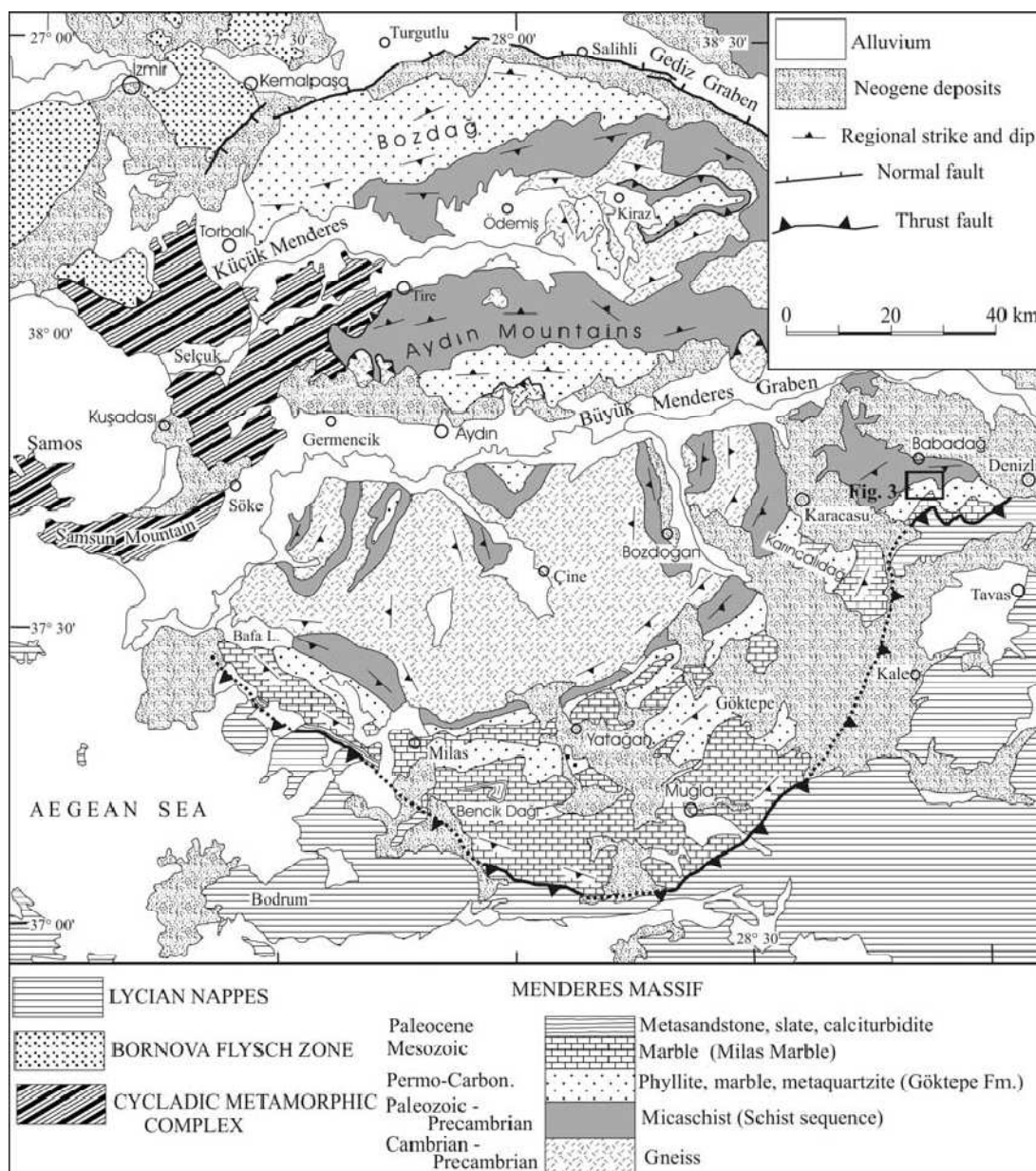


Figure 3.1 Geological map of the Menderes Massif based on the stratigraphic findings (Okay, 2001).

### 3.2 Tectonics

The structural characteristics of the Menderes Massif shows considerable complexity according to the rifting, metamorphism and settling of nappes.

The tectonic and geological events and related occurrence of the structures can be put in order due to Yılmaz (1997). Primarily, metamorphism by regional

compression caused by the collision of Sakarya plate and Anatolid-Torid plate in Paleocene-Eocene that resulted in the burial of the Menderes Massif. In the following time period, the compression continued and after the crust was thickened, the granitic magma was settled. Following this, the core complex was developed and the dom structures were formed. It is supposed that the occurrence of the dom structures lead to the graben development finally after the thermal depression in Early-Middle Miocene.

The recent researches show that the rotational movement of the Anatolian-Aegean plate is caused firstly by the collision of the Arabian and Eurasian plate in the east leading the movement towards west and secondly by the weight of the plunging oceanic crust leading the regression of the arc to south and relating tensional stress in the direction of NNE-SSW. According to this extensional tectonism, several grabens were formed in the direction of E-W and NW-SE (Şengör, 1982, 1987). These are Gökova, Büyük Menderes, Küçük Menderes, Gediz, Bakırçay and Simav rifts, Kütahya and Eskişehir grabens. Besides, the strike-slip faults with normal component in the direction of the normal of the NE-SW lines have an important role in the tectonic characteristics of this region. These strike-slip faults with normal component are Fethiye-Burdur fault zone and Bergama fault. Normal faults in the direction of NW-SE are generally located in the southwest Anatolia. In the middle of the West Anatolia, mainly the normal faults in the direction of E-W such as Gediz and Büyük Menderes faults are present (Figure 3.2). The Simav, Kütahya and Eskişehir faults also shows the similar characteristics which are located in northern part of the normal faults in the E-W direction. There are NE-SW oriented basins among the normal faults trending in E-W and NW-SE direction.

As a summary, the major tectonic features of Menderes Massif are E-W trending grabens due to the NNE-SSW trending extensional regime and NE-SW trending strike slip faults. Several NW-SE trending active normal faults cut across these E-W and NE-SW trending major structures.

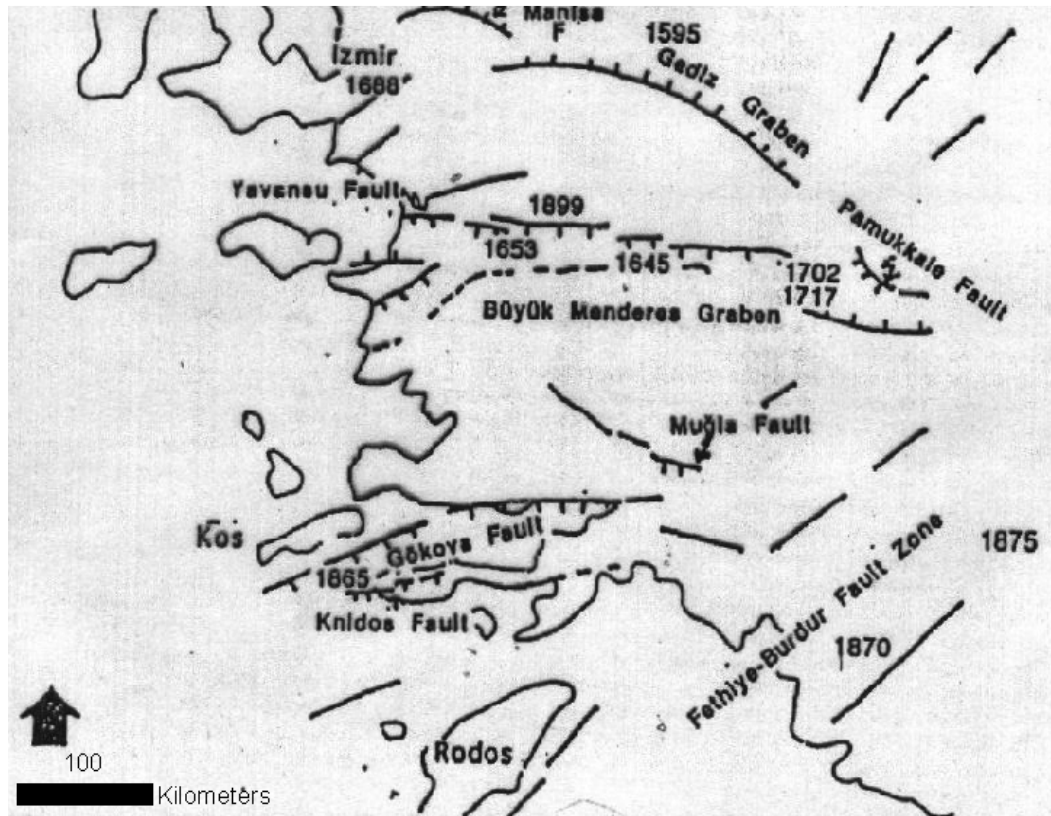


Figure 3.2 The active fault map of southwest Anatolia and the distribution of earthquakes occurred since 16<sup>th</sup> century (Barka & Reilinger, 1997; Ambraseys & Finkel, 1995).

### 3.2.1 *Büyük Menderes Graben*

Büyük Menderes graben is located between Denizli and the Aegean sea within the boundaries of Menderes Massif and is a plain approximately 200 km long. It represents similar lithologic characteristics as the Menderes Massif. The main fault runs along the northern border of the graben and dips to south.

NW-SE oriented basins are present in the southern part of the graben and it is proved that the faults along this strike are active with regard to the recent earthquakes (Price & Scott, 1994).

## **CHAPTER FOUR**

### **GEOLOGY OF THE STUDY AREA**

#### **4.1 Çine Submassif**

The southern part of the Menderes graben in the Menderes Massif was defined as Çine submassif. It is represented by coarse grained augen gneisses and fine grained mica-rich gneisses. Occasionally, augen gneisses are found to be involving K-feldspar and display morphologic and petrographic characteristics as granite, accordingly they are described as metagranites.

Bozkurt et al. (1993) determined approximately ten intrusive or dom structure in Çine submassif by the help of satellite images.

The albite bearing zone is extensively located in the southern part of the Çine submassif which settled along the NNE trending main tectonic zones from west to east; Bafa, Çomakdağ, Karadere, Olukbaşı, Çallı, Gökbel, Hisarardı, Karpuzlu, Topçarn, Güre, respectively.

It is supposed by Uygun and Gümüşçü (2000) that the aplites and pegmatites present in the Pan African aged granitic core complex in Çine submassif were formed to albitite due to anatexis, rejuvenation and metasomatism processes related to the main metamorphic event during the Alpine deformation.

The northern part of the Menderes Massif doesn't provide appropriate circumstances for albite formation as in the southern part. Uygun and Gümüşçü (2000) identify the case with either the primary alkaline character of orthogneisses in Çine submassif or late alkaline-metasomatism related to the alpine rejuvenation of the core rocks in south.

#### **4.2 Mineral Composition of Ore-Bearing Zone**

The orthogneisses which were derived from the granitic precursor rock can be divided into two types based on their mineralogical composition: "Biotite-rich orthogneisses" and "tourmaline-rich leucocratic orthogneisses" (Graciansky, 1965; Candan et al., 2006). However, in the study area, only the tourmaline-rich leucocratic

orthogneisses are exposed (Figure 4.1). Two types of the tourmaline-rich leucocratic orthogneisses have been recognized in the study area. First group consists of the orthogneisses which were derived from coarse grain granites with granoblastic texture. The mineral composition of these rocks is orthoclase (10 - 38%), plagioclase (14 - 27%), quartz (24 - 41%), muscovite (2 - 27%), tourmaline (2 - 16%), garnet (1-3%) and biotite (1 - 2%), zircon (trace), apatite (trace), rutile (trace) as accessory phases. The foliation planes of these rocks are defined by the parallel alignment of the muscovites. The second type is composed of medium grained, albite-rich leucocratic orthogneisses. The mineralogical composition of these leucocratic veins is albite (44 - 47%), orthoclase (1 - 5%), quartz (41 - 55%), rutile / sphene (1 - 7%). They have a medium grained ( $d < 0.4$  mm) granoblastic texture.

### **4.3 Occurrence of Albite Deposits**

The albite formation situated along shear planes or transverse fracture systems almost perpendicular to the main regional tectonic line, even the ones that along the S type folds on the margins of the main shear zones have an intrusive character and show a pronounced trending in NE - SW direction controlled by the old ductile shear zones (Uygun & Gümüşçü, 2000). Similarly, the ore-bearing zone with the mineralogical composition of Na-feldspar was developed along the shear zone in the study area. All of the geological units in the open pit albite mine were deformed by this shear zone trending in N25E direction (Figure 4.1).

According to the literature view, albite deposits are present only in core series as vein-type elongated masses with an outcrop width of 0.1- 0.7 km and nearly a length of 10 km (Figure 4.1).

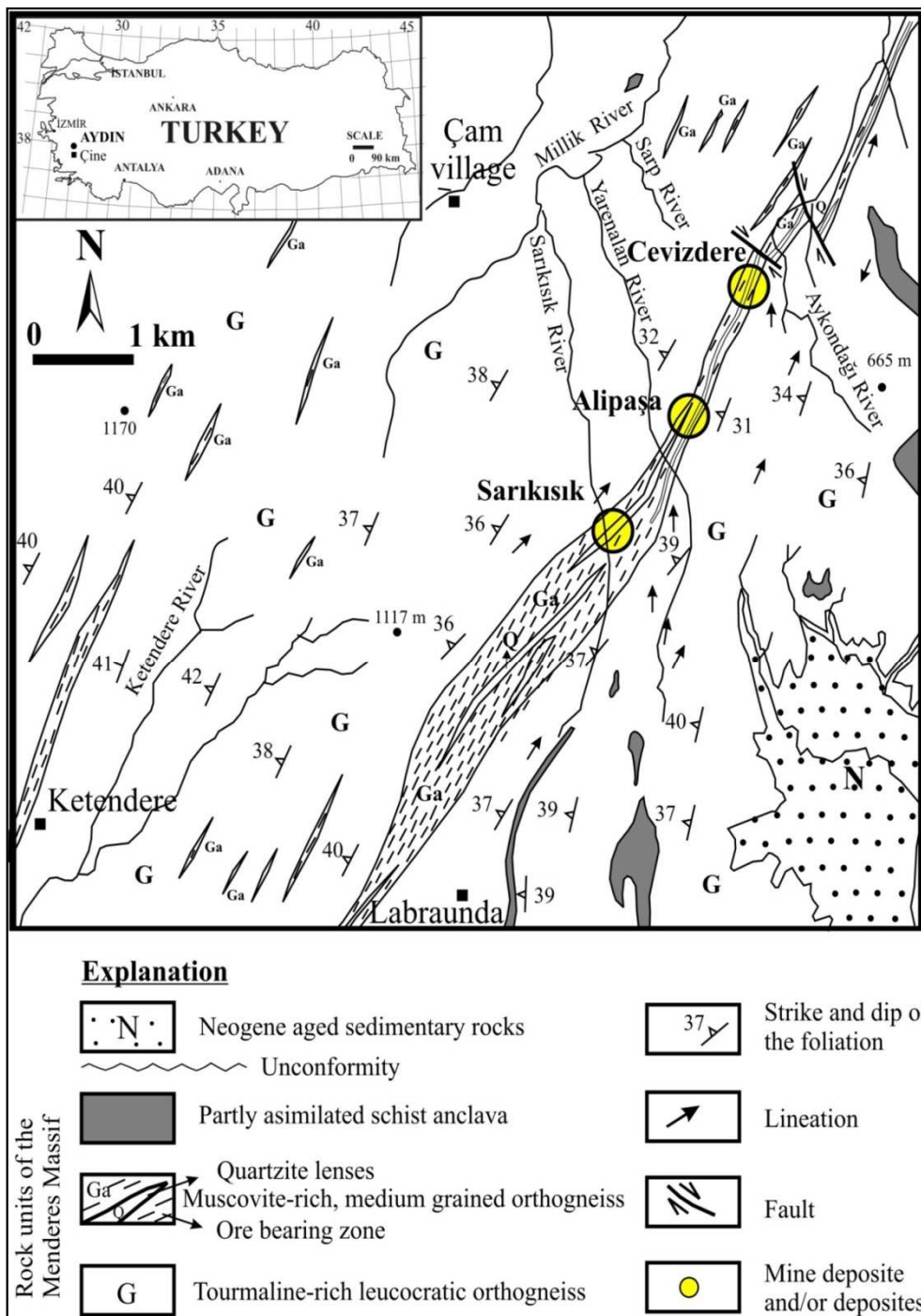


Figure 4.1 Location and geology map of the study area (Modified from Graciansky, 1965).

## **CHAPTER FIVE**

### **SEISMICITY**

Seismic activities are a major trigger for natural and man-made slope instabilities. Earthquake-induced slope failures are common phenomena. Accordingly, seismic effect is considered in the slope stability analysis of Alipaşa open pit mine since Aydın is a seismically active region located in the first-degree seismic zone.

The effect of earthquakes on the slope instabilities was evaluated using the historical seismicity within the vicinity of the open pit mine. In consequence, the recurrence rate and the extent of occurrence area of the previous earthquakes were investigated.

In the 17<sup>th</sup> and 18<sup>th</sup> centuries (1645, 1654, 1702), earthquakes correspond to the intensity of IX have occurred along the zone of the Menderes graben from Denizli to Aydın. Furthermore, an earthquake with a magnitude of 6.9 occurred on the 20<sup>th</sup> of September 1899 (Figure 5.1). Officially 1.100 fatalities were recorded for this earthquake (National Earthquake Information Center) and it led to form 1 to 2 m fault scarps (Altunel, 1998). The more recent intensive earthquake caused by a right handed strike slip movement in NE-SW direction with a magnitude of 6.8 occurred on 16<sup>th</sup> July 1955 on the west point of the graben (Altunel, 1999).

Pseudo-static analyses are widely used together with the slope stability analysis methods. It is based on modelling the earthquake as it acts on the center of the potential sliding mass like a static force represented by a constant horizontal ground-motion parameter named as seismic coefficient. In general, the seismic coefficients are determined by using the maximum horizontal acceleration.

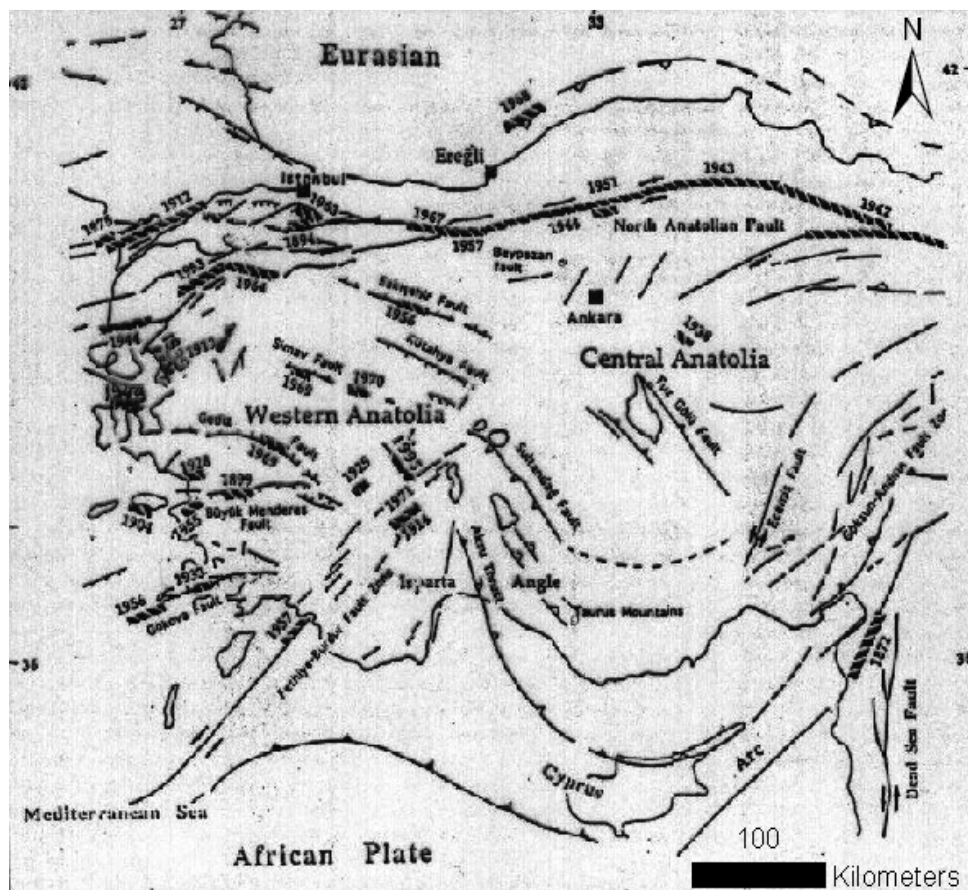


Figure 5.1 The distribution of earthquakes in terms of fault zones in west Anatolia in this century (Barka & Reilinger, 1997).

The researchers assumed that a possible future earthquake in the vicinity of Çine may occur along the Büyük Menderes fault with an extent of 110 km EW direction. The expected magnitude of the possible earthquakes along the fault zone was determined to be 5.5-6. The epicenters of such earthquakes can be located at any point within the active fault zone. Furthermore, the recurrence rate of the earthquakes in Aydın defined by an equation in terms of the relationship between magnitude and the frequency by Equation 3 ([www.jeofizik.comu.edu.tr](http://www.jeofizik.comu.edu.tr)).

$$\log N = 5.33 - 0.81M \quad (3)$$

where  $N$  is the frequency of earthquakes in a year and  $M$  is the magnitude of the earthquake. According to that correlation, the frequency for the earthquakes with a magnitude of 5.5 and 6.0 defined to be 2.39 and 1.59 years, respectively. These results implies that the recurrence of large earthquakes are frequent.



The values of maximum ground acceleration which would be generated by the Büyük Menderes graben fault computed by using the empirical attenuation formula proposed by Fukushima & Tanaka (1990) is presented in Table 5.1.

$$\log_{10} a = 0.42 M_w - \log(R + 0.025 \times 10^{0.42M_w}) - 0.0033R + 1.22 \quad (4)$$

a: Mean of the horizontal peak ground acceleration (cm/sec<sup>2</sup>)

M<sub>w</sub>: Moment magnitude

R: Shortest distance between site and fault rupture (km)

Table 5.1 The seismic acceleration values calculated by the the empirical attenuation formula proposed by Fukushima & Tanaka (1990) for various earthquake moment magnitudes.

Description	Values				
M <sub>w</sub>	5.5	5.8	6.0	6.5	7.0
R (km)	26.5	26.5	26.5	26.5	26.5
a (cm/sec <sup>2</sup> )	103	112	130	182	245
α <sub>s</sub> (g)	0.10	0.11	0.13	0.18	0.25

The seismic coefficient of 0.25g is defined as “violent” by Terzaghi (1950). Seed (1979) recommends to use seismic coefficient as 0.1 and 0.15 for the earthquakes of Richter’s magnitude 6.5 and 8.5, respectively in conjunction with the factor of safety as greater and/or equal to 1.15 in the absence of a excessive loss of strength during earthquake. On the other hand, Hynes-Griffin & Franklin (1984) suggest using seismic coefficient one-half of the peak ground acceleration for the preliminary assessment of slope stability in the case that factor of safety of the slope is obtained greater than 1, otherwise the analyses should be conducted particularly.

Although Table 5.1 proposes maximum seismic coefficient as 0.25g for the possible magnitude of the earthquake; in order not to obtain excessively conservative results and to investigate the earthquake effects on the rock slope stability extensively, seismic coefficient were taken into account in the analyses as 0g, 0.1g,

0.2g and 0.3g. The peak acceleration acts only momentarily in one direction in the analyses.

Furthermore, the calculated horizontal seismic coefficients were involved in the analyses as the seismic waves are coming from backward to the slope in a state of reducing the stability. Reversely, if the seismic waves were supposed to be coming from forward to the slope face, this would increase the stability of the slope by increasing the resisting forces. Accordingly, the SRF values would be expected to be greater safer. It should be noted that an engineering design firstly must be safe, economical and applicable.

## **CHAPTER SIX**

### **ENGINEERING GEOLOGY**

#### **6.1 Quantitative Description of Discontinuities in Rock Masses**

Rock mass description is only be useful for engineering designs and minimizes the expenses for in-situ testing when the field observation and also complete and unified description is done thoroughly.

The design of a rock slope requires adequate information on the mechanical properties of the discontinuities within the rock mass, since its stability depends on the nature of the discontinuities (Hoek & Bray, 1981).

Especially in low stress environments such as near surface excavations, engineering properties of discontinuities effect the strength and deformation characteristics of rock masses rather than the intact rock properties.

Engineering and geological properties of the rock mass and material exposed in the study area were determined on the basis of field observations and measurements and laboratory tests.

The rock mass characteristics investigated in this chapter was used in numerical analyses indirectly as a helpful parameter to determine Geological Strength Index (GSI),  $m_i$  (Hoek-Brown constant for rock material) and disturbance factor (D) which shows the signs of blasting damage on discontinuities (Table 6.1).

Table 6.1 Discontinuity properties obtained from the scan-lines

Mass Properties	Foliations	Joint sets		
	(F <sub>1</sub> , F <sub>2</sub> and F <sub>3</sub> )	(J <sub>1</sub> ) and (J <sub>4</sub> )	(J <sub>2</sub> )	(J <sub>3</sub> )
General attitudes of the discontinuities	F <sub>1</sub> : 300/32-40 F <sub>2</sub> : 273/32-40 F <sub>3</sub> : 243/32-40	325-340/80-87 290-320/80-90	190/70-85	250/80-90
Spacing (cm)	Minimum: 5 Maximum: 25 Mean:20 SD: 10 (Moderate spacing)	Minimum: 20 Maximum: 55 Mean:35 SD: 11 (Wide spacing)	Minimum: 15 Maximum:25 Mean:18 SD: 07 (Moderate spacing)	Minimum: 62 Maximum: 78 Mean:72 SD: 2.6 (Very wide spacing)
Persistence	4 m -12 m (Generally high persistence)	1.0 m – 4.5 m (Generally low persistence)	1.0 m – 2.0 m (Low persistence)	3.0 m – 8.5 m (Medium persistence)
Aperture	1 mm – 0.5 cm (Moderately wide gapped)	0.5 – 2.0 cm (Generally opened joints)	1 mm–1.0 cm (Moderately wide gapped)	0.5 cm – 3 cm (Very widely opened )
Roughness	Generally smooth and undulating (large wave length- little amplitude)			
Filling	Soft, damp filling			
Seepage	Minor seepage, specify dripping discontinuities			
Block size	Generally medium block size			
Weathering	Generally moderately weathered			

### 6.1.1 Type of Discontinuity

Discontinuities in the field vary from small scale fissures to huge faults. The type of a discontinuity indicates the past tectonic events and the formation of rock masses.

In the study area three different discontinuity types were defined for orthogneisses; these are tectonic originated joints and foliation planes related with metamorphism and tension cracks present on the berms due to small shear movements within the rock mass.

Tension cracks on the berms reached the length of 2-10 m and the widths of 1.0-5.0 cm in a few years with insignificant depth and are filled artificially with a impermeable material.

Their locations were derived from maximum tensile stresses in the mine which determined with an electronic distance-measuring instrument coupled with on precision theodolite. Bench number, the locations of survey monuments, directions and amount of the sliding movements occurred on these locations as well as bearings of the tension cracks were also recorded on the 1/500 scale topographical map of the study area (Figure 1.4).

Since the failure is expected to occur on the foliation planes, the description of foliation planes becomes important.

### ***6.1.2 Orientation of Discontinuities***

The orientation of discontinuities largely controls the possible instable conditions of the slope. Number of joint sets in conjunction with their orientations also determines the block shape of the rock mass which defines the mode of potential failure in open pit mine slopes and efficiency of mining the ore.

Discontinuity survey was performed in the eastern part of the open pit. In order to determine the pole concentrations of discontinuity sets, contour diagram was prepared. Accordingly, five tectonic joint sets and three differently oriented foliation planes were determined on the contour diagram (Figure 6.1). Besides,  $J_1$  and  $J_4$  joint sets are related to the same discontinuity set as like as the  $J_3$  and  $J_5$  joint sets. Discontinuity sets are classified in respect to their attitudes as in Table 6.2.

Table 6.2 Orientation of foliation planes and joint sets within the orthogneiss rock mass

Foliation planes		Joint sets	
F <sub>1</sub>	300/42	J <sub>1</sub>	332/88
F <sub>2</sub>	273/40	J <sub>2</sub>	190/85
F <sub>3</sub>	243/40	J <sub>3</sub>	250/88
		J <sub>4</sub>	312/89 and/or 130/89
		J <sub>5</sub>	221/84 and/or 41/84

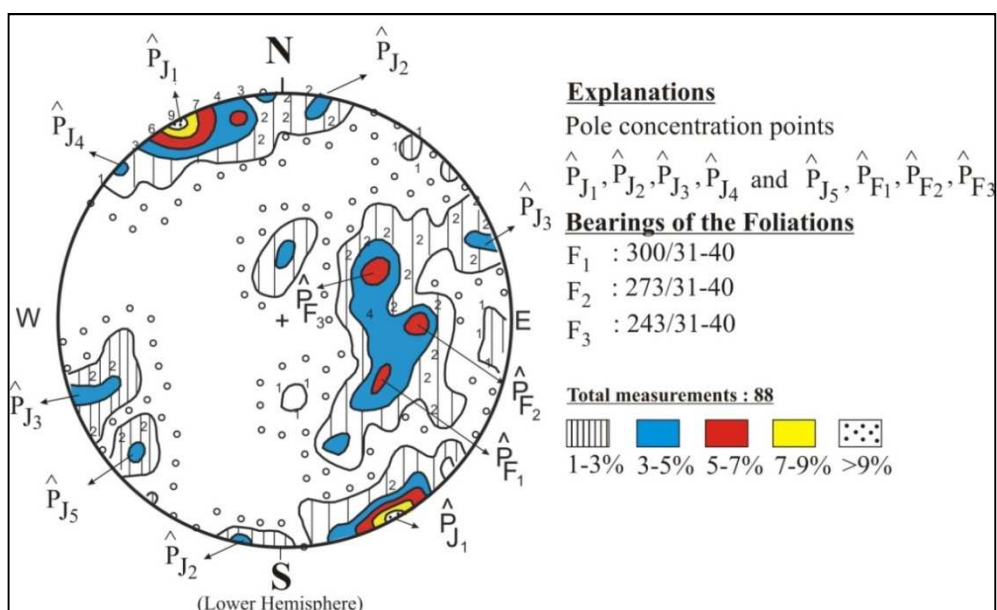


Figure 6.1 Schmidt contour diagram representing the orientation of joints plotted on a polar equal-area net.

### 6.1.3 Spacing of Discontinuities

Spacing is the shortest vertical distance between the discontinuities and it is determined by measuring this distance in a selected scan line.

As in the case of orientation, the importance of spacing increases when the other conditions for deformation are present, i.e. low shear strength and a sufficient number of discontinuities or joint sets for slips to occur (International Society for Rock Mechanics (ISRM), 1978a).

The distribution of spacing of joint sets and foliation planes varies between 5 cm to 78 cm. In respect to the mean spacing values, foliation planes are moderately spaced as like as joint set-2 ( $J_2$ ); joint set-4 ( $J_4$ ) together with joint set-1 ( $J_1$ ) are widely spaced and joint set-3 ( $J_3$ ) is very widely spaced according to the classification method suggested by ISRM, 1978a.

#### ***6.1.4 Persistence of Discontinuities***

Persistence signifies the length of traces of discontinuities within a plane on the outcrop. It can also be called as the continuity of a discontinuity. Determination of persistence of discontinuity sets is significant especially when the discontinuity set provides a failure surface for the rock mass. However, the real persistence determination is almost impossible but careful approaches can be useful.

The persistence measurements in the field were conducted in the direction of the related discontinuity set's dip. The discontinuities in the study area are commonly persistent and sub-persistent. In respect to the field measurements, foliation planes are dominantly high persistent to medium persistent, joint set-1 ( $J_1$ ) together with joint set-4 ( $J_4$ ) are low persistent to medium persistent, joint set-2 ( $J_2$ ) is low persistent and joint set-3 ( $J_3$ ) is medium persistent according to the classification method suggested by ISRM, 1978a.

#### ***6.1.5 Roughness of a Discontinuity Surface***

Roughness characterizes the condition of the discontinuity surface. On the other hand, waviness refers to larger scale undulations and is more resistant to deformation since it is too large to be sheared off.

The discontinuity surfaces in orthogneiss get involved in smooth, undulating (V) category in descriptive terms for small scale (several centimetres) observation according to ISRM, 1978a. The evidence of previous shear displacements were determined on several foliation planes, these were classified as slickensided, undulating (VI) category (Figure 6.2).



Figure 6.2 The view of slickensided and undulating foliation plane.

Beside the direct shear tests roughness profiles may provide an estimation of peak strength. In addition, according to typical roughness profiles for JRC range chart (ISRM 1978a), joint roughness coefficient (JRC) was defined in the range of 8 to 10. But at the same time, this classification is quite subjective.

The roughness of the discontinuity planes in the study area can be defined by large wavelength and little amplitude.

#### ***6.1.6 Discontinuity Wall Strength***

The compressive strength of the discontinuity wall (JCS) is an important parameter mainly if the walls are in contact with each other, in other words if the joints are infilled so that not controlled by the strength of the filling material.

The primary description of the rock mass must include the weathering grade. According to the weathering grade classification chart proposed after BS 5930 (1981), the rock mass is moderately weathered considering the distribution ratios of weathering grades in the orthogneiss rock mass, substantially as a result of the water



effect on the orthogneisses, rock mass weathered to high grade at some elevations. Afterwards a manual index test (ISRM, 1978a) was performed on the discontinuity wall reversely in the case of a filled discontinuity that the filling material influence the discontinuity strength, this test should be performed on the filling material in order to find the approximate range of uniaxial compressive strength. Consequently, according to the manual index test, foliation planes are medium strong rock (R2, 5.0-25 MPa) and moderately weathered and slightly discoloured as like as the joint surfaces, additional discolouration of joint surfaces are common.

### ***6.1.7 Discontinuity Aperture***

Aperture indicates the perpendicular distance between adjacent rock walls of an open discontinuity. Aperture is filled with secondary minerals, air or water.

Below the zone of weathering, all discontinuities of the fracture type are usually tight due to the state of stress in the rock mass including confining pressure (Beavis, 1985). The aperture on the exposure will be greater due to the disturbance on apertures by blasting and excavation modes or surface weathering effects.

The distribution of aperture of joint sets and foliation planes varies between 1 mm to 3 cm. In respect to the mean aperture values, foliation planes are moderately wide gapped as like as joint set-2 ( $J_2$ ), joint set-1 ( $J_1$ ) together with joint set-4 ( $J_4$ ) are wide gapped to opened and joint set-3 ( $J_3$ ) is very widely opened according to the classification method suggested by ISRM, 1978a.

### ***6.1.8 Filling of Discontinuity Apertures***

Filling is only determined on the 1-5 mm gapped foliation planes with a soft characteristic. The filling materials are at some point decomposed and at the other disintegrated. In this study, filling material was supposed to be a non-reducing factor for material strength; accordingly, only the wall strength regardless of the weathering grade was assumed in numerical analyses. As a determination of water content and permeability of the filled discontinuity, “The filling materials are damp but no free

water is present” description belongs to the W2 grade according to the chart proposed by Barton (1978).

### ***6.1.9 Seepage Through Discontinuity Planes***

The presence of water in a rock slope has a significant effect on stability since water accelerates weathering of rock, increases the weight of rock mass, its pressure reduces the shear strength of a potential sliding surfaces.

In fractured rocks, water flow occurs predominantly along discontinuities as they give the rock mass a secondary permeability.

The prediction of ground water level and likely seepage paths are major studies in an engineering problem. The filling materials were examined due to its seepage rating (W2) in terms of ISRM (1978a).

All the detailed ground water observations were discussed in this chapter under the title “Water Table Condition”.

### ***6.1.10 Block Size and Shape***

Block size/shape depends on the spacing, persistence of discontinuity sets and also the number of these sets.

Block size has an influence on slope stability as well as it designates the efficiency of the mining material in conjunction with the usage area of the ore.

Volumetric joint count ( $J_v$ ) is a way to define the block size of the rock mass. It is explained in Equation 5 or 6 as the sum of the number of joints per meter for each joint set present (Ulusay & Sönmez, 2007).

$$J_v = D_h (1/S) \quad (5)$$

$$J_v = 1/S_x + 1/S_y + 1/S_z + \dots \text{ (joint number/m}^3\text{)} \quad (6)$$

Where “ $D_h$ ” is the number of joint sets, “ $S$ ” is discontinuity spacing.

The orthogneiss is blocky as preferred in mining and due to the volumetric joint count calculation in a scan line approximately 10 m length indicates the medium block size according to the classification (Bell, 2007). Besides, the distribution of block size varies between small to medium block size in the eastern part of the open pit.

## 6.2 Rock Mass Strength

As a result of the water effect on the orthogneisses placed between the elevations of 500 m and 530 m, the rock mass weather to highly weathered rock mass (Figure 6.3). Engineering properties of the orthogneisses were fairly affected from the rock weathering. In addition, the orthogneisses placed between the elevations of 500 m and 530 m have frequently jointed rock mass property due to the stress relaxation.



Figure 6.3 A view of seepage point into the crack opened by rock movement and planar foliations in the orthogneiss rock mass.

### 6.3 In-situ Tests

#### 6.3.1 Tilt Tests

Tilt tests are performed on discontinuities which provide a failure plane within the rock mass in order to determine the surface friction of these discontinuities (Koca & Kınca, 2004). It is based on slipping the two discontinuity planes on each other as applying shear forces. As a result of tilt tests, the friction angle of the undulated discontinuity planes is approximately  $36^{\circ} \pm 2.11$  (Table 6.3).

Table 6.3 Tilt test results for the discontinuities in eastern part of the Alipaşa open pit mine

Test Number	Description of Discontinuity Plane	Mean Test Result
10	Slightly weathered, very thin filled and slightly undulated foliation planes	$36^{\circ} \pm 2.11$

The mean friction angle value obtained from tilt tests was used as a base in kinematical analyses.

### 6.4 Laboratory Tests

#### 6.4.1 Unit Weight Determination

Unit weight of orthogneiss was determined in traditional way with digital precision balance and compass by measuring the weight and volume of the core samples. The mean unit weight value with standard deviation obtained was shown in Table 6.4.

#### 6.4.2 Uniaxial Compressive Strength Test

The principle of uniaxial compressive strength test is that the specimens are loaded axially up to failure or any other prescribed level whereby the specimen is

deformed. As a result, the applied load at which the rock material starts deforming provides the ultimate uniaxial strength of it. This test was performed according to ISRM, 1978 b on core samples with diameter of 54 mm ( $N \times$  core diameter) and length to diameter ratio as 2 ( $L=2D$ ). Loading rates on the rock specimens were set as 0.5-1.0 MPa/sec.

The mean uniaxial compressive strength and unit weight values of orthogneiss rock material were used as a base in numerical analyses and were shown in Table 6.4. Besides, the uniaxial compressive strength test results were shown in Appendix A, collectively.

Table 6.4 The physico-mechanical properties of the orthogneisses required in numerical analyses

Some physico-mechanical properties of the orthogneisses (n: test number)		Test results
$\gamma_n$ (kN/m <sup>3</sup> )	n: 18	25.9±0.01
$\sigma_{ci}$ (MPa)	n: 12	27.34±5.30

The uniaxial compressive strength test results for the rock material found to be 27.34 MPa and classified as moderately strong rock without considering anisotropy effect according to Anon (1977). This classification fits the ones obtained from charts (ISRM, 1978a) based on field observations.

## 6.5 Kinematic Analysis Of The Eastern Slope of Alipaşa Open Pit Mine

In engineering geology, permanent stable slopes are important criteria for safety and cost. Kinematical analyses are helpful only in determining possible kinematic type of failure such as planar, wedge and toppling. They do not consider forces acting on a slope forming material (height of slope and important geotechnical parameters such as cohesion of discontinuities and unit weight). Furthermore, kinematical analysis sometimes does not work for rock having close-very close spacing and low persistent joints and if rotational failure is expected.

On the stereonets, type of the failure can be identified together with the direction of the slide. Although kinematic analyses provide prevision for the stability condition of a slope, water and earthquake or other triggering effects for slope instabilities are not taken into account. For the kinematical analyses, the lower hemispheres

stereographical projection method described by Hoek and Bray (1981) and Goodman (1989) was used. Plane failure possibility along the two sets of foliation planes ( $F_1$  and  $F_2$ ) for each slope angle ( $30^\circ$ ,  $32^\circ$ ,  $34^\circ$ ,  $36^\circ$ ,  $40^\circ$ ) was kinematically investigated by utilizing a program generated by real person thus the program is not commercially available. The projections for each slope angle are presented in Figure 6.4.

According to the pole concentrations of all sets of foliation planes,  $F_3$  (243/40) set was not taken into account in kinematic analyses due to its difference from the dip direction of slope face bigger than  $20^\circ$ . The dip direction of the discontinuities influence the stability as well as the dip angle of the discontinuities. The dip angle of the discontinuity plane should be less than the ones of slope; in other words discontinuity plane should be daylighted on the slope face to lead to a planar failure. If only the slope angle is taken as less than  $40^\circ$ , the stable conditions are provided. The overall slope reaches the critical balance if the dip angles of discontinuities are steeper ( $40^\circ$  -  $42^\circ$ ) than the slope face.

The daylight envelope which represents planar sliding area within the  $\pm 20^\circ$  boundary was generated by plotting the poles of the slope face with rotating the great circle of the slope on various slope angles and related strikes. Whether the pole points of discontinuities are located within this daylight up to the boundary of friction cone or not was investigated. As a result, the dip angle of the foliation planes are higher than the dip angle of the slope, thus not providing failure. Although the angles between the pole point of overall slope and the pole points of the foliation planes are less than  $20^\circ$  since the pole points of the foliation planes are not located in the daylight envelope, it is not possible that deep failures along the foliation planes are taken place in the eastern part of the mine if only the slope angle is less than  $40^\circ$ .

One should note that kinematic analysis can only be used for preliminary design of non-critical slopes since it neglects the physical properties of discontinuities and the external forces that influence stability.

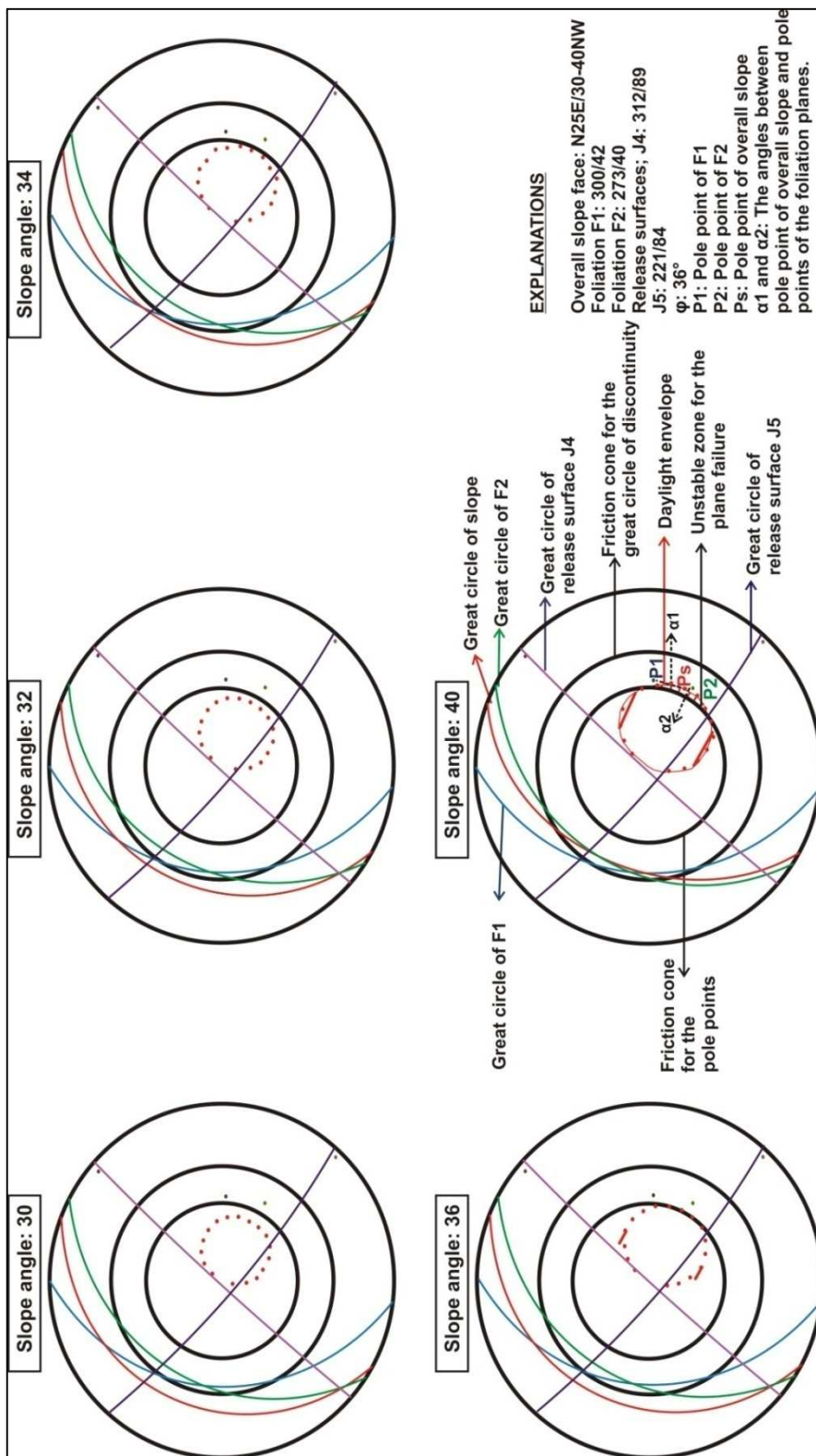


Figure 6.4 Kinematic analyses of the overall slope of the eastern part of the open pit considering various slope angles.

## 6.6 Water Table Condition

Tension cracks present on the berms can be filled with water after a heavy rainstorm unless effective surface drainage has been provided. On the basis of previous failures on benches, it is estimated that the visible tension cracks signifies slow movements that already occurred therefore the filling of tension cracks with water means reducing rock strength due to increasing water pressure.

Water flow is a common indicator for slope instabilities in the mine. In jointed rock masses as such, it is expected that the water pressure in the discontinuities will build up and disperse more rapidly than those in the pores of the intact rock blocks. Especially in winter, as the amount of rainfall increases, water seeps towards the base of the mine increases. In January, after the heavy rainstorms, the seepage points observed in the field were plotted on the map (Figure 6.5).

In rock slopes, discontinuities give the rock mass secondary permeability that provide important channels for water flow within the rock mass. Although the permeability of the rock material is low, when the rock mass is considered together with the discontinuities, secondary permeability becomes significant. The orientation, frequency and openness of discontinuities acts on the secondary permeability of the rock mass. The most dangerous conditions which would develop in this case would be those given by prolonged heavy rain.

It is interpreted that the opened shear joints and also the topographic conditions would support path for water flow. In parallel with this idea, shear joints perpendicular to the foliation planes were examined in the field and plant growings on a line along these joints were determined (Figure 6.6). This proves the water follows the path along the joints and daylights on the slope face.

Apart from the surface water condition in the mine, as seen in Figure 6.5, almost all water seepage points are located under the elevation of 462.5 m and their distribution generates a line for water table location. Only two water seepage points located above the elevation of 462.5 m are considered as wet discontinuity zone. During previous drilling at the base of the mine, ground water level was not



discovered until 30 m below surface. Further drilling operations were conducted in order to evaluate the water table condition within the mining area. Ten drill holes were observed during May and June in terms of the changes of the water table level. The locations of ten boreholes were shown in Figure 6.5. Consequently, the depth of water and the elevation of the water table level for each date were recorded (Appendix B). The topography of the eastern slope of the mine associated with the water table levels measured in each date and drill holes were illustrated in Figure 6.7.

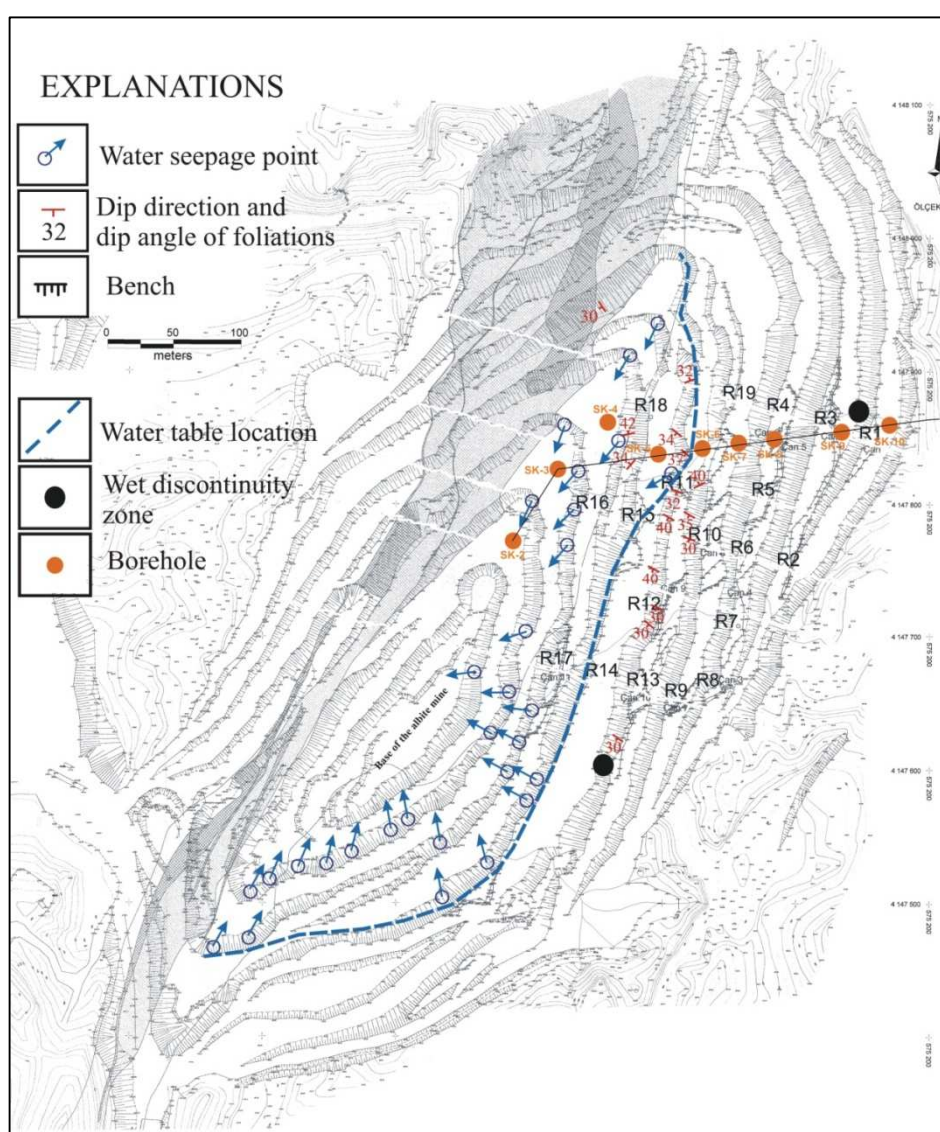


Figure 6.5 The location of seeps, wet discontinuity zones, boreholes and estimated water table level in the eastern part of the Alipaşa albite open pit mine.



Figure 6.6 Plant growings and damp areas along the shear joint zones.

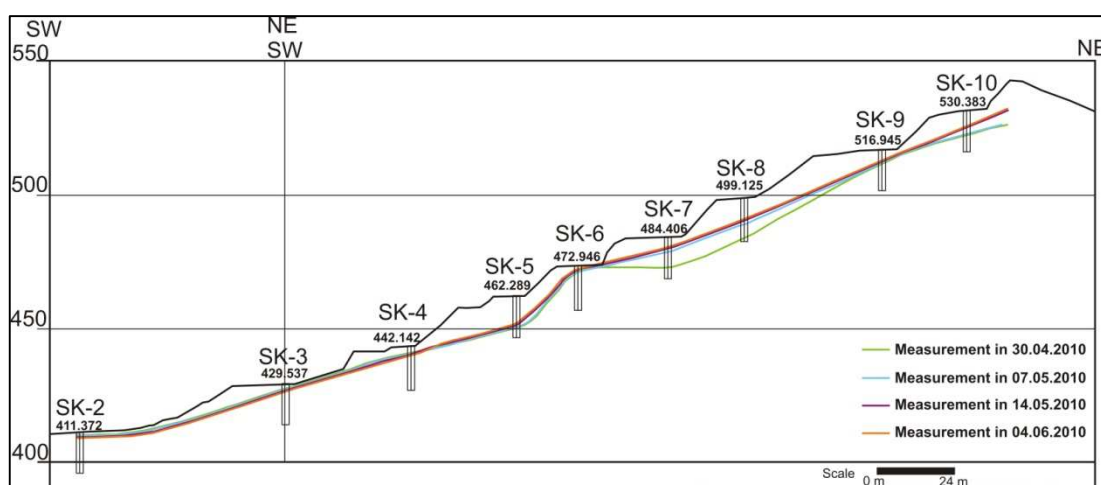


Figure 6.7 The change of water table levels in each drill hole due to various months.

According to the wet discontinuity zones and the water table levels measured in the boreholes, the peak elevation that the water rises in the slope is supposed to be 462.5 m; relatingly this peak elevation for each cross-section lines are; 454 m, 452.5 m, 462 m, 462 m, 462,5 m, respectively. This means that at which time seepage points were investigated (10.01.2010), the water table level located at maximum 462.5 m for E-E' cross-section. This nearly equals to the  $\approx 62.5\%$  water saturation according to the final geometry of the albite mine (the base elevation of 350 m). The average annual precipitation is 619 mm, the average precipitation in January and December are 96 mm and 110.4 mm, respectively. This water saturation degree can

be at the very most  $\approx 73.08\%$  if the amount of precipitations in January and December are correlated.

The investigated rock slope supposed to consist of various lithologic facies since the water seeps daylighted on the slope face designate that the water infiltration continues down to an impermeable layer and the water is accumulated as an perched water. The water table location shown in Figure 6.5 can be considered as a perched water table level.

In finite element slope stability analysis, degree of water saturation of orthogneisses was considered as 50%, %70, %100, respectively.

**CHAPTER SEVEN**  
**SLOPE STABILITY ANALYSIS CONSIDERING THE GENERALIZED**  
**HOEK-BROWN FAILURE CRITERION**

**7.1 Applicability of the Generalized Hoek-Brown Failure Criterion**

In order to determine the rock material strength In jointed rock masses, core samples are taken to use in the laboratory tests. Merely, the test results show very conservative values on the rock strength since the specimen is an intact rock, on the other hand rock mass as a whole consists of discontinuities such as bedding, foliations, naturally occurred joints, faults etc. In this case, as sample size taken for laboratory test is limited, the specimens are not representative of the jointed rock mass. In parallel with requirement to estimate the realistic rock mass strength, Hoek-Brown Failure Criterion was proposed by Hoek and Brown (1980a, 1980b). Besides, this criterion can only be used for jointed rock masses that show isotropic character. In other words, it is unsuitable for slope stability problems where shear failures are generated by a single discontinuity set or combination of seldom discontinuity sets (e.g. sliding over inclined bedding planes, toppling due to near-vertical discontinuity, or wedge failure over intersecting discontinuity planes) (Li et al., 2009). The Generalized Hoek-Brown Failure Criterion can be applied on the intact rock or heavily jointed rock mass that show isotropic character as in this study (Figure 7.1).

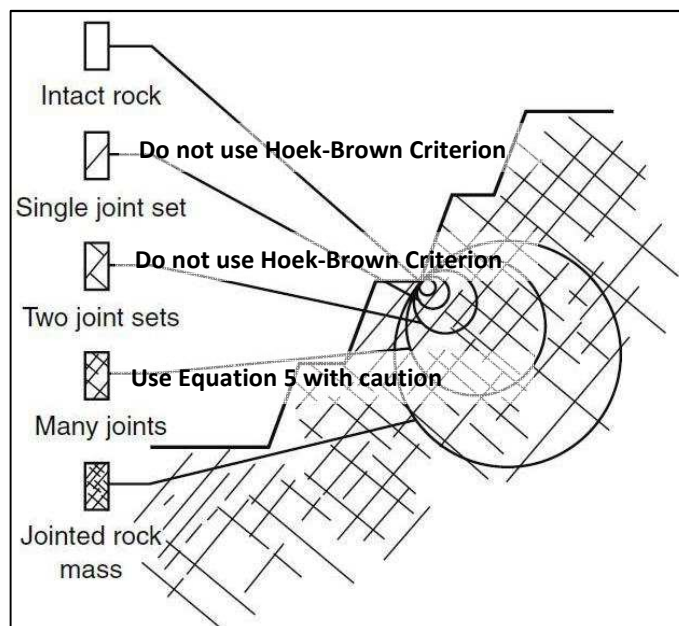


Figure 7.1. Idealised diagram showing the transition from intact to heavily jointed rock mass with increasing sample size (Modified from Hoek, 2006).

As a summary, Generalized Hoek-Brown Failure Criterion provides a good estimate for the shear strength of closely jointed rock masses.

## 7.2. Input Data for Slope Stability Analyses Based on Generalized Hoek-Brown Criterion

In a site investigation performed for an engineering design, collecting data about rock mass properties, taking rock samples for laboratory tests and correlating the data obtained from either field survey or laboratory tests provide quantitative information about the rock mass. In the case of in-situ testing methods are unavailable or costly, a relation between the data derived from field observations and laboratory tests is required to estimate the strength properties of rock mass. At this stage, Hoek and Brown (1980a, 1980b) proposed a method for estimating the strength of jointed rock masses, based on an assessment of the interlocking of rock blocks and the condition of the surfaces between these blocks. Several modifications were performed in order to supply the requirements due to limitations of criterion. The final form of the criterion named as Generalized Hoek-Brown Criterion defines the non-linear

relationship between the minor and major principal stresses and the shear strength for jointed rock masses (Hoek et al., 2002). The empirical relationship for the Generalized Hoek-Brown Failure Criterion for jointed rock masses is;

$$\sigma_1' = \sigma_3' + \sigma_{ci} \left[ m_b \cdot \frac{\sigma_3}{\sigma_{ci}} + s \right]^a \quad (7)$$

For the intact rock pieces that make up the rock mass is defined by;

$$\sigma_1' = \sigma_3' + \sigma_{ci} \left[ m_i \cdot \frac{\sigma_3}{\sigma_{ci}} + s \right]^{0.5} \quad (8)$$

where  $\sigma_1'$  and  $\sigma_3'$  are the maximum and minimum effective principal stresses at failure,  $m_b$  is a Hoek-Brown constant that represents the rock mass and  $m_i$  is a Hoek-Brown constant that represents the rock material,  $s$  and  $a$  are constants which depend upon the rock mass characteristics,  $\sigma_{ci}$  is the uniaxial compressive strength of the intact rock pieces.

The rock mass constants are found by Generalized Hoek-Brown Failure Criterion in association with the geological strength index (GSI). When the criterion was firstly introduced, they were estimated directly from rock mass rating system (RMR). However the correlation was proved to be unreliable. At present, the latest revision (Marinos & Hoek, 2001) of GSI chart is used to estimate the appropriate GSI value as an input to the equations relevant for the prediction of rock mass strength and deformation parameters (Figure 7.2). Consequently, GSI system provides information for estimating the reduction in rock mass strength for different geological conditions of rock material by considering the engineering discontinuity properties such as block size and surface conditions. The GSI ratings vary between 10 to 100 representing very weak rock and intact rock, respectively.









<p><b>GEOLOGICAL STRENGTH INDEX FOR JOINTED ROCKS (Hoek and Marinos, 2000)</b></p> <p>From the lithology, structure and surface conditions of the discontinuities, estimate the average value of GSI. Do not try to be too precise. Quoting a range from 33 to 37 is more realistic than stating that GSI = 35. Note that the table does not apply to structurally controlled failures. Where weak planar structural planes are present in an unfavourable orientation with respect to the excavation face, these will dominate the rock mass behaviour. The shear strength of surfaces in rocks that are prone to deterioration as a result of changes in moisture content will be reduced if water is present. When working with rocks in the fair to very poor categories, a shift to the right may be made for wet conditions. Water pressure is dealt with by effective stress analysis.</p>		<p><b>SURFACE CONDITIONS</b></p> <p><b>VERY GOOD</b> Very rough, fresh unweathered surfaces</p> <p><b>GOOD</b> Rough, slightly weathered, iron stained surfaces</p> <p><b>FAIR</b> Smooth, moderately weathered and altered surfaces</p> <p><b>POOR</b> Slickensided, highly weathered surfaces with compact coatings or fillings or angular fragments</p> <p><b>VERY POOR</b> Slickensided, highly weathered surfaces with soft clay coatings or fillings</p> <p>DECREASING SURFACE QUALITY →</p>				
<p><b>STRUCTURE</b></p> <p> <b>INTACT OR MASSIVE</b> - intact rock specimens or massive in situ rock with few widely spaced discontinuities</p> <p> <b>BLOCKY</b> - well interlocked undisturbed rock mass consisting of cubical blocks formed by three intersecting discontinuity sets</p> <p> <b>VERY BLOCKY</b> - interlocked, partially disturbed mass with multi-faceted angular blocks formed by 4 or more joint sets</p> <p> <b>BLOCKY/DISTURBED/SEAMY</b> - folded with angular blocks formed by many intersecting discontinuity sets. Persistence of bedding planes or schistosity</p> <p> <b>DISINTEGRATED</b> - poorly interlocked, heavily broken rock mass with mixture of angular and rounded rock pieces</p> <p> <b>LAMINATED/SHEARED</b> - Lack of blockiness due to close spacing of weak schistosity or shear planes</p> <p>DECREASING INTERLOCKING OF ROCK PIECES ↓</p>		<p>90</p> <p>80</p> <p>70</p> <p>60</p> <p>50</p> <p>40</p> <p>30</p> <p>20</p> <p>10</p> <p>N/A</p> <p>N/A</p>				
		N/A	N/A	N/A	N/A	N/A
		90	80	70	60	50
		80	70	60	50	40
		70	60	50	40	30
		60	50	40	30	20
		50	40	30	20	10
		40	30	20	10	N/A

Figure 7.2 Geological Strength Index based on geological descriptions (Marinos & Hoek, 2001).

Following equations represent the relationship between GSI and the Hoek-Brown constants (Hoek et al., 2002).

$$m_b/m_i = \exp\left(\frac{GSI-100}{28-14D}\right) \quad (9)$$

$$s = \exp\left(\frac{GSI-100}{9-3D}\right) \quad (10)$$

$$a = 1/2 + 1/6 (e^{-GSI/15} - e^{-20/3}) \quad (11)$$

where D is a factor which depends on the degree of disturbance due to blast damage and stress relaxation. It is obvious that the appearance of a rock face which has been excavated by controlled blasting and a face which has been damaged by bulk blasting show differences. The rating of D varies between 0 to 1, representing the undisturbed in situ rock masses and very disturbed rock masses, respectively (Table 7.1).

Table 7.1 Disturbance factor chart

Description of rock mass	Suggested value of “D”
Small scale blasting in civil engineering slopes results in modest rock damage, particularly if controlled blasting is used. However, stress relief results in some disturbance.	D = 0.7 Good blasting D = 1.0 Poor blasting
Very large open pit mine slopes suffer significant disturbance due to heavy production blasting and also due to stress relief from overburden removal. In some softer rocks excavation can be carried out by ripping and dozing and the degree of damage to the slopes is less.	D = 1.0 Production blasting D = 0.7 Mechanical Excavation.



The values of the Hoek-Brown constants that represent the rock material and mass symbolised by  $m_i$  and  $m_b$ , respectively, depend on the rock type, the size, geometry and interlocking degree of the rock forming grains. In this study,  $m_i$  value was selected from the chart (Hoek, 2006) (Table 7.2)

Table 7.2 Proposed  $m_i$  values for various rock types (Hoek, 2006).

Rock type	Class	Group	Texture			
			Coarse	Medium	Fine	Very fine
SEDIMENTARY	Clastic		Conglomerates* (21 ± 3)	Sandstones 17 ± 4	Siltstones 7 ± 2	Claystones 4 ± 2
			Breccias (19 ± 5)		Greywackes (18 ± 3)	Shales (6 ± 2) Marls (7 ± 2)
	Non-Clastic	Carbonates	Crystalline Limestone (12 ± 3)	Sparitic Limestones (10 ± 2)	Micritic Limestones (9 ± 2)	Dolomites (9 ± 3)
		Evaporites		Gypsum 8 ± 2	Anhydrite 12 ± 2	
	Organic				Chalk 7 ± 2	
METAMORPHIC	Non Foliated		Marble 9 ± 3	Hornfels (19 ± 4) Metasandstone (19 ± 3)	Quartzites 20 ± 3	
	Slightly foliated		Migmatite (29 ± 3)	Amphibolites 26 ± 6		
	Foliated**		Gneiss 28 ± 5	Schists 12 ± 3	Phyllites (7 ± 3)	Slates 7 ± 4
IGNEOUS	Plutonic	Light	Granite 32 ± 3	Diorite 25 ± 5	Granodiorite (29 ± 3)	
		Dark	Gabbro 27 ± 3	Dolerite (16 ± 5)	Norite 20 ± 5	
	Hypabyssal		Porphyries (20 ± 5)		Diabase (15 ± 5)	Peridotite (25 ± 5)
	Volcanic	Lava		Rhyolite (25 ± 5) Andesite 25 ± 5	Dacite (25 ± 3) Basalt (25 ± 5)	Obsidian (19 ± 3)
		Pyroclastic	Agglomerate (19 ± 3)	Breccia (19 ± 5)	Tuff (13 ± 5)	

\* Conglomerates and breccias may present a wide range of  $m_i$  values depending on the nature of the cementing material and the degree of cementation, so they may range from values similar to sandstone to values used for fine grained sediments.

\*\* These values are for intact rock specimens tested normal to bedding or foliation. The value of  $m_i$  will be significantly different if failure occurs along a weakness plane.

One of the Hoek-Brown rock mass constants,  $s$  value varies between 0 and 1 and depends on the interlocking degree of the grains in the rock mass,  $s = 0$  signifies very weak rock that has approximately zero cohesion and tensile strength.

The uniaxial compressive strength of the rock mass can also be defined by the Hoek-Brown parameters by setting  $\sigma_3' = 0$  in Equation 12 (Hoek, 2006);

$$\sigma_c = \sigma_{ci} \cdot s^a \quad (12)$$

and the tensile strength is calculated as follows (Hoek, 2006);

$$\sigma_t = -\frac{s\sigma_{ci}}{m_b} \quad (13)$$

Hoek and Diederichs (2006) proposed an equation to define the deformation modulus of rock mass by utilizing the deformation modulus of intact rock obtained from the strain gauge test (Equation 14) However, if the strain gauge test is unavailable, elasticity modulus of intact rock can be determined from the Equation 15 proposed by Deere (1968).

$$E_{rm} = E_i \left( 0.02 + \frac{1-(D/2)}{1 + e^{((60+15D-GSI)/11)}} \right) \quad (14)$$

$$E_i = MR \times \sigma_{ci} \quad (15)$$

where MR is a value identified as modulus ratio and selected from the chart generated by the data from Deere (1968), Palmstrom and Singh (2001) in Hoek and Diederichs (2006) in terms of various rock types. For foliated gneiss, MR is suggested to be between 300 and 750. Though, in order to obtain an unconservative result, other approaches for estimating the elasticity modulus of rock material were taken into account.

Accordingly, an empirical equation proposed by Hoek et al. (2002) based on  $\sigma_{ci}$ , GSI and D values (Eq. 16) was used together with Equation 14 for the cases  $\sigma_{ci} \leq 100$  MPa. These calculations were conducted by putting the  $E_{rm}$  values found by Eq. 16 into the Eq. 14 to find out the  $E_i$  values.

$$E_{rm} = (1 - D/2) \sqrt{\sigma_{ci}/100} \times 10^{(GSI-10)/40} \quad (16)$$

Following that, the  $E_i$  values obtained from Equation 15 and Equations 14 and 16 were compared (Figure 7.3). As a result, Eq. 15 was considered to be slightly subjective, so that the elasticity modulus of rock material was taken as 33500 MPa as an input data for finite element method based on Generalized Hoek-Brown Criterion and equivalent Mohr-Coulomb parameters.

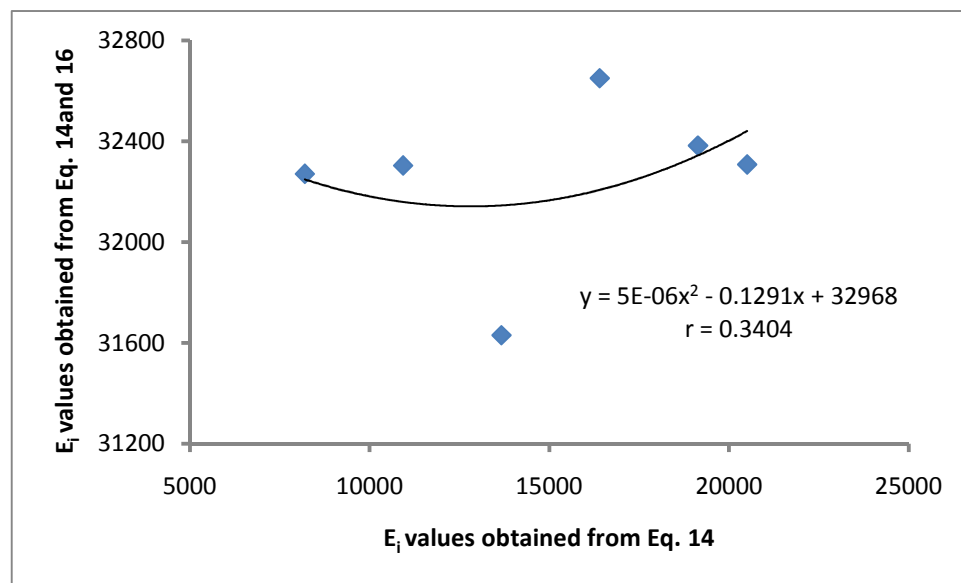


Figure 7.3 The simple correlation of  $E_i$  values obtained from Equation 15 and Equations 14, 16 considering  $D$ : 0.7,  $\sigma_{ci}$ : 27.34 MPa and the GSI variations of 35 to 47 and the MR variations of 300 to 750.

Furthermore the  $E_{rm}$  values obtained from Equations 14 and 16 were also compared in order to crosscheck the reliability of the both approaches for estimating  $E_{rm}$  in the case of same  $D$  and GSI values, for a selected  $E_i$  and laboratory established  $\sigma_{ci}$ . The simple regression analysis results showed that the both  $E_{rm}$  values have a significant relationship with coefficient of correlation of  $r$ : 0.9999 (Figure 7.4). In other words, both the Equations 14 and 16 can be convenient approaches for determining the  $E_{rm}$  values.

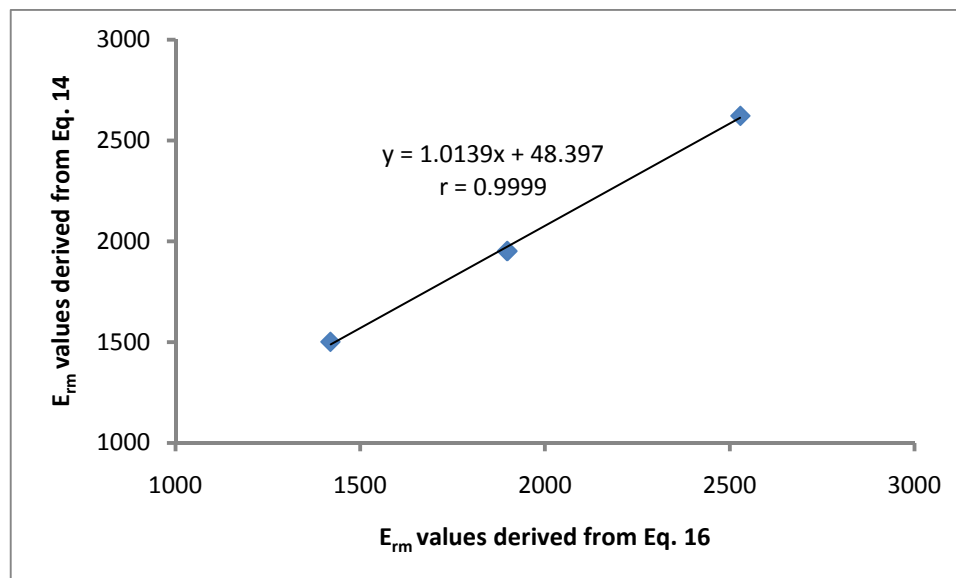


Figure 7.4 The simple correlation of the  $E_{rm}$  values obtained from Equations 14 and 16; in the case  $D: 0.7$ ,  $E_i: 33500$  MPa,  $\sigma_{ci}: 27.34$  MPa and for the GSI variations of 35, 40, 45.

As a summary, in order to run the Generalized Hoek-Brown Failure Criterion for estimating the strength and deformability of rock masses,  $\sigma_{ci}$ ,  $m_i$ , GSI,  $D$  and  $E_i$  values are required (Table 7.3).

The Poisson's's ratio is the ratio of the transverse strain to longitudinal strain in compressional or tensional stress condition. The Poisson's ratio of rocks varies in very narrow range and according to the chart (Gerçek, 2004) Poisson's's ratio for gneiss is in the range 0.1 to 0.3. In this study, Poisson's's ratio of 0.25 was approved to be taken into account in the FEM analysis.

When utilising the Generalized Hoek-Brown Criterion in FE slope stability analysis program Phase<sup>2</sup>, firstly, mesh setup and field stress properties are defined in "Define Material Properties" command, then Young's modulus, Poisson's's ratio, unit weight of rock material, uniaxial compressive strength of intact rock,  $m_b$ ,  $s$  and  $a$  parameters are required to be defined and dilation angle which controls an amount of plastic volumetric strain developed during plastic shearing and assumed to be constant during plastic yielding was taken as zero. In other words, in the case of a very weak rock in which elastic-perfectly plastic behaviour, it is assumed that there is no volume change (Figure 7.5). Rock material and rock mass properties taken into

account for the numerical analyses considering Generalized Hoek-Brown Criterion were given in Table 7.4.

Table 7.3 The required input data in Generalized Hoek-Brown Criterion and relevant outputs

Input Data	Output		
	Generalized Hoek-Brown Criterion	Mohr-Coulomb fit	Rock Mass Parameters
Uniaxial compressive strength of rock material, $\sigma_{ci}$	Hoek-Brown constant for rock mass, $m_b$	Equivalent Mohr-Coulomb parameter, cohesion, $c$	Tensile strength of rock mass, $\sigma_{tm}$
Geological Strength Index, GSI	Hoek-Brown constant for rock mass, $s$		Uniaxial compressive strength of rock mass, $\sigma_c$
Hoek-Brown constant for intact rock pieces, $m_i$	Hoek-Brown constant for rock mass, $a$	Equivalent Mohr-Coulomb parameter, internal friction angle, $\Phi$	Global strength of rock mass, $\sigma_{ci}$
Disturbance Factor, $D$			Deformation modulus of rock mass, $E_{rm}$
Deformation modulus of intact rock, $E_i$			

RocLab program involved in the software Phase<sup>2</sup> provides easy calculation of  $m_b$ ,  $s$ ,  $a$ , Young's modulus and strength parameters of rock mass required in FE modelling by entering the values of  $\sigma_{ci}$ ,  $m_i$ ,  $D$ , GSI and intact rock modulus ( $E_i$ ).

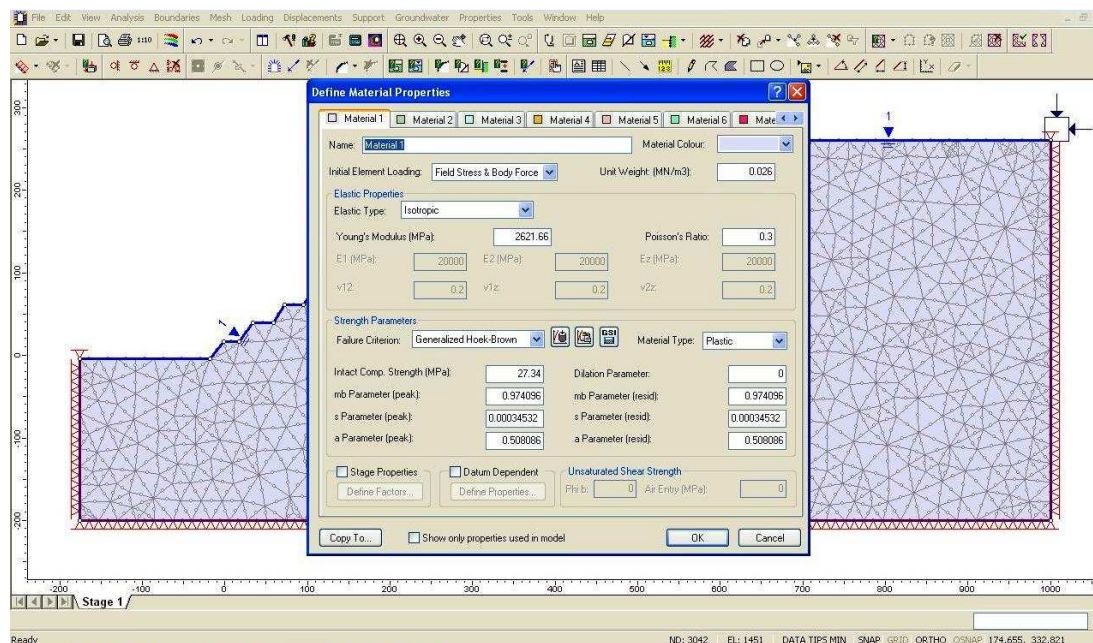


Figure 7.5 Defining the material properties in Phase<sup>2</sup>.

When defining the material properties, initial element loading was set to Field stress & Body Force. This means numerical analyses were conducted through self-weight of material itself that is derived from unit weight together with the loading parameters defined as gravity field stress. If just body force was assumed, the material would settle under Its own weight and the top surface would move down, besides if the material had just initial stress it would expand and the top surface would move up. Therefore, firstly the both was defined then the material assumed to be in equilibrium.

The following process is defining the water table location and in the case of earthquake effect, the seismic load coefficient should be entered to the program. Furthermore, the slope is assumed to be loaded under gravity with a horizontal and vertical stress ratio of 1. This assumption should be put in the numerical model under the Field Stress command in the Loading menu.

Finally, calculations are conducted. The software performs the calculations through each element generated by meshing with respect to the rock mass properties derived from Generalized Hoek-Brown Criterion, piezometric and seismic properties entered to program.

Table 7.4 Rock material and rock mass properties used in numerical analyses considering Generalized Hoek-Brown Criterion

Rock Type	Intact Rock Properties			D	Rock Mass Properties				
	Dilation parameter: 0				Poisson's ratio: 0.25				
	Unit Weight: 0.026 MN/m <sup>3</sup>								
Orthogneiss	m <sub>i</sub>	σ <sub>ci</sub> (MPa)	E <sub>i</sub> (MPa)	0.7	GSI	s	a	m <sub>b</sub>	E <sub>rm</sub> (MPa)
					35	0.0001	0.516	0.562	1500.76
					40	0.0002	0.511	0.740	1950.72
	20	27.34	33500		45	0.0003	0.508	0.974	2621.66

*m<sub>i</sub>, m<sub>b</sub>: Hoek-Brown constants for intact rock and rock mass, respectively; σ<sub>ci</sub>: uniaxial compressive strength of intact rock pieces; E<sub>i</sub> and E<sub>rm</sub>: deformation modulus of intact rock and rock mass, respectively; D: disturbance factor; GSI: geological strength index; s and a: Hoek-Brown constants which depend upon the rock mass characteristics.*

### 7.3 The Slope Stability Analyses Results Based on Generalized Hoek-Brown Criterion

Slope failure occurs since the shear strength of the material on the sliding surface remain incapable to resist the actual shear stress. As a result of FEM analyses, for all anticipated cases, SRF values that implies the stability state of slopes were determined. The critical SRF values for the open pit albite mine was considered to be 1.15-1.30 especially for the worst conditions modelled, such as fully saturated, seismically active and lower GSI value cases.

In order to obtain more realistic and reliable SRF values, variations of GSI, water table location, seismic coefficient and slope angle for each cross-section which have different slope heights were considered in the slope stability analyses. The SRF values were collectively shown in Appendix C. Additionally, the effect of variants on the SRF values were investigated by multivariate analysis with a commercially available software SPSS (Statistical Package for the Social Sciences) (Appendix E). Besides, linear regression analysis between the dependent variable (SRF) and

independent variables (GSI, seismic coefficient, slope angle, water table location and slope height) was performed. Consequently, one linear equation was obtained (Equation 17).

$$\text{SRF} = 2.060 - 0.399\alpha_s - 0.039\alpha_{\text{slope}} + 0.017\text{GSI} - 0.002\text{WTL} - 0.002H_{\text{slope}} \quad r: 0.696 \quad (17)$$

( $\alpha_s$ : seismic coefficient;  $\alpha_{\text{slope}}$ : slope angle; GSI: geological strength index; WTL: water table location;  $H_{\text{slope}}$ : slope height)

Statistical analyses showed that the most effective parameter on slope stability is  $\alpha_{\text{slope}}$ , after which GSI, WTL,  $\alpha_s$  and  $H_{\text{slope}}$  are nominated, respectively.

In parallel with the requirements of determining a optimum overall slope angle for the eastern slope of the open pit, the change of SRF values according to the variables (water condition, seismic coefficient, slope angle and GSI) were investigated for each cross-section. The SRF values for the most appropriate condition can be defined readily by the graphs generated (Figures 7.6-7.8). On this basis, in the case of 70% saturated condition together with 0.1g seismic coefficient and GSI value as 42, the optimum overall slope angle can not be higher than 32° in terms of Generalized Hoek-Brown Criterion.



## Water Table Level: 100% (Generalized Hoek-Brown)

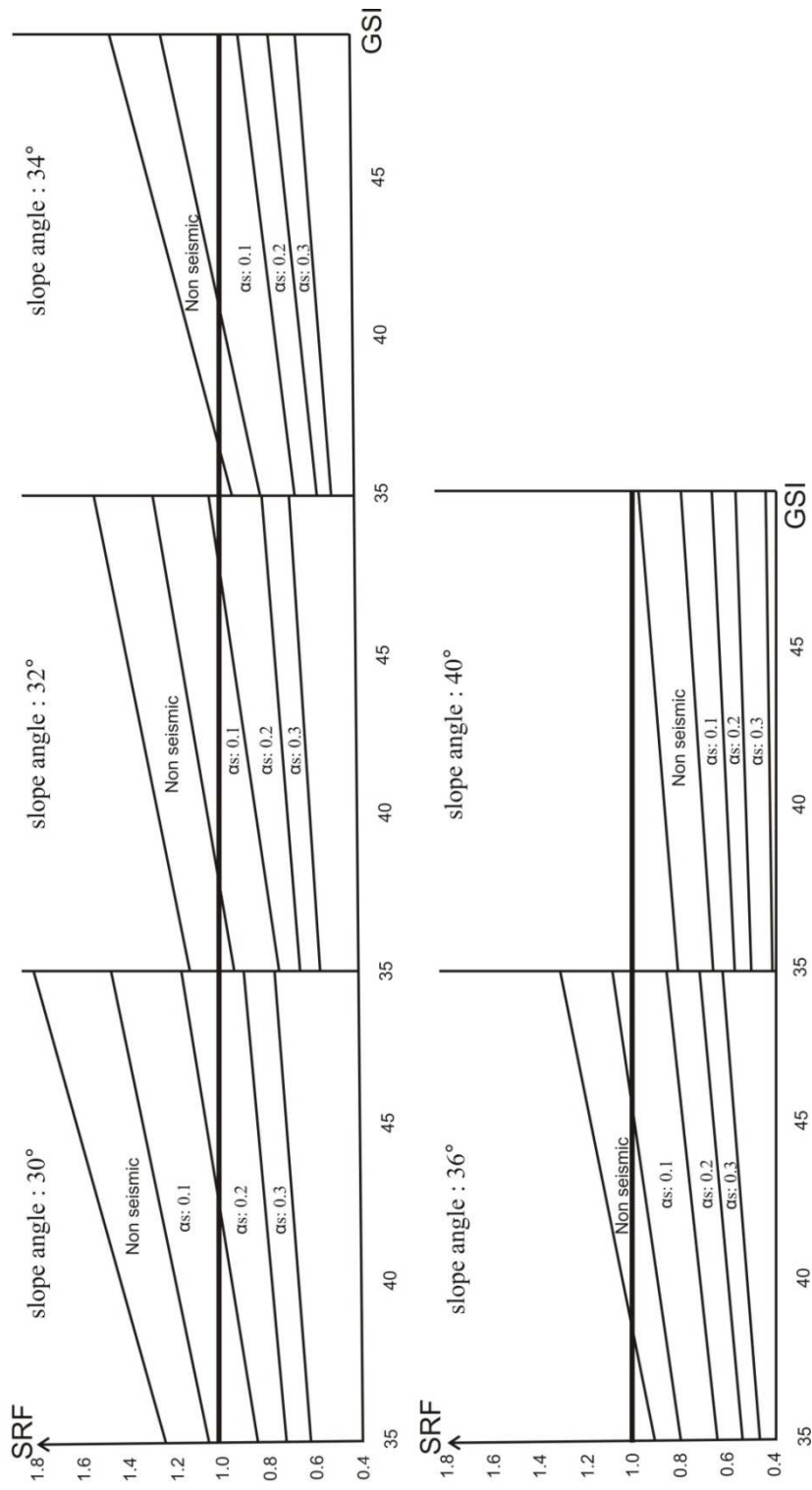


Figure 7.6 Relationship between GSI ratings and SRF values considering the different slope angles, seismic coefficients for all cross sections in 100% saturated condition for Generalized Hoek-Brown Criterion.

## Water Table Level: 70% (Generalized Hoek-Brown)

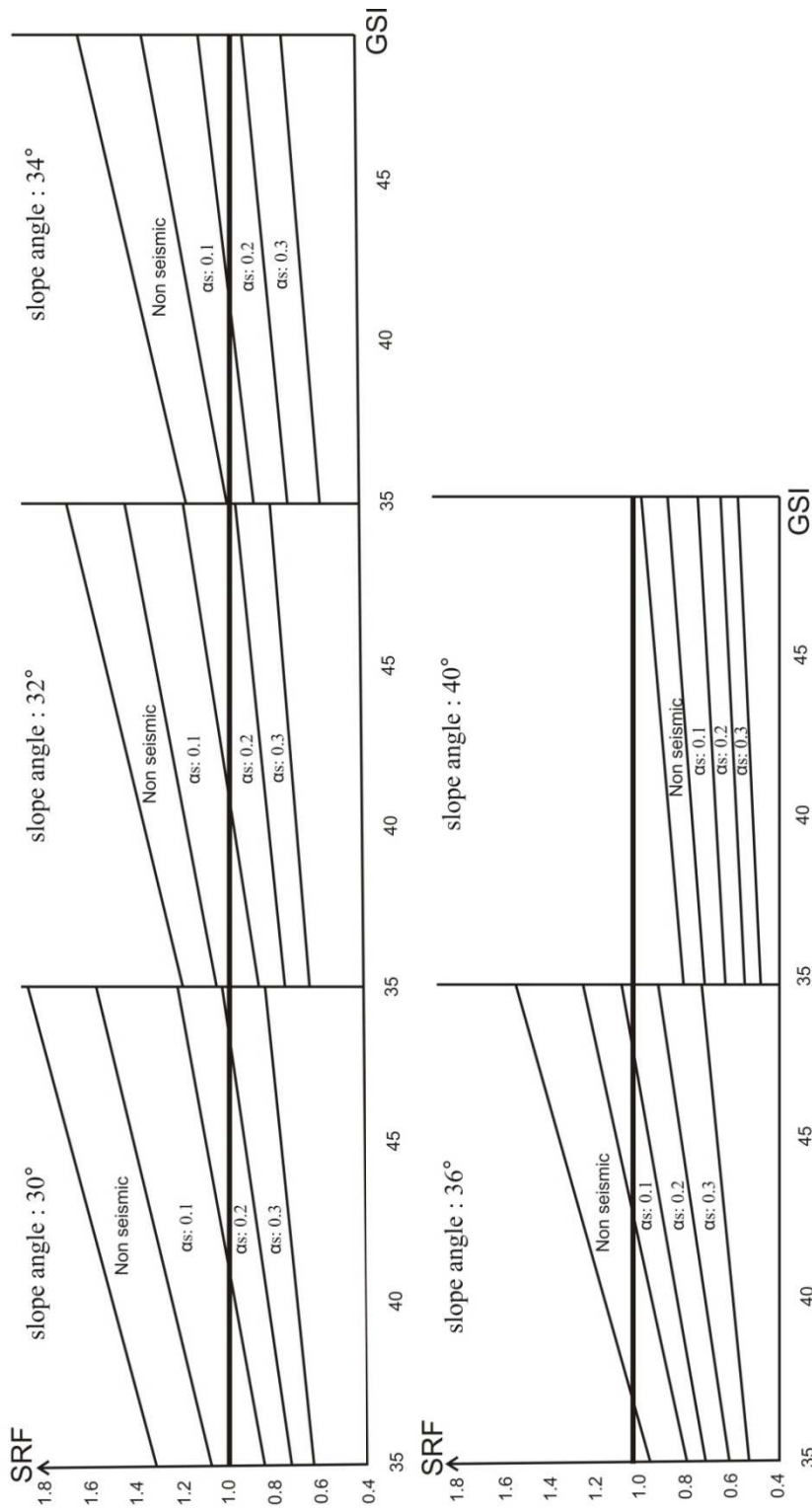


Figure 7.7 Relationship between GSI ratings and SRF values considering the different slope angles, seismic coefficients for all cross sections in 70% saturated condition for Generalized Hoek-Brown Criterion.

### Water Table Level: 50% (Generalized Hoek-Brown)

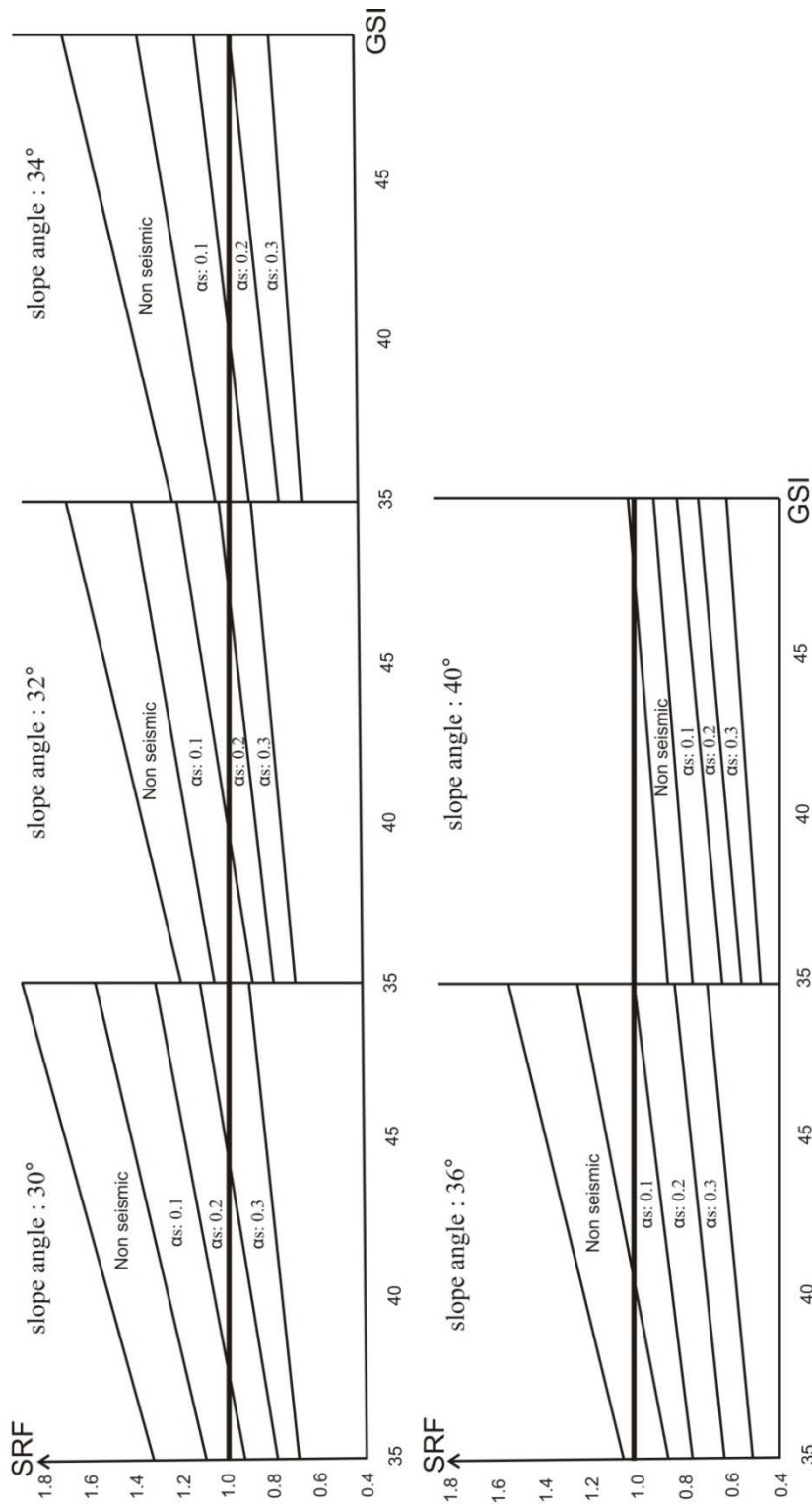


Figure 7.8 Relationship between GSI ratings and SRF values considering the different slope angles, seismic coefficients for all cross sections in 50% saturated condition for Generalized Hoek-Brown Criterion.

## CHAPTER EIGHT

### SLOPE STABILITY ANALYSIS USING THE EQUIVALENT MOHR COULOMB PARAMETERS

#### 8.1 Applicability of Equivalent Mohr-Coulomb Criterion

Since many geotechnical software programs are written in terms of the Mohr-Coulomb Failure Criterion, it is sometimes necessary to determine equivalent friction angles and cohesive strengths for each rock mass and stress range (Hoek, 2006). The equivalent Mohr-Coulomb parameters are defined by Hoek et al. (2002) as which over a specified stress interval minimizes the area between linear Mohr-Coulomb and the Hoek-Brown curve. In other words, this procedure involves fitting a Mohr-Coulomb curve geometrically that equalize the sum of positive areas (areas above the Mohr-Coulomb line) to the sum of negative areas (areas below the line) (Figure 8.1).

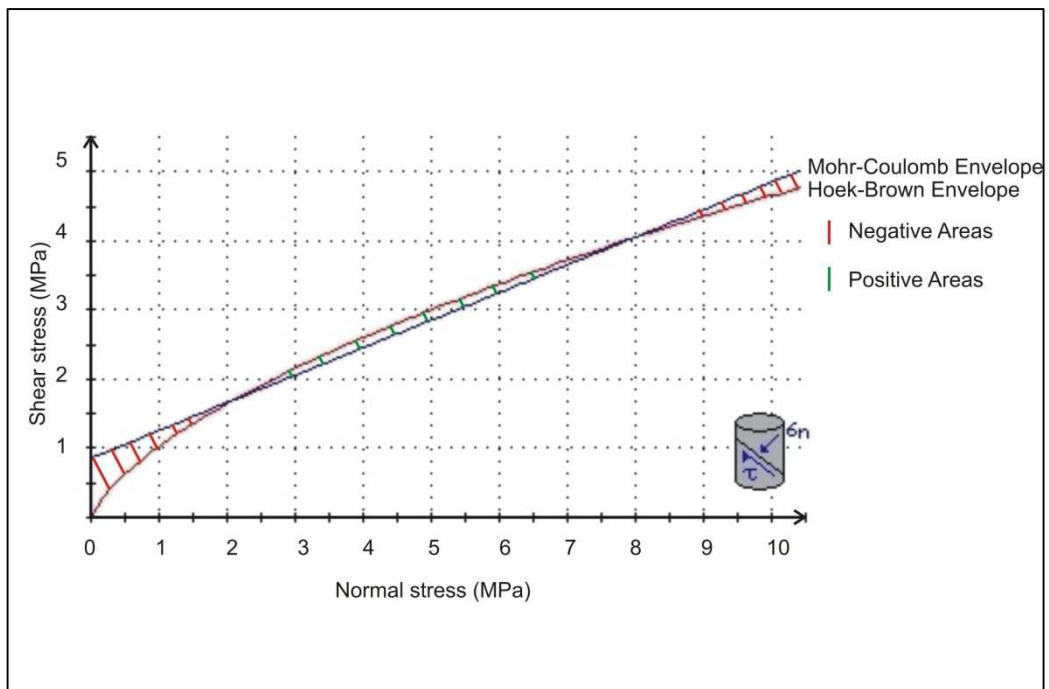


Figure 8.1 The imaged definition of the positive and negative areas between linear Mohr-Coulomb and non-linear Hoek-Brown failure envelopes (The image was captured from RocLab program and modified for illustration).

As a summary, Hammah et al., (2004) defined this method as it involves primarily determining a Mohr-Coulomb envelope equivalent to a Hoek-Brown model, and then applying the resulting equivalent cohesion and friction angle values in the standart SSR technique.

## 8.2 Input Data for Slope Stability Analyses Based on Equivalent Mohr-Coulomb Criterion

The fitting procedure is conducted over a stress range from tensile strength to the maximum compressive strength in the slope. The equivalent Mohr-Coulomb parameters were calculated by the equations below (Hoek, 2006);

$$\Phi' = \sin^{-1} \left[ \frac{6am_b(s+m_b\sigma'_{3n})^{a-1}}{2(1+a)(2+a)+6am_b(s+m_b\sigma'_{3n})^{a-1}} \right] \quad (18)$$

$$c' = \frac{\sigma_{ci}[(1+2a)s+(1-a)m_b\sigma'_{3n}](s+m_b\sigma'_{3n})^{a-1}}{(1+a)(2+a)+\sqrt{1+6am_b(s+m_b\sigma'_{3n})^{a-1}}/(1+a)(2+a)} \quad (19)$$

where  $\sigma'_{3n} = \frac{\sigma'_{3max}}{\sigma_{ci}}$  and the maximum compressive strength is calculated from the equation;

$$\sigma'_{3max} = 0.72 \sigma'_{cm} \left[ \frac{\sigma'_{cm}}{gH} \right]^{0.91} \quad (20)$$

Where  $g$  is the rock mass unit weight,  $H$  is the slope height and  $\sigma'_{cm}$  is the global rock mass strength that can be defined by the equation below;

$$\sigma'_{cm} = \sigma_{ci} \frac{(m_b+4s-a(m_b-8s))\left(\frac{m_b}{4}+s\right)^{a-1}}{2(1+a)(2+a)} \quad (21)$$

According to the equations (18-21) the equivalent Mohr-Coulomb parameters were calculated by the utilizing the RocLab program involved in the Phase<sup>2</sup> software. Results were shown in the Table 8.1.

Table 8.1 The equivalent Mohr-Coulomb parameters used in analyses according to the various GSI values and the slope heights relevant to the five cross-sections

Intact Rock Properties		D	Slope Height	Orthogneiss Rock Mass Properties														
Properties				Dilation angle ( $\psi$ ): 0														
$m_i$ : 20		GSI																
$\sigma_{ci}$ (MPa) : 27.34 $E_i$ (MPa): 33500		35				40				45								
		$c$ (MPa)	$\Phi$ (°)	$\sigma_t$ (MPa)	$E_{rm}$ (MPa)	$c$ (MPa)	$\Phi$ (°)	$\sigma_t$ (MPa)	$E_{rm}$ (MPa)	$c$ (MPa)	$\Phi$ (°)	$\sigma_t$ (MPa)	$E_{rm}$ (MPa)					
		135	0.436	29.46	0.497	31.83	0.562	34.17	0.531	34.87	0.526	35	0.554	34.34	0.471	36.38	1950.72	2621.66
		123	0.412	30.14	0.470	32.53	0.491	32	0.465	32.65	0.491	32	0.465	32.65	0.416	34.01	1500.76	
		132	0.430	29.62	0.491	32	0.491	32	0.465	32.65	0.491	32	0.465	32.65	0.416	34.01	1500.76	
121	0.408	30.26	0.465	32.65	0.465	32.65	0.465	32.65	0.465	32.65	0.465	32.65	0.416	34.01	1500.76			
101	0.365	31.58	0.416	34.01	0.416	34.01	0.416	34.01	0.416	34.01	0.416	34.01	0.416	34.01	1500.76			

$m_i$  : Hoek-Brown constants for intact rock;  $\sigma_{ci}$ : uniaxial compressive strength of intact rock pieces;  $E_i$  and  $E_{rm}$ : deformation modulus of intact rock and rock mass, respectively;  $D$ : disturbance factor;  $GSI$ : geological strength index;  $c$ : cohesion of rock mass;  $\Phi$ : internal friction angle of rock mass;  $\sigma_t$ : tensile strength of rock mass.

### 8.3 The Slope Stability Analyses Results Based on Equivalent Mohr Coulomb Parameters

The SRF values obtained by using Mohr-Coulomb Criterion with equivalent strength parameters were collectively shown in Appendix D. The multivariate analysis and other statistical analyses were performed as applied for the Generalized Hoek-Brown Criterion results (Appendix E). As a result of linear regression analysis, one linear equation was obtained (Equation 22).

$$\text{SRF} = 3.037 - 0.593\alpha_s - 0.060\alpha_{\text{slope}} + 0.021\text{GSI} - 0.006\text{WTL} - 0.003H_{\text{slope}} \quad r: 0.680 \quad (22)$$

( $\alpha_s$ : seismic coefficient;  $\alpha_{\text{slope}}$ : slope angle; GSI: geological strength index; WTL: water table location;  $H_{\text{slope}}$ : slope height)

Statistical analyses showed that the most effective parameter on slope stability is  $\alpha_{\text{slope}}$  after which WTL, GSI,  $\alpha_s$  and  $H_{\text{slope}}$  are nominated, respectively.

Investigation of the change of SRF values according to the various water condition, seismic coefficient, slope angle and GSI values by graphs readily provide estimation of stability state for various geological conditions with reference of 1.00 line (Figures 8.5-8.7) as well as in some conditions 1.3 can be taken as a critical SRF value.

The SRF values belonging to the slope angle of 40° were obtained significantly low such as in the range of 0.01 to 0.25. The reason for these cases was supposed to be the occurrence of bench failures in the early stages of SRF values, therefore SRF values are increased until the overall slope failure occurs on the model in order to obtain more reasonable results. For rare conditions (non seismic and GSI value as 40-45), even the SRF values are increased, overall slope failure did not occur (Figure 8.2). Furthermore, for some conditions (especially for slope angle 34°), rotational failure surface did not cut the toe of the slope (Figure 8.3), as well as some models showed deformation like swelling, displacement towards up to the ground right before the overall slope failure (Figure 8.4).

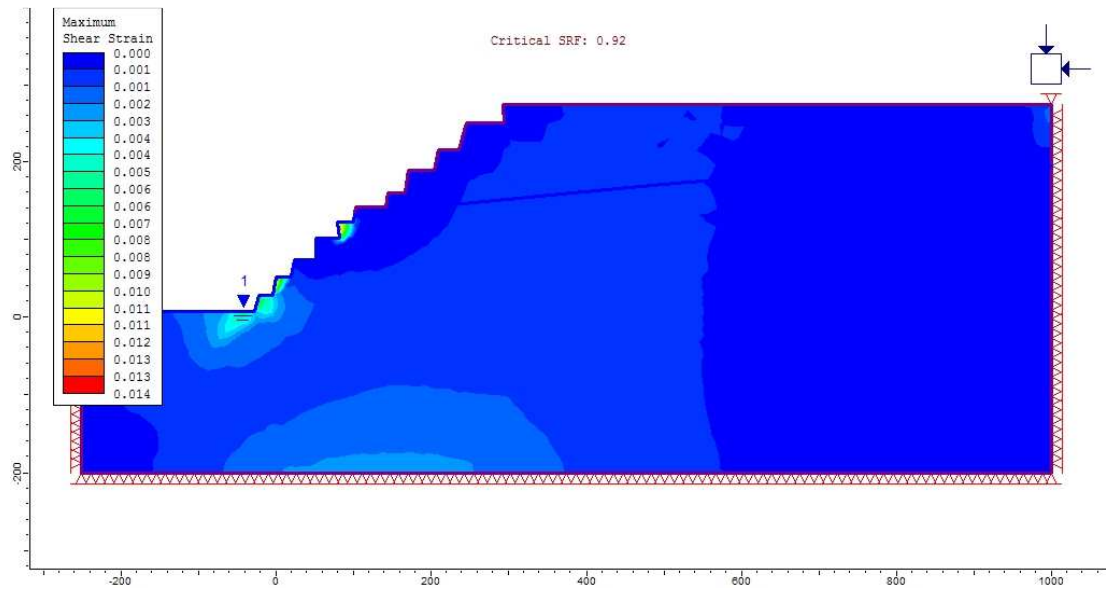


Figure 8.2 The illustration of the underestimated critical SRF value due to the bench failure (Even if the SRF value is increased manually until 1.00, overall slope failure did not occur.) (GSI:35, slope angle:  $40^\circ$ , non seismic, 50% saturated, C-C' cross section, Mohr-Coulomb Criterion).

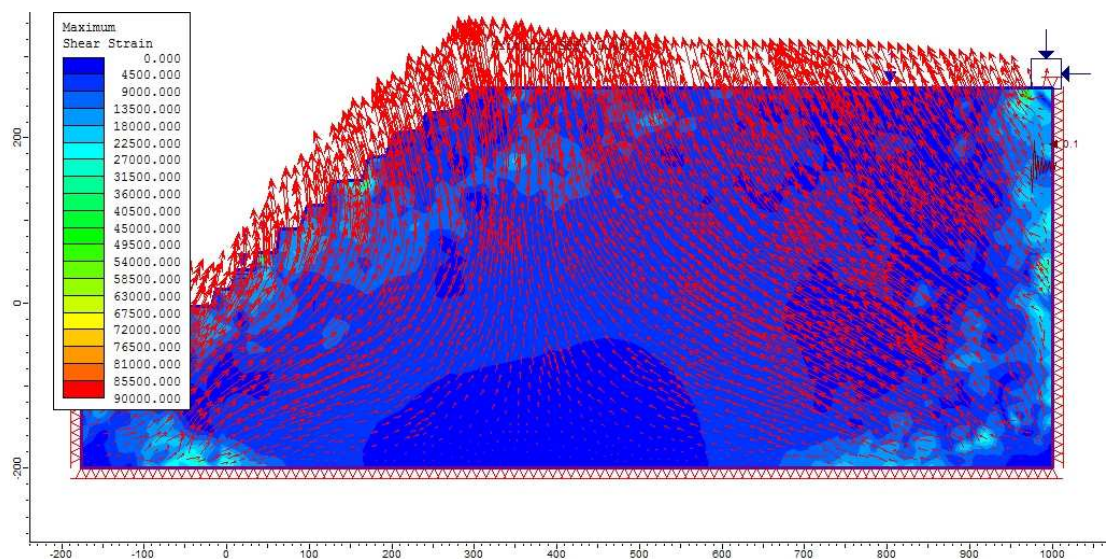


Figure 8.3 The display of deformation vectors that implying a deformation upwards as swelling (GSI:35, slope angle:  $40^\circ$ ,  $\alpha_s$ : 0.1g, 100% saturated, A-A' cross section, Mohr-Coulomb Criterion).



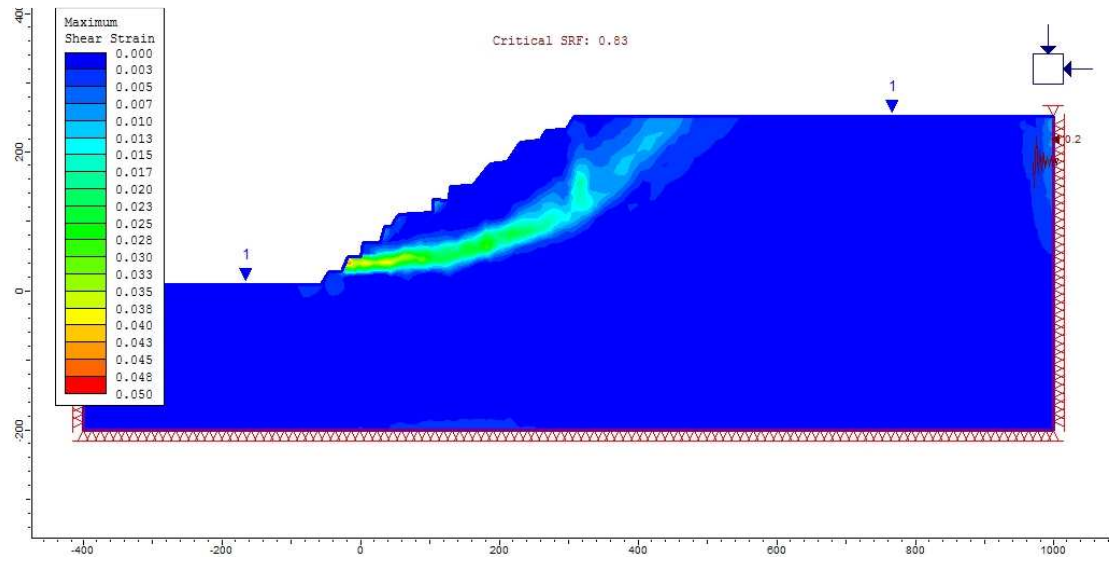


Figure 8.4 The illustration of failure surface not cutting the toe of the slope (GSI:40, slope angle:  $34^\circ$ ,  $\alpha_s$ : 0.2g, 100% saturated, D-D' cross section, Mohr-Coulomb Criterion).

In the case of 70% saturated condition together with 0.1g seismic coefficient and GSI value as 42, the optimum overall slope angle can not be higher than  $34^\circ$  in terms of Mohr-Coulomb Criterion performed by equivalent strength parameters.

## Water Table Level: 100% (Equivalent Mohr-Coulomb)

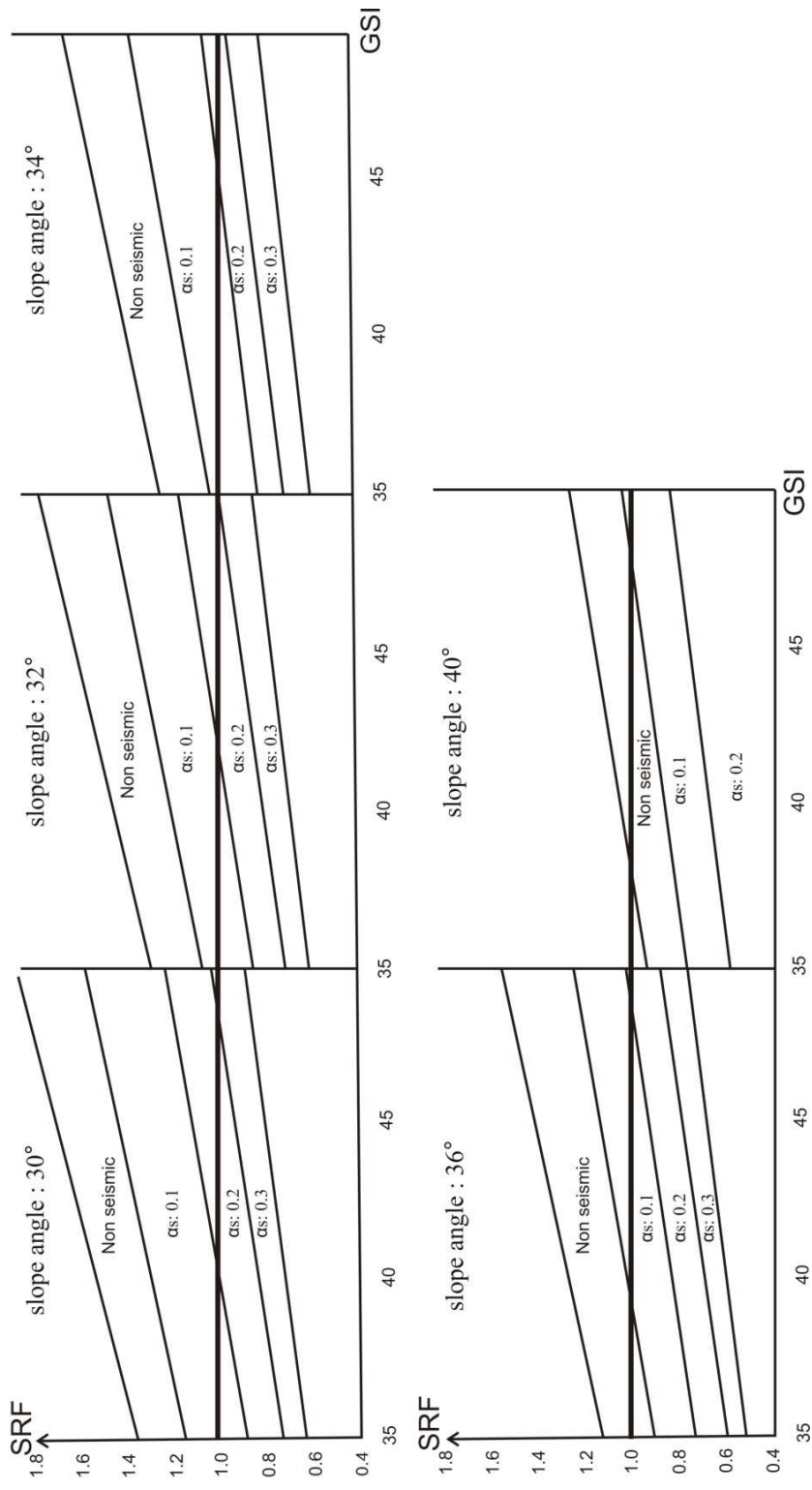


Figure 8.5 Relationship between GSI ratings and SRF values considering the different slope angles, seismic coefficients for all cross sections in 100% saturated condition for Mohr-Coulomb Criterion.

## Water Table Level:70% (Equivalent Mohr-Coulomb)

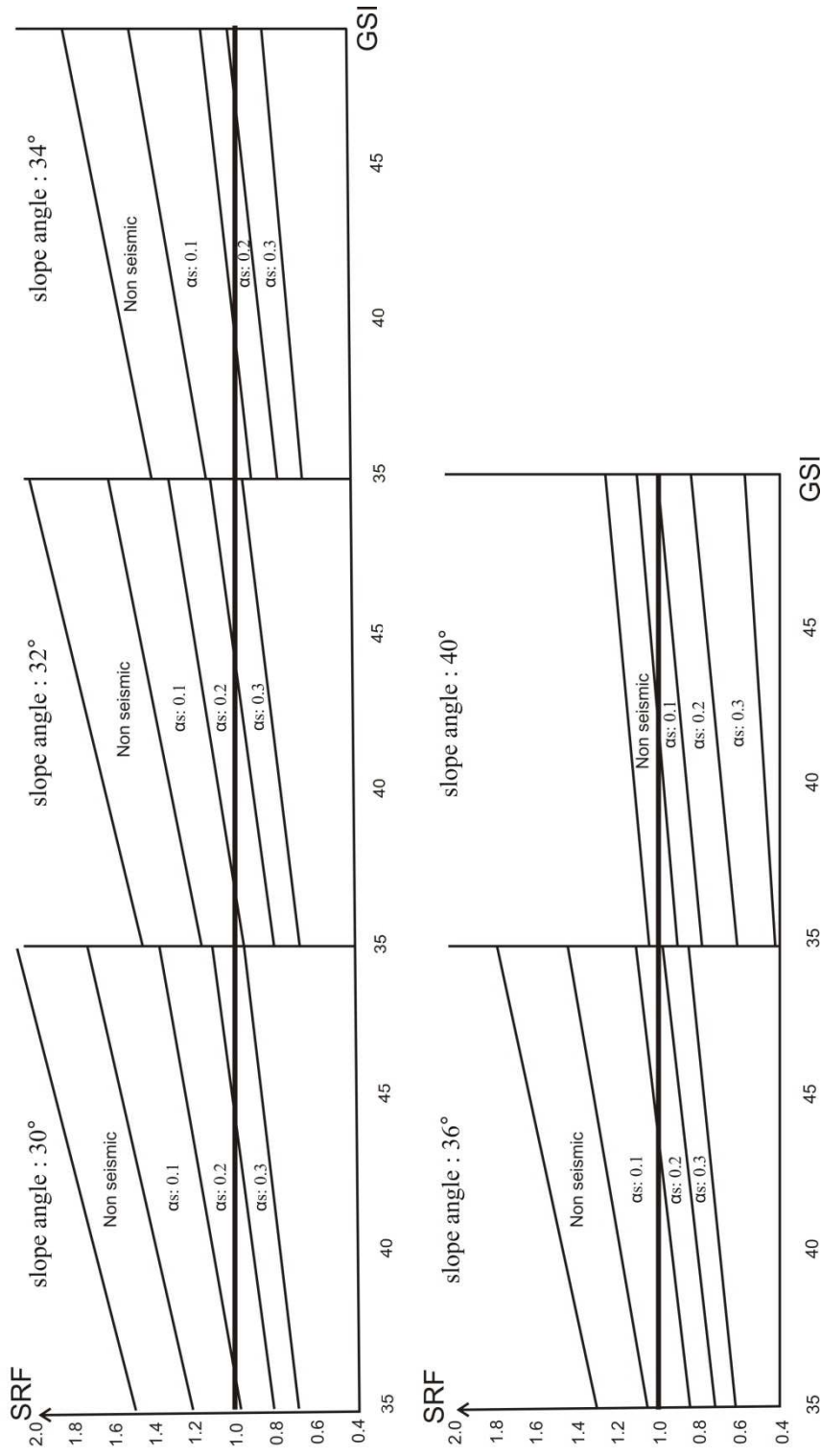


Figure 8.6 Relationship between GSI ratings and SRF values considering the different slope angles, seismic coefficients for all cross sections in 70% saturated condition for Mohr-Coulomb Criterion.

## Water Table Level: 50% (Equivalent Mohr-Coulomb)

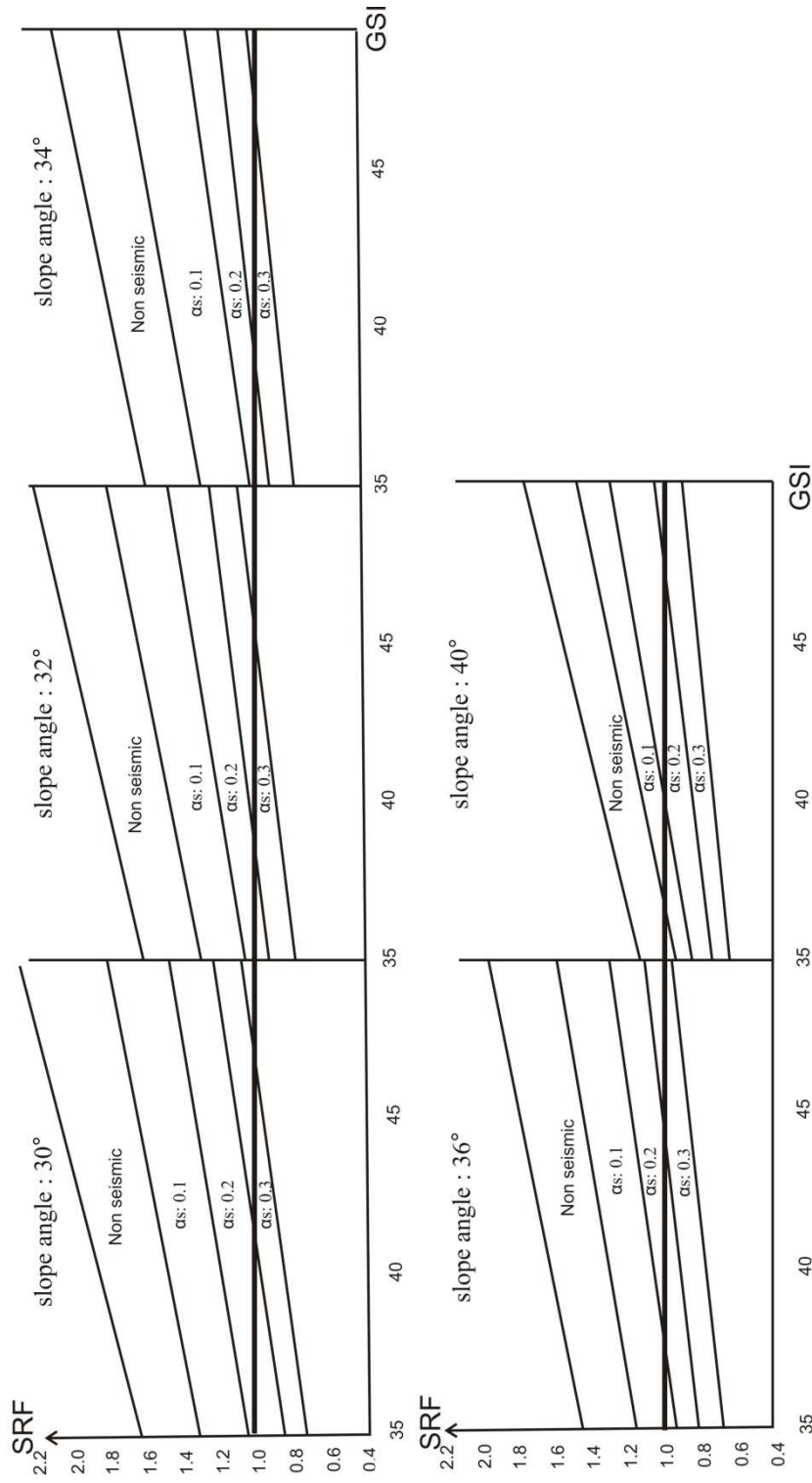


Figure 8.7 Relationship between GSI ratings and SRF values considering the different slope angles, seismic coefficients for all cross sections in 50% saturated condition for Mohr-Coulomb Criterion.

## **CHAPTER NINE**

### **COMPARISON OF THE RESULTS OBTAINED FROM TWO METHODS**

In order to compare the SRF values obtained from both methods, paired samples T test was performed with regard to five slope angles used in numerical analyses. This test computes the difference between the two variables for each case and gives significance degree in terms of the difference of means of each variable. The test results for each slope angle are shown in Appendix F.

The correlation coefficients of results for each slope angle are; 0.961, 0.920, 0.931, 0.916, 0.645, respectively.

Additionally, the T test results showed that for slope angles 30°, 32°, 34°, 36°, the SRF values obtained from Mohr-Coulomb Criterion are higher than the ones obtained from Generalized Hoek-Brown Criterion. Reversely, this overestimation of SRF values yield to a underestimation through the analyses for slope angle 40°.

The distribution of correlation coefficients with regard to various slope angles were illustrated in Figure 9.1. According to the distribution of correlation coefficients, it was revealed that the correlation between the SRF values obtained from both methods in terms of various slope angles have a strong negative, polynomial character.

Inversely to well correlation of SRF values throughout the computation for slope angles 30°, 32° and significant overestimation of SRF values throughout the computation for slope angles 34° and 36°, the SRF values were underestimated substantially for slope angle 40°. It is supposed that the reason is; when one of the benches constitute the overall slope have failed, the software detects these deformation as an overall slope failure and computes the SRF values in parallel with this. As a result, the SRF values can be found less than it is expected to be. According to that underestimated SRF values, the SRF values were manually increased and the critical SRF values for the overall slope named increased SRF were determined. These values were considered when evaluating the results. Besides, in

some models, even if the SRF values intend to be increased, the software did not permit. In this case, it was considered to be a stable condition for the overall slope except the bench failures (Figure 9.3).

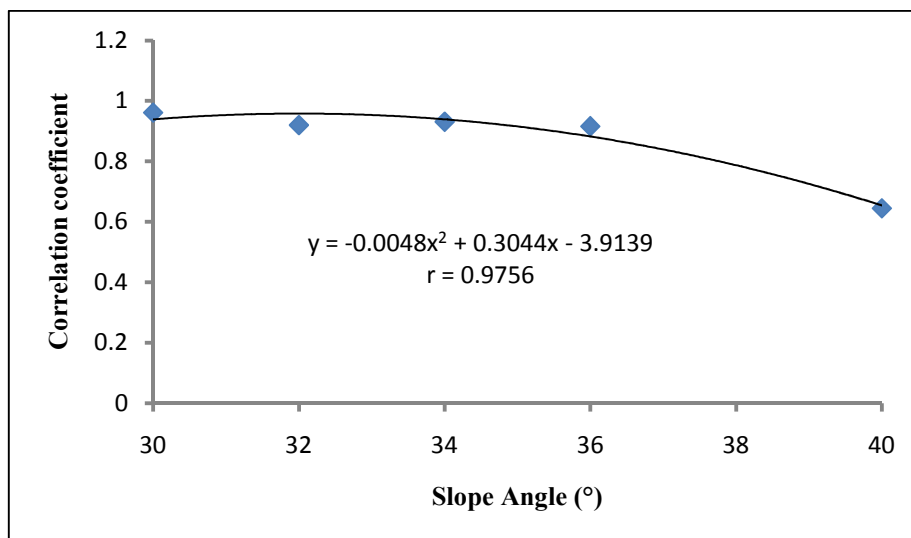


Figure 9.1 The relation between the correlation coefficients and slope angles.

Furthermore, the distribution of mean differences for all slope angles showed significant polynomial relation (Figure 9.2). In other words, as the slope angle increases until 34°, the mean difference increases. Although for 40°, the mean difference reaches the minimum value, the correlation becomes weak.

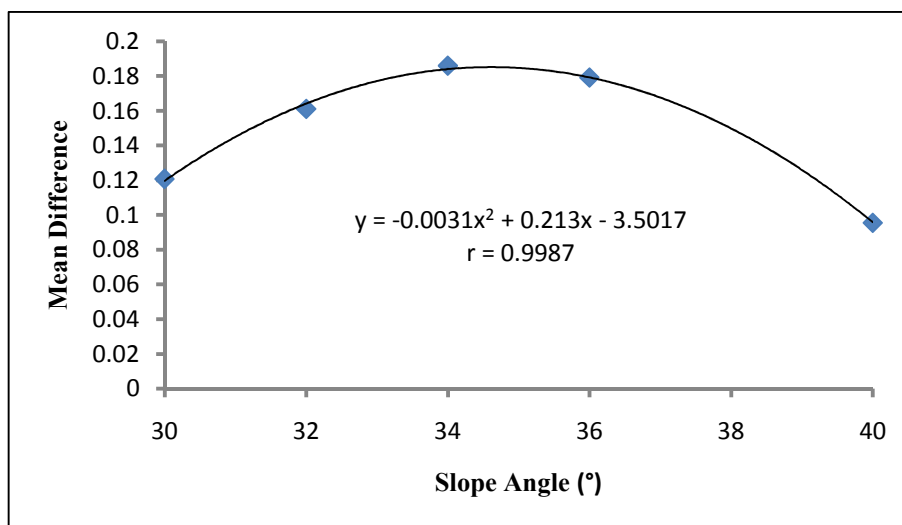


Figure 9.2 The relation between the mean differences of both method results and slope angles.

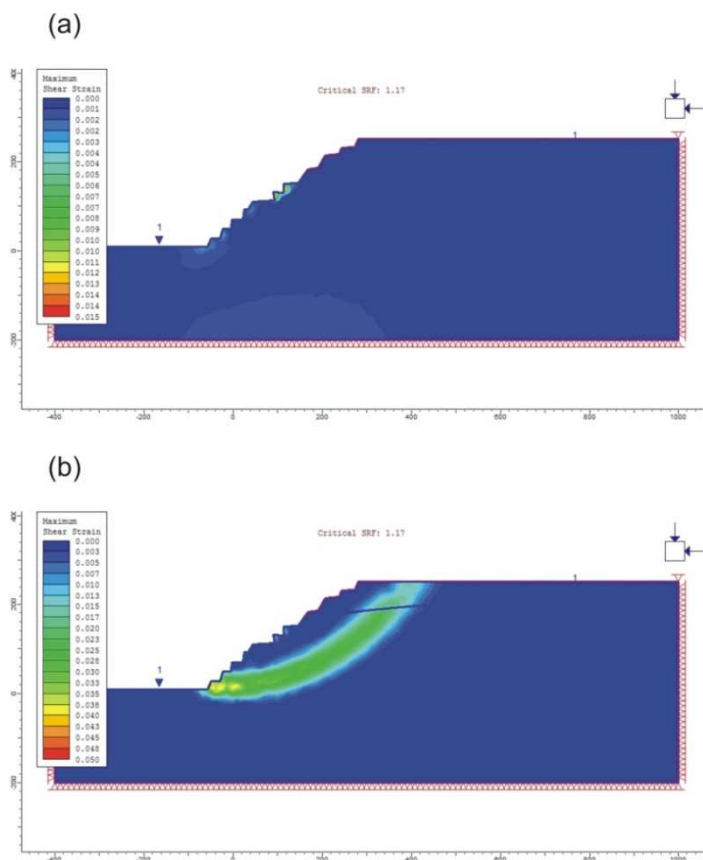


Figure 9.3 (a) Bench scale failure related to the critical SRF value;  
 (b) Overall slope failure related to the increased SRF value (GSI:45,  
 slope angle:  $36^\circ$ , non seismic, 70% saturated, D-D' cross section,  
 Mohr-Coulomb Criterion).

Consequently, for all outputs, the mean difference between the SRF values obtained from Generalized Hoek-Brown and Mohr-Coulomb Criterion is statistically significant at the level  $p < 0.01$ . This means, the results obtained from Generalized Hoek-Brown and Mohr-Coulomb Criterion did not match well. For slope angles  $30^\circ$  and  $32^\circ$ , the difference is fractional. Except that, starting from the slope angles  $34^\circ$  and  $36^\circ$ , the difference is getting greater and as Generalized Hoek-Brown Criterion estimates the SRF values less than 1, equivalent Mohr-Coulomb Criterion still estimates the SRF values greater than 1. This circumstance can lead the designer to suppose that the slope would stay stable, although the SRF values were overestimated.

As the SRF values obtained from Generalized Hoek-Brown Criterion decreases proportionally due to increasing of slope angle, the SRF values obtained from Mohr-Coulomb Criterion has shown a sudden decrease starting from the slope angle  $40^\circ$ .



## CHAPTER TEN

### CONCLUSIONS

Right after the the field survey and laboratory tests, numerical analyses performed on the rock slope models considering two methods using the two-dimensional finite element analysis program. The type of failure and optimum overall slope angle were estimated, furthermore the effect of variable parameters on the slope stability was investigated.

1. The resulting failure mode involved slip along the dominant joints and starts from the tension cracks on the crest of the slope and continues with a rotational character (Figure 10.1). This failure surface commonly cuts to the toe of the slope, rarely daylight on the slope face involving most of the benches. Underestimation of the SRF values in both methods depending on the steepness of the benches. As the dip angle of bench increases, the probability of failure of this bench increases. Consequently, FEM analysis estimates the SRF values very low according to the bench failures as supposing them the ultimate failure.

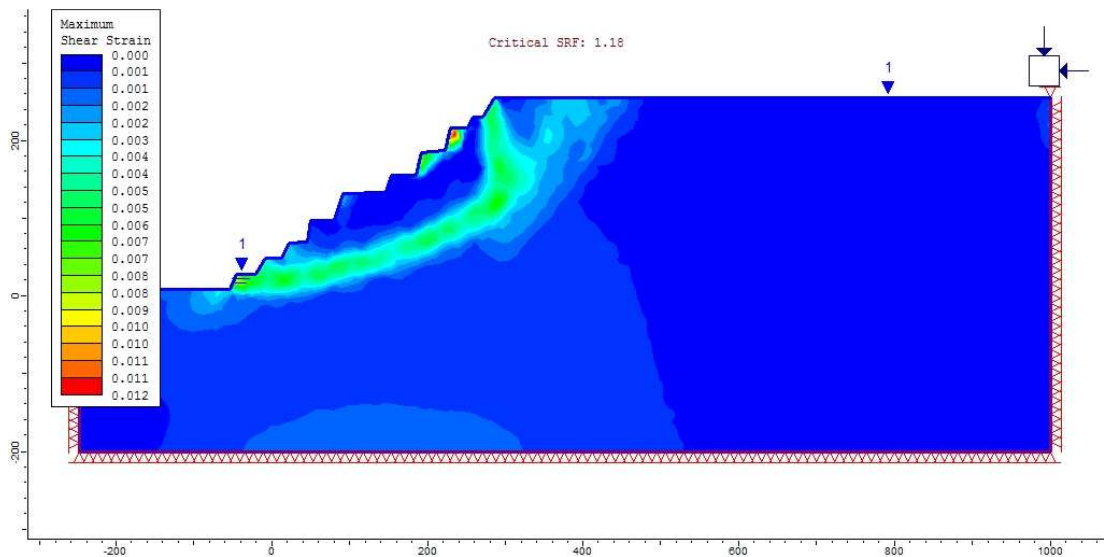


Figure 10.1 The illustration of failure mode (GSI:40, slope angle: 36°, non seismic, 100% saturated, B-B' cross section, Mohr-Coulomb Criterion).

2. As a result of the multivariate correlation of independent variables (GSI, seismic coefficient, slope angle, water table location and slope height) and dependent variable (SRF) considering the both methods; the slope angle was determined to be the most effective parameter on the slope stability, then which water table location, GSI, seismic coefficient and slope height are nominated, respectively.

3. Various slope angles ( $30^\circ$ ,  $32^\circ$ ,  $34^\circ$ ,  $36^\circ$ ,  $40^\circ$ ) were considered in FEM analyses. It was determined that the stability of slopes belonging to the eastern part of the open pit is sensitive to small changes of slope angle. With respect to the requirement of the optimum overall slope angle belonging to the future geometry and height of the overall slope, the models generated dependent on slope angle, water table location, GSI, seismic coefficient and slope height provides estimation for the critical SRF value for each condition of the slope (Figure 10.2).

It was determined from the graphs (Figures 7.6-7.8, 8.5-8.7) that it would not be possible to keep the overall slope stable for the dip angles of  $36^\circ$  and  $40^\circ$  unless the non seismic condition is considered. On the other hand, optimum overall slope angle was determined to be  $32^\circ$  under the conditions of WTL as 70%, seismic acceleration as 0.10 g and GSI as 42. The proposed optimum overall slope angle can be applied for the best way if only the present overall slope is trimmed from the upper slope face to the base of the mine as shown in Figure 10.2.

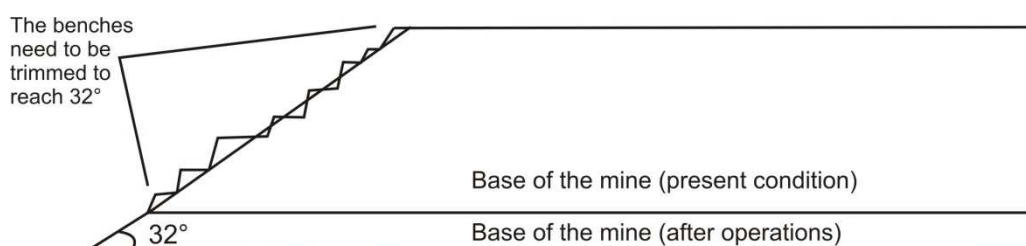


Figure 10.2 The illustration of the required operation in order to apply the proposed optimum overall slope angle fits the slope conditions.

4. Various water saturation degrees (100%, 70%, 50%) were considered in FEM analyses according to the levels of water seepage points observed in the field and also the meteorologic data for the study area obtained from DMİ's website.

Apart from the disturbing effect of water on slope stability, water content also increases the excavation costs. In terms of economical perspective, this case is undesirable.

It is useful to take some precautions for some slopes that does not permit the water table level to exceed 50% to stay stable. Hence, one of the remedial measures is the surface drainage of the slide area. Although surface drainage in itself is seldom sufficient for the stabilization of a slope in motion, it can contribute substantially to the drying and thus, controlling of the slides. Furthermore, all streams and temporary watercourses should be prevented. In addition, all springs issuing within the slide area, especially at its head must be entrapped and diverted outside of the slide area. For the immediate provisional diversion of water any pipes available may be used and for long term solution, drainage ditches paved by concrete tiles can be used.

5. GSI ratings were selected in the range between 35 and 45 for FEM analyses. As a result of the analyses, a GSI rating in the range between 40 and 45 is defined to be more appropriate for the orthogneiss since the critical SRF-values obtained from the method considering the Generalized Hoek-Brown Criterion are in agreement with the ones from Mohr-Coulomb in this interval.

6. Various seismic coefficients with respect to the seismicity of the study area (non-seismic, 0.1g, 0.2g, 0.3g) were considered in FEM analyses.

It was determined that the high seismic loading leads to tensile stresses within the rock mass. Since the rocks have very low tensile strength, failure occurs. This case is significant especially for steep slopes with high water saturation.

Analyses results showed that the depth of plastic zone remains almost unchanged for various seismic coefficients. In other words, the shape of the potential failure surface is almost independent of the magnitude of horizontal seismic coefficient ( $\alpha_s$ ) for each cross-section in jointed orthogneisses.

7. The slopes belonging to the five cross-sections taken perpendicular to the shear zone were considered as slope models in FEM analyses. The heights of these slopes are, 135 m, 123 m, 132 m, 121 m, 101 m, respectively.

Especially for the slope angle  $40^\circ$  in Generalized Hoek-Brown Failure Criterion, the SRF values related to slopes of each cross-section are very close to each other. This implies that the variation in the slope geometry and height does not have a significant effect on the SRF values when the other conditions remain the same, (Figure 10.3). However, commonly, E-E' cross-section is the most stable one than the others since its height is the shortest.

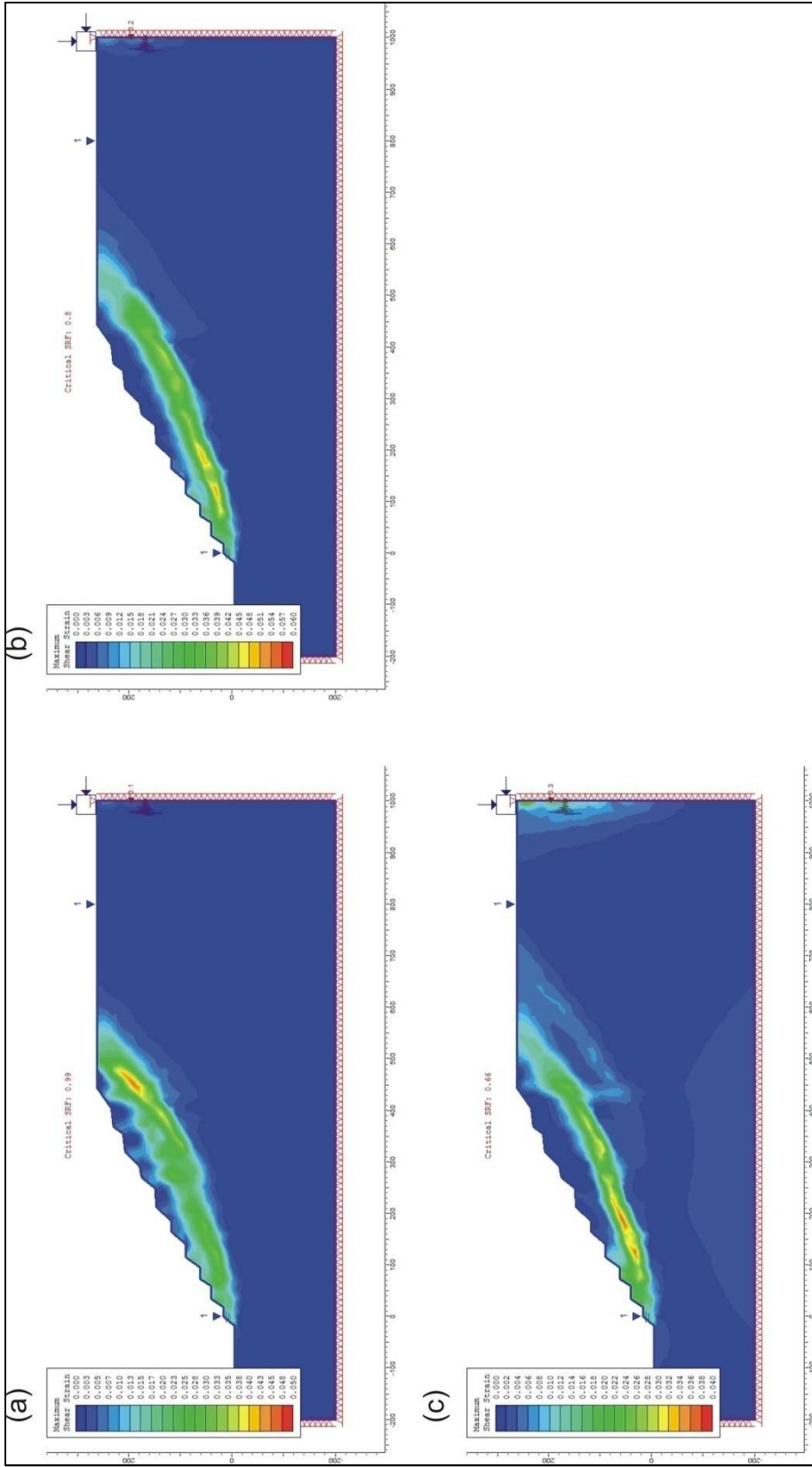


Figure 10.3 Comparisons between the depth of plastic zones for various seismic coefficients (a)  $\alpha_s$ : 0.1g; (b)  $\alpha_s$ : 0.2g; (c)  $\alpha_s$ : 0.3g (GSI:35, slope angle: 30°, 100% saturated, A-A' cross section, Mohr-Coulomb Criterion).

## REFERENCES

- Ambraseys, N. N., Finkel, C. F., (1995). *The seismicity of Turkey and adjacent areas, a historical review*, İstanbul: Eren Yayıncılık.
- Altunel, E., (1999). Geological and morphological observations in relation to the 20 September 1899 Menderes Earthquake, Western Turkey. *J. Geol. Soc. London*, 156, 241-246.
- Altunel, E., (1998). Evidence for damaging historical earthquakes at Priene, Western Turkey. *Turkish J. Earth Sci.*, 7, 25-35.
- Anon, (1977a). The description of rock masses for engineering purposes. *Quarterly Journal of Engineering Geology*, 10, 43–52.
- Barka, A., & Reilinger, R., (1997). Active tectonics of the Eastern Mediterranean Region: Deduced from GPS, neotectonic and seismicity data. *Annali de Geofisica*, 40(3), 587-610.
- Barton, N., (1978). Suggested methods for the quantitative description of discontinuities in rock masses, ISRM Commission on Standardization of Laboratory and Field Tests. *Int. J. Rock Mech. Min. Sci. Geomech., Abstr.* 15, 319–368.
- Beavis, F.C., (1985). *Engineering geology*. Melbourne, Boston: Blackwell Scientific Publications.
- Bell, F.G., (2007). *Engineering Geology* (2nd ed.). Oxford: Elsevier Linacre House.
- Bozkurt, E., Park, G.R., Winchester, J.A., (1993). Evidence against the core/cover interpretation of the Southern sector of the Menderes massif, West Turkey, *Terra Nova*, 145-151.
- BS 5930, (1981). *Code of Practice for Site Investigation*. London: British Standards Institution.

- Candan, O., Dora, O.Ö., (1998). Menderes masifinde granülit, eklojit ve mavi şist kalıntıları: Pan-Afrikan ve Tersiyer metamorfik evrimine bir yaklaşım. *Türkiye Jeoloji Bült.*, 41(1),1-35.
- Candan, O., Koralay, E., Dora, O.Ö., Chen, F., Oberhanslı, R., Çetinkaplan, M. et al., (2006). *Stratigraphy of the Pan – African Basement of the Menderes Massif and the primary contact relationship between core and cover series*. In Proceedings of Colloquium of the Menderes Massif, İzmir, Turkey, 8-14.
- Dawson, E.M., Roth, W.H., Drescher, A., (1999). Slope stability analysis by strength reduction. *Geotechnique*, 49 (6), 835-840.
- Deere, D.U., (1968). Geological considerations. In K.G. Stagg & O.C. Zienkiewicz (Ed.), *Rock Mechanics in Engineering Practice* (1-20). London: John Wiley and Sons.
- Depremsellik*. (n.d.). Retrieved January 11, 2011, from [http://www.jeofizik.comu.edu.tr/egitim/egitim/ders\\_notlari/.../jf407deprem.ppt](http://www.jeofizik.comu.edu.tr/egitim/egitim/ders_notlari/.../jf407deprem.ppt)
- Dora, O.Ö., Savaşçın, M.Y., Kun, N., Candan, O., (1987). Menderes Masifinde Post Metamorfik Plütonlar, *Yerbilimleri*, 14, 79-89.
- Fukushima, Y., Tanaka, T., (1990). A new attenuation relation for peak horizontal acceleration of strong earthquake ground motion in Japan. *Bull. Seism. Soc. Am.* 80, 757-783.
- Gerçek, H., (2004). *Kayaçların Poisson oranlarına göre sınıflanması*. In Proceedings of KayaMek'2004-VII. Bölgesel Kaya Mekaniği Sempozyumu, Sivas, Turkey.
- Goodman, Richard E., (1989). *Introduction to Rock Mechanics* (2nd ed.). London: John Wiley & Sons.
- Graciansky, P., (1965). Précisions sur le métamorphisme du massif de Menderes le long de sa bordure meridionale. *Bulletin of the Mineral Research and Exploration Institute of Turkey*, 64, 9-23.

- Hammah, R.E, Curran, J.H., Yacoub, T.E., & Corkum, B., (2004). *Stability analysis of rock slopes using the finite element method*. In Proceedings of the ISRM Regional Symposium EUROCK 2004 and the 53<sup>rd</sup> Geomechanics Colloquium, Salzburg, Austria.
- Hammah, R.E., Yacoub, T.E., Corkum, B., Curran, J.H., (2005). *The Shear strength reduction method for the Generalized Hoek-Brown Criterion*. In Proceedings of the 40<sup>th</sup> U.S. Symposium on Rock Mechanics, AlaskaRocks 2005, Anchorage, Alaska.
- Hoek, E., (1994). Strength of rock and masses, *ISRM News Journal*, 2 (2), 4-16.
- Hoek, E., (2006). Rock Mass Properties. In *Practical Rock Engineering* (1-47). Canada: The University of Toronto Press.
- Hoek, E. and Bray, J.W., (1981). *Rock Slope Engineering* (3rd ed.). London: Institution of Mining and Metallurgy.
- Hoek, E., Brown, E.T., (1980a). *Underground excavations in rock*. London: Inst. Min. Metall.
- Hoek, E., Brown, E.T., (1980b). Empirical strength criterion for rock masses. *Jour. Geotech. Engrg. Div., ASCE*, 106 (9), 1013-1035.
- Hoek, E., Carranza-Torres, C. and Corkum, B. (2002). *Hoek-Brown criterion-2002 edition*. In Proceedings of North American Rock Mechanics Symp., Toronto, Canada, 1, 267-273.
- Hoek, E and Diederichs, M.S. (2006). Empirical estimation of rock mass modulus. *International Journal of Rock Mechanics and Mining Sciences*, 43, 203–215.
- Hynes-Griffin, M.E. and A.G. Franklin, A.G., (1984). *Rationalizing the Seismic Coefficient Method*. Miscellaneous Paper GL-84-13, U.S. Department of the Army, Corps of Engineers, Waterways Experiment Station, Vicksburg, MS.



- ISRM, (1978a). Suggested Methods for the Quantitative Description of Discontinuities in Rock Masses. *Int. J. Rock Mech. Min. Sei. And Geomech. Abstr.*, 15, 319-368.
- ISRM, (1978b). Suggested Methods for Determining the Uniaxial Compressive Strength and Deformability of Rock Materials. *Int. J. Rock Mech. Min. Sei. and Geomech. Abstr.*, 16, 135-140.
- Koca, M.Y., Kahraman, B., Kınca, C., (2009). Observational geological report on eastern slope of the Alipaşa albite deposit in Karpuzlu, Çine. *Dokuz Eylül University, Engineering Faculty, Geological and Mining Engineering Department*, pp. 49.
- Koca, M.Y. and Kınca, C., (2004). Abandoned stone quarries in and around the Izmir city centre and their geo-environmental impacts-Turkey. *Engineering Geology*, 75, 49-67.
- Li, A.J., Lyamin, A.V., Merifield, R.S., (2009). Seismic rock slope stability charts based on limit analysis methods. *Computers and Geotechnics*, 36 (1-2), 135-148.
- Lorig, L., Varona, P., (2004). Numerical analysis. In D. C. Wyllie & C. W. Mah, (Ed.). *Rock slope Engineering, Civil and Mining* (4th ed.) (218-244). New York: Spon Press.
- Marinos, P., & Hoek, E., (2001). Estimating the geotechnical properties of heterogeneous rock masses such as flysch. *Bulletin of the Engineering Geology & the Environment (IAEG)*, 60, 85-92.
- National Earthquake Information Center (NEIC)*. Retrieved December 20, 2010 from <http://earthquake.usgs.gov/earthquakes/world/historical.php/>
- Okay, A.I., (2001). Stratigraphic and metamorphic inversions in the central Menderes Massif: A new structural model. *International Journal of Earth Sciences*, 91 (1), 173-178.

- Okay, A. I., (1989). Denizli'nin Güneyinde Menderes Masifi ve Likya Naplarının Jeolojisi. *MTA Dergisi*, 109, 45-58.
- Palmstrom, A., Singh, R., (2001). The deformation modulus of rock masses: comparisons between in situ tests and indirect estimates. *Tunnelling and Underground Space Technology*, 16, 115-131.
- Phase 2 V 7.013 Two-dimensional finite element analysis program. Rocscience Inc., 2010.
- Price, S. and Scott, B., (1994). Fault-block rotations at the edge of a zone of continental extension; southwest Turkey. *Journal of Structural Geol.*, 16, 381-392.
- Seed, H.B., (1979). Considerations in the earthquake-resistant design of earth and rockfill dams. *Geotechnique*, 29, 215–263.
- Şengör, A.M.C., (1982). *Ege'nin neotektonik evrimini yöneten etkenler, Batı Anadolu'nun genç tektoniği ve volkanizması*. In Proceedings of Türkiye Jeoloji Kurultayı panel, 59-71.
- Şengör A.M.C., (1987). Cross-faults and differential stretching of hanging walls in regions of low-angle normal faulting: examples from western Turkey. In M. P. Coward, J. F. Dewey, P. L. Hancock (Ed.). *Continental Extensional Tectonics*, Geological Society (28th ed.) (575–589). London: Geological Society.
- Terzaghi, K., 1950. Mechanism of landslides. In S. Paige, (Ed.). *Application of Geology to Engineering Practice* (Berkey Volume) (83–123). New York: Geological Society of America.
- Ulusay, R., Sönmez, H., 2007. *Kaya Kütlelerinin Mühendislik Özellikleri* (2nd ed.). Ankara: TMMOB Jeoloji Mühendisleri Odası.

Uygun, A., Gümüřcü, A., (2000). Geology and origin of the albite deposite of the Çine submassif, southern Menderes Massif (SW-Turkey). *Mineral Res. Expl. Bul.*, 122, 23-30.

Yılmaz, Y. (1997). Geology of Western Anatolia. In C. Schindler and M. Pfister (Ed.). *Active tectonics of NW Anatolia -The Marmara poly-project* (31-54). VDF, ETH Zurich.

**APPENDICES**  
**APPENDIX A – LABORATORY TEST RESULTS**

Test Number	Uniaxial Compressive Strength Test Results (MPa)	Unit Weight Determination Test (kN/m <sup>3</sup> )
1	24.08	25.90
2	36.30	25.91
3	23.20	25.91
4	33.30	25.91
5	22.04	25.90
6	21.02	25.90
7	29.03	25.90
8	30.12	25.93
9	26.00	25.89
10	35.01	25.91
11	20.02	25.89
12	28.01	25.92
13		25.89
14		25.90
15		25.91
16		25.91
17		25.90
18		25.90

## APPENDIX B – MEASUREMENTS OF WATER TABLE LEVEL

Table 1 The measurements of depth of water and elevation of water in drill holes along a selected line in the eastern slope of the Alipaşa open pit mine

Date	SK2		SK3		SK4		SK5		SK6		SK7		SK8		SK9		SK-10	
	D.W.	E.W.	D.W.	E.W.	D.W.	E.W.	D.W.	E.W.	D.W.	E.W.	D.W.	E.W.	D.W.	E.W.	D.W.	E.W.	D.W.	E.W.
<b>30.04.10</b>	1.05	410.32	1.30	428.24	2.00	440.14	13.90	448.39	1.45	471.50	11.30	473.11	14.50	484.63	5.10	511.85	9.20	521.18
<b>07.05.10</b>	1.28	410.09	1.37	428.17	2.96	439.18	11.30	450.99	1.40	471.55	5.30	479.11	9.40	489.73	5.10	511.85	6.00	524.38
<b>14.05.10</b>	1.30	410.07	1.35	428.19	3.45	438.69	11.40	450.89	1.50	471.45	4.85	479.56	8.25	490.88	5.10	511.85	5.70	524.68
<b>28.05.10</b>	1.10	410.27	1.25	428.29	1.90	440.24	11.20	451.09	1.20	471.75	4.05	480.36	7.95	491.18	4.80	512.15	6.00	524.38
<b>04.06.10</b>	1.30	410.07	1.40	428.14	2.60	439.54	11.20	451.09	1.30	471.65	3.80	480.61	7.95	491.18	4.70	512.25	6.20	524.18
<b>11.06.10</b>	1.30	410.07	1.40	428.14	2.95	439.19	11.30	450.99	1.20	471.75	3.70	480.71	7.95	491.18	4.40	512.25	6.50	523.88

*D.W.* : Depth of water, *E.W.* : Elevation of water, *SK* : Drill hole

## APPENDIX C - GENERALIZED HOEK-BROWN ANALYSES RESULTS

Table 1 SRF-values for the discontinuous rock mass under the water table level of 100% considering both non-seismic and seismic effects (slope stability analysis were conducted by using the Generalized Hoek & Brown Failure Criterion)

Slope Angle	Seismic Coefficient	GSI	SRF					
			A-A'	B-B'	C-C'	D-D'	E-E'	
30°	0	35	1.14	1.10	1.22	1.15	1.20	
		40	1.27	1.24	1.35	1.30	1.41	
		45	1.41	1.39	1.49	1.46	1.61	
	0.1	35	0.88	0.98	0.95	0.95	1.02	
		40	0.99	1.10	1.05	1.05	1.14	
		45	1.07	1.22	1.15	1.17	1.26	
	0.2	35	0.74	0.80	0.76	0.74	0.84	
		40	0.80	0.88	0.83	0.80	0.92	
		45	0.87	0.95	0.90	0.89	1.02	
	0.3	35	0.61	0.69	0.64	0.62	0.69	
		40	0.66	0.76	0.70	0.68	0.77	
		45	0.72	0.83	0.76	0.74	0.85	
32°	0	35	1.10	1.09	1.06	1.05	1.15	
		40	1.22	1.25	1.2	1.23	1.29	
		45	1.34	1.39	1.34	1.38	1.41	
	0.1	35	0.85	0.86	0.86	0.87	0.86	
		40	0.94	0.96	0.94	0.96	0.95	
		45	1.04	1.07	1.02	1.07	1.07	
	0.2	35	0.71	0.73	0.71	0.72	0.74	
		40	0.77	0.79	0.78	0.79	0.80	
		45	0.83	0.86	0.85	0.86	0.86	
	0.3	35	0.59	0.59	0.61	0.62	0.65	
		40	0.66	0.67	0.68	0.68	0.71	
		45	0.71	0.71	0.74	0.74	0.76	
34°	0	35	0.95	0.85	0.96	0.90	0.96	
		40	1.07	0.90	1.07	1.05	1.11	
		45	1.19	1.04	1.19	1.25	1.31	
	0.1	35	0.77	0.81	0.76	0.79	0.86	
		40	0.83	0.88	0.83	0.86	0.96	
		45	0.87	0.92	0.89	0.93	1.09	
	34°	0.2	35	0.65	0.68	0.63	0.63	0.75
			40	0.71	0.74	0.67	0.70	0.82
			45	0.76	0.80	0.74	0.76	0.89
		0.3	35	0.53	0.57	0.53	0.53	0.62
			40	0.58	0.63	0.59	0.58	0.68
			45	0.63	0.69	0.63	0.64	0.72
36°		0	35	0.86	0.86	0.84	0.89	0.86
			40	0.95	0.96	0.90	1.02	0.97
			45	1.07	1.12	1.00	1.15	0.995
		0.1	35	0.74	0.79	0.71	0.78	0.79
			40	0.80	0.85	0.78	0.85	0.86
			45	0.86	0.91	0.83	0.93	0.91
	0.2	35	0.59	0.65	0.59	0.66	0.65	
		40	0.65	0.71	0.65	0.72	0.71	
		45	0.70	0.78	0.70	0.79	0.74	
	0.3	35	0.48	0.52	0.50	0.56	0.55	
		40	0.56	0.58	0.55	0.61	0.60	
		45	0.59	0.63	0.59	0.66	0.65	
40°	0	35	0.73	0.75	0.79	0.56	0.55	
		40	0.79	0.60	0.86	0.60	0.58	
		45	0.84	0.77	0.93	0.62	0.61	
	0.1	35	0.60	0.50	0.65	0.54	0.54	
		40	0.67	0.54	0.69	0.58	0.57	
		45	0.69	0.56	0.76	0.62	0.60	
	0.2	35	0.50	0.50	0.51	0.47	0.50	
		40	0.54	0.53	0.56	0.51	0.54	
		45	0.57	0.55	0.60	0.55	0.57	
	0.3	35	0.39	0.43	0.43	0.32	0.40	
		40	0.42	0.47	0.46	0.32	0.42	
		45	0.45	0.48	0.51	0.39	0.49	

Table 2 SRF-values for the discontinuous rock mass under the water table level of 70% considering both non-seismic and seismic effects (slope stability analysis were conducted by using the Generalized Hoek & Brown Failure Criterion)

Slope Angle	Seismic Coefficient	GSI	SRF				E-E'
			A-A'	B-B'	C-C'	D-D'	
30°	0	35	1.20	0.99	1.33	1.15	1.25
		40	1.37	1.17	1.47	1.30	1.47
		45	1.52	1.39	1.62	1.46	1.70
	0.1	35	0.90	0.98	1.04	1.01	1.07
		40	1.00	1.12	1.15	1.17	1.21
		45	1.12	1.26	1.28	1.30	1.41
	0.2	35	0.78	0.90	0.82	0.81	0.92
		40	0.84	1.02	0.90	0.88	1.02
		45	0.90	1.13	0.99	0.95	1.13
	0.3	35	0.65	0.74	0.69	0.69	0.77
		40	0.71	0.83	0.75	0.75	0.86
		45	0.77	0.89	0.81	0.80	0.93
32°	0	35	1.13	1.07	1.11	1.07	1.21
		40	1.27	1.26	1.26	1.02	1.37
		45	1.41	1.43	1.40	1.23	1.56
	0.1	35	0.88	0.94	0.92	0.86	1.02
		40	0.99	1.06	1.03	0.96	1.14
		45	1.11	1.22	1.13	1.09	1.26
0.2	35	0.74	0.82	0.75	0.79	0.79	
	40	0.82	0.88	0.83	0.86	0.84	
	45	0.90	0.93	0.90	0.91	0.92	
0.3	35	0.64	0.70	0.64	0.69	0.71	
	40	0.70	0.76	0.70	0.75	0.78	
	45	0.76	0.83	0.76	0.82	0.83	
34°	0	35	0.96	0.84	0.98	0.84	1.16
		40	1.09	0.89	1.10	0.86	1.31
		45	1.22	0.98	1.25	0.92	1.50
	0.1	35	0.80	0.84	0.83	0.83	0.97
		40	0.86	0.89	0.86	0.89	1.08
		45	0.91	0.96	0.91	0.95	1.23

Slope Angle	Seismic Coefficient	GSI	SRF				E-E'	
			A-A'	B-B'	C-C'	D-D'		
34°	0.2	35	0.71	0.77	0.63	0.72	0.83	
		40	0.77	0.83	0.67	0.77	0.89	
		45	0.83	0.89	0.74	0.83	1.00	
	0.3	35	0.60	0.65	0.53	0.60	0.71	
		40	0.66	0.72	0.59	0.67	0.77	
		45	0.72	0.78	0.63	0.72	0.85	
	36°	0	35	0.85	0.96	0.84	0.81	0.89
			40	0.91	1.08	0.90	0.70	1.06
			45	1.02	1.24	1.00	1.06	1.36
		0.1	35	0.77	0.85	0.71	0.80	0.86
			40	0.84	0.90	0.78	0.86	0.93
			45	0.90	1.02	0.83	0.91	1.10
40°	0.2	35	0.65	0.76	0.59	0.74	0.74	
		40	0.72	0.83	0.65	0.81	0.84	
		45	0.76	0.89	0.70	0.86	0.90	
	0.3	35	0.53	0.64	0.50	0.62	0.63	
		40	0.59	0.70	0.55	0.68	0.70	
		45	0.63	0.76	0.59	0.74	0.79	
40°	0	35	0.74	0.51	0.79	0.56	0.64	
		40	0.79	0.54	0.86	0.60	0.68	
		45	0.86	0.56	0.93	0.62	0.71	
	0.1	35	0.64	0.49	0.65	0.75	0.56	
		40	0.69	0.52	0.69	0.80	0.59	
		45	0.74	0.54	0.76	0.86	0.61	
40°	0.2	35	0.58	0.65	0.51	0.65	0.51	
		40	0.62	0.66	0.56	0.71	0.56	
		45	0.66	0.73	0.60	0.78	0.59	
	0.3	35	0.52	0.57	0.43	0.58	0.46	
		40	0.55	0.63	0.46	0.63	0.51	
		45	0.60	0.69	0.51	0.69	0.56	

Table 3 SRF-values for the discontinuous rock mass under the water table level of 50% considering both non-seismic and seismic effects (slope stability analysis were conducted by using the Generalized Hoek & Brown Failure Criterion).

Slope Angle	Seismic Coefficient	GSI	SRF				
			A-A'	B-B'	C-C'	D-D'	E-E'
30°	0	35	1.26	1.09	1.33	1.18	1.24
		40	1.42	1.24	1.52	1.30	1.50
		45	1.58	1.39	1.69	1.46	1.73
	0.1	35	0.94	1.07	1.09	1.03	1.07
		40	1.05	1.12	1.21	1.17	1.21
		45	1.18	1.28	1.35	1.33	1.41
	0.2	35	0.80	0.90	0.87	0.86	0.98
		40	0.87	1.02	0.97	0.92	1.11
		45	0.92	1.17	1.05	1.05	1.25
	0.3	35	0.69	0.81	0.76	0.77	0.84
		40	0.75	0.87	0.82	0.83	0.92
		45	0.82	0.94	0.87	0.88	1.01
32°	0	35	1.12	1.25	1.06	0.91	1.16
		40	1.27	1.24	1.24	1.06	1.31
		45	1.44	1.46	1.46	1.25	1.53
	0.1	35	0.93	0.98	0.94	0.86	1.04
		40	1.05	1.12	1.05	0.995	1.16
		45	1.16	1.27	1.16	1.15	1.24
	0.2	35	0.79	0.85	0.80	0.83	0.85
		40	0.85	0.90	0.86	0.89	0.93
		45	0.91	1.03	0.91	0.94	0.99
	0.3	35	0.67	0.75	0.69	0.76	0.77
		40	0.75	0.82	0.76	0.84	0.83
		45	0.81	0.89	0.83	0.90	0.88
34°	0	35	0.97	1.10	0.93	0.86	1.18
		40	1.10	1.23	1.06	0.94	1.34
		45	1.27	1.40	1.20	1.13	1.50
	0.1	35	0.85	0.86	0.82	0.84	1.03
		40	0.90	0.95	0.88	0.89	1.15
		45	1.01	1.12	0.92	0.97	1.33

Slope Angle	Seismic Coefficient	GSI	SRF				
			A-A'	B-B'	C-C'	D-D'	E-E'
34°	0.2	35	0.76	0.83	0.72	0.79	0.86
		40	0.82	0.89	0.78	0.84	0.93
		45	0.88	0.98	0.83	0.89	1.08
	0.3	35	0.66	0.74	0.65	0.71	0.80
		40	0.74	0.80	0.70	0.78	0.86
		45	0.78	0.86	0.75	0.85	0.91
36°	0	35	0.86	1.06	0.86	0.86	0.99
		40	0.96	1.19	1.00	0.995	1.19
		45	1.11	1.34	1.11	1.12	1.38
	0.1	35	0.83	0.87	0.79	0.83	0.86
		40	0.88	0.98	0.87	0.89	0.95
		45	0.92	1.13	0.92	0.95	1.13
	0.2	35	0.69	0.82	0.70	0.79	0.83
		40	0.73	0.87	0.76	0.85	0.88
		45	0.80	0.92	0.81	0.91	0.93
	0.3	35	0.54	0.72	0.63	0.72	0.73
		40	0.60	0.80	0.69	0.78	0.79
		45	0.65	0.86	0.74	0.84	0.85
40°	0	35	0.81	0.83	0.79	0.56	0.76
		40	0.87	0.85	0.84	0.59	0.82
		45	0.91	0.90	0.89	0.62	0.85
	0.1	35	0.76	0.79	0.74	0.59	0.67
		40	0.82	0.84	0.80	0.63	0.74
		45	0.88	0.89	0.85	0.66	0.87
	0.2	35	0.68	0.75	0.64	0.54	0.70
		40	0.74	0.82	0.69	0.59	0.76
		45	0.80	0.86	0.75	0.65	0.80
	0.3	35	0.58	0.81	0.55	0.48	0.65
		40	0.64	0.89	0.61	0.54	0.70
		45	0.70	0.97	0.67	0.57	0.75



## APPENDIX D - MOHR-COULOMB ANALYSES RESULTS

Table 1 SRF-values for the discontinuous rock mass under the water table level of 100% considering both non-seismic and seismic effects (slope stability analysis were conducted by using the Mohr-Coulomb Failure Criterion).

Slope Angle	Seismic Coefficient	GSI	SRF				
			A-A'	B-B'	C-C'	D-D'	E-E'
30°	0	35	1.19	1.29	1.24	1.27	1.36
		40	1.33	1.44	1.38	1.42	1.52
		45	1.48	1.59	1.53	1.57	1.69
	0.1	35	0.95	1.03	0.98	1.00	1.08
		40	1.06	1.15	1.09	1.12	1.20
		45	1.18	1.27	1.21	1.24	1.33
	0.2	35	0.78	0.85	0.80	0.82	0.88
		40	0.87	0.95	0.89	0.92	0.98
		45	0.97	1.05	0.99	1.02	1.09
	0.3	35	0.65	0.71	0.66	0.68	0.73
		40	0.73	0.79	0.74	0.77	0.81
		45	0.81	0.88	0.82	0.85	0.90
32°	0	35	1.12	1.21	1.15	1.19	1.27
		40	1.26	1.35	1.28	1.32	1.42
		45	1.39	1.50	1.42	1.47	1.58
	0.1	35	0.90	0.96	0.92	0.96	1.01
		40	1.01	1.08	1.02	1.07	1.13
		45	1.12	1.19	1.14	1.19	1.26
0.2	35	0.73	0.80	0.76	0.78	0.84	
	40	0.82	0.90	0.85	0.88	0.94	
	45	0.91	0.995	0.94	0.97	1.04	
0.3	35	0.61	0.67	0.64	0.65	0.70	
	40	0.68	0.74	0.72	0.72	0.78	
	45	0.76	0.83	0.79	0.81	0.87	
34°	0	35	1.05	1.13	1.07	1.12	1.21
		40	1.18	1.26	1.20	1.25	1.35
		45	1.31	1.40	1.33	1.39	1.49
	0.1	35	0.86	0.91	0.86	0.91	0.97
		40	0.96	1.02	0.96	1.02	1.08
		45	1.06	1.13	1.07	1.13	1.20

Slope Angle	Seismic Coefficient	GSI	SRF				
			A-A'	B-B'	C-C'	D-D'	E-E'
34°	0.2	35	0.70	0.75	0.70	0.74	0.80
		40	0.79	0.84	0.79	0.83	0.89
		45	0.87	0.93	0.88	0.92	0.995
	0.3	35	0.58	0.62	0.59	0.61	0.67
		40	0.65	0.70	0.66	0.69	0.75
		45	0.73	0.78	0.73	0.77	0.83
36°	0	35	0.98	1.05	0.99	1.05	1.12
		40	1.10	1.18	1.11	1.17	1.25
		45	1.22	1.31	1.23	1.30	1.39
	0.1	35	0.80	0.85	0.79	0.85	0.90
		40	0.89	0.95	0.89	0.95	1.01
		45	0.99	1.06	0.98	1.06	1.12
0.2	35	0.66	0.70	0.64	0.71	0.73	
	40	0.74	0.79	0.71	0.79	0.82	
	45	0.82	0.88	0.79	0.88	0.91	
40°	0.3	35	0.55	0.58	0.53	0.59	0.59
		40	0.61	0.66	0.60	0.66	0.66
		45	0.68	0.73	0.67	0.73	0.74
	0	35	0.48	0.52	0.50	0.53	0.52
		40	0.56	0.60	0.54	0.60	0.64
		45	0.64	0.69	0.63	0.69	0.74
0.1	35	0.48	0.52	0.50	0.53	0.52	
	40	0.56	0.60	0.54	0.60	0.64	
	45	0.64	0.69	0.63	0.69	0.74	
40°	0.2	35	0.38	0.42	0.40	0.43	0.44
		40	0.46	0.50	0.44	0.50	0.54
		45	0.54	0.58	0.52	0.58	0.62
	0.3	35	0.30	0.33	0.31	0.34	0.35
		40	0.36	0.39	0.36	0.39	0.41
		45	0.42	0.45	0.42	0.45	0.47

Table 2 SRF-values for the discontinuous rock mass under the water table level of 70% considering both non-seismic and seismic effects (slope stability analysis were conducted by using the Mohr-Coulomb Failure Criterion).

Slope Angle	Seismic Coefficient	GSI	SRF					
			A-A'	B-B'	C-C'	D-D'	E-E'	
30°	0	35	1.30	1.41	1.36	1.40	1.52	
		40	1.45	1.57	1.52	1.56	1.69	
		45	1.61	1.74	1.68	1.73	1.87	
	0.1	35	1.04	1.14	1.09	1.12	1.21	
		40	1.16	1.27	1.22	1.25	1.35	
		45	1.29	1.41	1.35	1.39	1.50	
	0.2	35	0.84	0.94	0.89	0.91	0.98	
		40	0.94	1.04	1.00	1.02	1.10	
		45	1.05	1.16	1.11	1.13	1.22	
	0.3	35	0.70	0.78	0.73	0.75	0.81	
		40	0.78	0.87	0.81	0.84	0.90	
		45	0.87	0.97	0.90	0.94	1.00	
32°	0	35	1.24	1.35	1.30	1.33	1.45	
		40	1.39	1.50	1.45	1.48	1.62	
		45	1.54	1.67	1.61	1.65	1.80	
	0.1	35	1.00	1.09	1.05	1.08	1.17	
		40	1.12	1.22	1.18	1.20	1.31	
		45	1.25	1.35	1.31	1.33	1.45	
	0.2	35	0.82	0.88	0.86	0.89	0.96	
		40	0.92	0.99	0.96	0.995	1.07	
		45	1.03	1.10	1.07	1.10	1.19	
	0.3	35	0.68	0.74	0.71	0.74	0.80	
		40	0.76	0.82	0.79	0.82	0.89	
		45	0.85	0.91	0.88	0.92	0.99	
34°	0	35	1.18	1.29	1.23	1.27	1.39	
		40	1.32	1.44	1.37	1.42	1.55	
		45	1.46	1.59	1.52	1.57	1.72	
	0.1	35	0.96	1.05	1.00	1.04	1.12	
		40	1.07	1.17	1.12	1.16	1.26	
		45	1.19	1.30	1.25	1.29	1.39	
	36°	0	35	1.11	1.23	1.17	1.21	1.32
			40	1.25	1.37	1.30	1.34	1.47
			45	1.39	1.52	1.45	1.49	1.63
		0.1	35	0.92	1.01	0.96	0.99	1.07
			40	1.02	1.13	1.07	1.09	1.19
			45	1.14	1.25	1.19	1.21	1.33
0.2		35	0.76	0.84	0.80	0.83	0.88	
		40	0.85	0.94	0.90	0.93	0.99	
		45	0.94	1.04	1.00	1.03	1.10	
0.3		35	0.63	0.69	0.66	0.69	0.73	
		40	0.71	0.77	0.75	0.77	0.82	
		45	0.79	0.86	0.83	0.86	0.92	
40°	0	35	0.97	1.02	0.95	0.98	1.04	
		40	1.09	1.14	1.02	1.05	1.08	
		45	1.21	1.26	1.13	1.16	1.21	
	0.1	35	0.80	0.84	0.84	0.84	0.95	
		40	0.89	0.99	0.94	0.94	1.05	
		45	1.00	1.06	1.05	1.07	1.16	
	0.2	35	0.61	0.68	0.68	0.68	0.85	
		40	0.69	0.87	0.76	0.76	0.95	
		45	0.77	0.97	0.85	0.85	1.06	
	0.3	35	0.44	0.66	0.56	0.62	0.72	
		40	0.49	0.74	0.63	0.63	0.81	
		45	0.55	0.82	0.70	0.70	0.90	

Table 3 SRF-values for the discontinuous rock mass under the water table level of 50% considering both non-seismic and seismic effects (slope stability analysis were conducted by using the Mohr-Coulomb Failure Criterion).

Slope Angle	Seismic Coefficient	GSI	SRF				
			A-A'	B-B'	C-C'	D-D'	E-E'
30°	0	35	1.39	1.51	1.46	1.51	1.64
		40	1.56	1.68	1.63	1.68	1.83
		45	1.73	1.86	1.80	1.86	2.03
	0.1	35	1.12	1.22	1.18	1.22	1.32
		40	1.25	1.36	1.31	1.36	1.47
		45	1.38	1.50	1.45	1.50	1.63
	0.2	35	0.91	1.00	0.97	1.00	1.08
		40	1.02	1.12	1.08	1.12	1.20
		45	1.13	1.23	1.20	1.24	1.33
	0.3	35	0.77	0.85	0.80	0.84	0.89
		40	0.86	0.94	0.90	0.93	0.99
		45	0.95	1.04	1.00	1.04	1.10
32°	0	35	1.33	1.45	1.39	1.44	1.58
		40	1.48	1.61	1.55	1.61	1.76
		45	1.65	1.79	1.71	1.78	1.95
	0.1	35	1.08	1.17	1.11	1.18	1.27
		40	1.21	1.31	1.24	1.31	1.42
		45	1.34	1.45	1.38	1.45	1.58
0.2	35	0.90	0.96	0.91	0.98	1.05	
	40	1.00	1.07	1.01	1.09	1.17	
	45	1.11	1.19	1.12	1.21	1.30	
34°	0	35	0.75	0.80	0.75	0.82	0.88
		40	0.84	0.89	0.84	0.92	0.98
		45	0.93	0.995	0.94	1.02	1.09
	0.1	35	1.27	1.39	1.33	1.37	1.51
		40	1.42	1.55	1.49	1.53	1.68
		45	1.58	1.72	1.65	1.73	1.86
0.2	35	1.04	1.13	1.08	1.13	1.23	
	40	1.16	1.27	1.21	1.26	1.37	
	45	1.29	1.40	1.34	1.41	1.52	

Slope Angle	Seismic Coefficient	GSI	SRF					
			A-A'	B-B'	C-C'	D-D'	E-E'	
34°	0.2	35	0.86	0.94	0.90	0.96	1.01	
		40	0.97	1.05	1.01	1.06	1.13	
		45	1.07	1.16	1.12	1.18	1.26	
	0.3	35	0.73	0.78	0.76	0.82	0.85	
		40	0.81	0.88	0.85	0.91	0.95	
		45	0.90	0.97	0.94	1.01	1.05	
	36°	0	35	1.22	1.33	1.28	1.32	1.44
			40	1.36	1.49	1.43	1.47	1.61
			45	1.51	1.65	1.58	1.63	1.78
		0.1	35	1.00	1.10	1.05	1.09	1.18
			40	1.12	1.23	1.18	1.22	1.32
			45	1.24	1.36	1.30	1.35	1.46
40°	0.2	35	0.83	0.91	0.88	0.91	0.98	
		40	0.93	1.01	0.99	1.02	1.09	
		45	1.03	1.13	1.09	1.13	1.21	
	0.3	35	0.70	0.76	0.75	0.78	0.83	
		40	0.79	0.86	0.84	0.87	0.92	
		45	0.88	0.95	0.93	0.97	1.02	
40°	0	35	1.11	1.11	1.11	1.11	1.15	
		40	1.24	1.24	1.24	1.24	1.26	
		45	1.37	1.37	1.37	1.37	1.41	
	0.1	35	0.91	1.02	0.94	1.03	1.06	
		40	1.02	1.11	1.06	1.11	1.16	
		45	1.14	1.27	1.17	1.27	1.33	
0.2	35	0.77	0.85	0.82	0.82	0.90		
	40	0.86	0.95	0.92	0.92	1.00		
	45	0.96	1.05	1.01	1.02	1.10		
0.3	35	0.64	0.81	0.70	0.64	0.79		
	40	0.72	0.91	0.78	0.72	0.88		
	45	0.80	1.01	0.87	0.80	0.98		

## APPENDIX E – MULTIVARIATE ANALYSES RESULTS

Table 1 The correlations between SRF values obtained from Generalized Hoek-Brown Criterion and the variants used in the FEM analyses

SRF	SRF	GSI	watertablelocation	seismiccoefficient	slopeheight	slopeangle
Pearson Correlation	1	.286(**)	-.208(**)	-.186(**)	-.116(**)	-.559(**)
Sig. (2-tailed)		.000	.000	.000	.000	.000
N	900	900	900	900	900	900
Pearson Correlation	.286(**)	1	.000	.000	.000	.000
Sig. (2-tailed)	.000	1.000	1.000	1.000	1.000	1.000
N	900	900	900	900	900	900
Pearson Correlation	-.208(**)	.000	1	.000	.000	.000
Sig. (2-tailed)	.000	1.000	1.000	1.000	1.000	1.000
N	900	900	900	900	900	900
Pearson Correlation	-.186(**)	.000	.000	1	.000	.000
Sig. (2-tailed)	.000	1.000	1.000	1.000	1.000	1.000
N	900	900	900	900	900	900
Pearson Correlation	-.116(**)	.000	.000	.000	1	.000
Sig. (2-tailed)	.000	1.000	1.000	1.000	1.000	1.000
N	900	900	900	900	900	900
Pearson Correlation	-.559(**)	.000	.000	.000	.000	1
Sig. (2-tailed)	.000	1.000	1.000	1.000	1.000	1.000
N	900	900	900	900	900	900

\*\* Correlation is significant at the 0.01 level (2-tailed).

Table 2 The correlations between SRF values obtained from Mohr-Coulomb Criterion and the variants used in the FEM analyses

	SRF	GSI	water table location	seismic coefficient	slope height	slope angle
SRF	1	.224(**)	-.318(**)	-.169(**)	-.080(*)	-.526(**)
		.000	.000	.000	.016	.000
	900	900	900	900	900	900
GSI	.224(**)	1	.000	.000	.000	.000
	.000	1.000	1.000	1.000	1.000	1.000
	900	900	900	900	900	900
water table location	-.318(**)	.000	1	.000	.000	.000
	.000	1.000	1.000	1.000	1.000	1.000
	900	900	900	900	900	900
seismic coefficient	-.169(**)	.000	.000	1	.000	.000
	.000	1.000	1.000	1.000	1.000	1.000
	900	900	900	900	900	900
slope height	-.080(*)	.000	.000	.000	1	.000
	.016	1.000	1.000	1.000	1.000	1.000
	900	900	900	900	900	900
slope angle	-.526(**)	.000	.000	.000	.000	1
	.000	1.000	1.000	1.000	1.000	1.000
	900	900	900	900	900	900

\*\* Correlation is significant at the 0.01 level (2-tailed).

\* Correlation is significant at the 0.05 level (2-tailed).

## APPENDIX F - PAIRED SAMPLES T TEST RESULTS

Table 1 Paired samples (Hoek-Brown and Mohr Coulomb criterions) T test results for slope angle 30°

		Paired Samples Test							
		Paired Differences							
		Mean	Std. Deviation	Std. Error Mean	95% Confidence Interval of the Difference		t	df	Sig. (2-tailed)
					Lower	Upper			
Pair 1	Hoek30 - Mohr30	-.12083	.09183	.00684	-.13434	-.10733	-17.653	179	.000

Table 2 Paired samples (Hoek-Brown and Mohr Coulomb criterions) T test results for slope angle 32°

		Paired Samples Test							
		Paired Differences							
		Mean	Std. Deviation	Std. Error Mean	95% Confidence Interval of the Difference		t	df	Sig. (2-tailed)
					Lower	Upper			
Pair 1	Hoek32 - Mohr32	-.16109	.12340	.00920	-.17924	-.14295	-17.515	179	.000

Table 3 Paired samples (Hoek-Brown and Mohr Coulomb criterions) T test results for slope angle 34°

		Paired Differences							
		Mean	Std. Deviation	Std. Error Mean	95% Confidence Interval of the Difference		t	df	Sig. (2-tailed)
					Lower	Upper			
Pair 1	Hoek - Mohr	-.18594	.11110	.00828	-.20229	-.16960	-22.455	179	.000

Table 3 Paired samples (Hoek-Brown and Mohr Coulomb criterions) T test results for slope angle 36°

		Paired Differences							
		Mean	Std. Deviation	Std. Error Mean	95% Confidence Interval of the Difference		t	df	Sig. (2-tailed)
					Lower	Upper			
Pair 1	Hoek - Mohr	-.17917	.13277	.00990	-.19869	-.15964	-18.105	179	.000

Table 3 Paired samples (Hoek-Brown and Mohr Coulomb criterions) T test results for slope angle 40°

		Paired Differences					t	df	Sig. (2-tailed)
		Mean	Std. Deviation	Std. Error Mean	95% Confidence Interval of the Difference				
Pair 1	Hoek - Mohr							Lower	Upper
		.09556	.38005	.02833	.03966	.15145	3.373	179	.001